Department of Geomatics Engineering

Design and Analysis of Inertial Navigation Systems with Skew Redundant Inertial Sensors

(URL: http://www.geomatics.ucalgary.ca/graduatetheses)

by

Yigiter Yuksel

March 2011

UNIVERSITY OF CALGARY

DESIGN AND ANALYSIS OF INERTIAL NAVIGATION SYSTEMS WITH SKEW

REDUNDANT INERTIAL SENSORS

by

YIGITER YUKSEL

A THESIS

SUBMITTED TO THE FACULTY OF GRADUATE STUDIES

IN PARTIAL FULFILMENT OF THE REQUIREMENTS FOR THE

DEGREE OF DOCTOR OF PHILOSPHY

DEPARTMENT OF GEOMATICS ENGINEERING

CALGARY, ALBERTA

March, 2011

Abstract

The performance of current MEMS based inertial units is usually insufficient to be used in applications for which high accuracy is required. For such applications, if the size and power constraints do not allow the use of traditional high-end inertial sensors, an alternative solution is strongly required. In this study such an alternative INS design method using redundant low cost inertial sensors is described.

In the first part of this study the solution of the optimum inertial sensor fusion problem is derived. In the skew redundant inertial measurement units (SRIMU), the redundancy of the sensors generates additional observations which can be used to estimate the sensor errors without requiring any external aid. In this study, it is proved that the projection of raw sensor outputs to the left null space of the sensor configuration matrix can be used to define these redundancy observations. Based on these observations, the computation of best acceleration and rotation rate which can be used to execute the standard INS equations in an SRIMU based navigation system is explained.

In the second part, the optimum navigation solution for the SRIMU based INSs is defined. In general, such optimum configurations are hard to implement due to the structure of the navigation filters. Therefore, in this study, alternative suboptimal SRIMU based INS configurations are introduced and the conditions for which these alternative configurations become optimal are described. These configurations can be conveniently implemented in the existing navigation software/libraries without requiring any significant modification.

Finally, the comparison of SRIMU based single-INS configurations with the multi-INS configurations is presented. In the existing literature, the multi inertial sensor navigation

problems are usually handled within multi-INS approaches. However, such multi-INS

approaches i) are numerically very problematic, ii) require extensive modification in the

existing navigation libraries and iii) cannot be used when sensors are arbitrarily oriented.

In this study it is shown that the proposed single-INS configurations for SRIMU systems

are theoretically equivalent to the multi-INS configurations and hence can be

implemented instead of any multi-INS configuration without dealing with any of the

aforementioned problems.

To my father Vedat and my mother Melek Yuksel, for their endless love and support.

To my brother Uygar Cagdas, who has always been an inspiration to me.

Table of Contents

List of Figures and Illustrations

List of Abbreviations

Symbol	Definition
ARW	Angle Random Walk
DoF	Degree of Freedom
DSR	Dynamical System Representation
FDI	Fault Detection and Identification
FOG	Fibre Optic Gyroscope
GPS	Global Positioning System
IMU	Inertial Measurement Unit
INS	Inertial Navigation System
MAP	Maximum A-Posteriori
MEMS	Micro-Electromechanical Systems
MISO	Multiple input Single Output
ML	Maximum Likelihood
MMSE	Minimum Mean Square Estimate
MVU	Minimum Variance Unbiased
PVA	Position, Velocity, Attitude
RIMU	Redundant Inertial Measurement Unit
RLG	Ring Laser Gyroscope
SRIMU	Skew Redundant Inertial Measurement Unit
VRW	Velocity Random Walk
WLS	Weighted Least Square

Chapter One: **Introduction**

1.1 Background and Problem Definition

With the emergence of MEMS (micro-electromechanical system) inertial sensors in the

commercial markets in the 1990s, the researches in the inertial navigation technologies

gained another dimension. Until that time, inertial navigation systems (INS) were

designed using only high end components such as fibre optic gyroscopes (FOG) and ring

laser gyroscopes (RLG). Over the years, as new and better INS algorithms were

developed specifically for these high-end inertial measurement units (IMU), it became

possible to reach very precise 6DoF navigation solutions even under complete

autonomous mode of operations. On the other hand, despite their spectacular precision,

these high-end IMUs had 2 major drawbacks which render them unsuitable for a wider

range of consumer applications: i) They were too expensive, ii) They were too heavy

(and usually too large) to be employed in applications for lightweight systems.

Because of these problems, the new MEMS based inertial sensor products were

immediately accepted by INS designers as an alternative for the existing navigation

systems. Their low costs, ultra small sizes and very low power requirements provided

INS designers endless opportunities to develop inertial navigation products for new

applications for which high-end IMUs cannot be employed. Especially, thanks to their

affordable prices and ultra small sizes, new concepts which are impossible to realize with

high-end IMUs such as indoor personal navigation and (commercial) automotive driver

assistance have emerged among navigation community. These new exiting application

areas make MEMS based sensors an indispensible part of every design affords.

On the other hand, despite the fact that over 20 years had passed since the first MEMS based inertial units appeared in the commercial markets, the INS community has not been able to fulfill most of the navigation system demands of the consumers with these low-cost MEMS units. For many fields such as mobile mapping, autonomous robotics and personal navigation, the existing MEMS based INSs are still not sufficient to provide as accurate navigation solution as required by these applications. Still, in many cases, high-end IMUs stand as the only possible choice for system designers if relatively long term stable autonomous navigation solution is desired.

The primary reason for the insufficiency of the MEMS based IMUs is that their outputs are corrupted by several high power error components. During the unaided mode of operation, these high power error components quickly accumulate in the navigation states leading to unacceptable navigation solutions in a very short period of time. The most basic solution to such fast error build up is to aid (integrate) IMUs with the external navigation devices such as GPS. Even without absolute positioning aids, promising navigation results can be still obtained with the (almost) standard Kalman filtering methods as long as some form of external aids can be generated from either the environment or application specific constraints. Some recent examples with these kind of aids can be found in [Tardif et al., 2010] (for visual odometry), [Skog et al., 2010] (for zero-velocity updates) and [Kleinert et al., 2010] (for monocular SLAM). However, such a strong dependence of the INSs to external measurement sources usually contradicts with the main motivation behind the INS concept: INSs must be autonomous and self sufficient. Such dependence on the external sources ruins this self-sufficiency property of the INSs and makes the final navigation product less attractive for some applications.

Over the years, increasingly complex and innovative solutions have been proposed by several research groups to decrease the dependence of INS stability to the external navigation aids. For instance, along with numerous other studies, [Kaygisiz et al., 2003] and [Noureldin et al., 2011] propose neural networks, [Carvalho et al., 1997] and [Nordlund et al., 2001] employ particle filters, [Noureldin et al., 2007] and [Sasiadek et al., 2000] uses fuzzy logic to adaptively adjust parameters of the main estimation algorithms. Essentially, most of such proposed solutions focus on developing more efficient algorithms to estimate the navigation information and IMU errors under limited external navigation aids. However, to the best knowledge of the author, no such solution has been able to permanently supersede the (almost) standard Kalman filtering based INS aiding methods. Therefore, the problem of developing a method (or an algorithm) which leads to accurate and sufficiently autonomous navigation solutions for MEMS based inertial sensors has yet to be solved.

1.2 Thesis Objectives

In this thesis, the objective is to solve the problem of designing stable INSs with only MEMS inertial sensors using a completely new point of view. Instead of focusing on developing a new (and hopefully more efficient) algorithm for better error estimation, it is aimed to employ redundant (abundant) number of inertial sensors in the IMU to achieve high accuracy acceleration/rotation rate measurements which eventually leads to better and more stable autonomous navigation solutions for extended durations. In such design approach, extra inertial sensors (without any orientation constraint) are added to the IMUs until the overall accuracy of the final IMU configuration becomes sufficient to

satisfy the specified mission/application requirements. As the final IMU contains both redundant and skewed (not aligned with body frame) inertial sensors, in this thesis it will be called as SRIMU (skew redundant inertial measurement unit).

Despite this simple objective definition, the implementation and the design aspects of this concept entail a large number of ambiguities. First of all, the existing INS design methods (and practices) are not capable of answering any questions regarding the use of SRIMUs in the INSs. In the standard approach, the INS algorithms take 3 acceleration/rotation rates (for 6DoF navigation) and generate the navigation solution. This computed navigation solution is then considered as a nominal solution around which the linearized INS error propagation models are defined. These error models are then utilized in a Kalman filter to estimate both the sensors and navigation errors whenever an external observation becomes available.

On the other hand, when an SRIMU is used in the INS, the above steps of standard approach become quite ambiguous: Which inertial sensors of the SRIMU should be used to run the INS algorithms? If a combination of all sensors is to be used, how this combination should be formed? Does the redundancy of the sensors provide any information other than the raw outputs? If the redundancy provides such additional information, how should it be mathematically represented? What is the optimal navigation solution for such SRIMU based INSs? Is it sufficient to run an INS with optimally combined (fused) SRIMU outputs to reach the optimal navigation solution?

The main objective of this thesis is to provide a general framework to answer these types of questions regarding the SRIMU based INS designs. As will be explained in the following chapters, in the developed framework, the real kinematic variables measured

by the inertial sensors (i.e. acceleration and rotation rates defined for the fictitious body frame of reference) are also considered as unknowns to be estimated (computed) together with the other navigation and IMU states. However, in contrast to the navigation and IMU related states, no stochastic descriptors are associated with these unknown kinematic variables. Therefore, the entire framework is constructed on a mixed stochastic and deterministic estimation problem.

In the course of describing a main theoretical framework for optimal processing of redundant inertial systems, the following topics/questions will also be addressed in this thesis:

i. How can an SRIMU based navigation system be formulated?

ii. How can a cost function be associated with the selected formulation to specify the optimality?

iii. How can this optimization problem be solved?

iv. How can all the inertial sensor outputs be combined (fused) to form a single "optimal" measurement?

v. What is the optimal navigation solution for SRIMU based systems?

vi. What is the relation between the optimally fused sensor outputs and optimal navigation solution?

vii. Which kind of navigation structures can be used for SRIMU based systems

viii. What is the error model of the optimally fused sensor outputs?

ix. Is it possible to processes subsets of sensors individually and combine the navigation solution later?

x. What are the conditions for which the separate processing of sensors provides the optimal solution?

xi. How can the external measurements be handled when the sensors are processed separately?

1.3 Review of the Existing Literature

The initial studies about the redundant inertial sensor configurations were mostly focused on the reliability issues of the navigation systems. Several studies investigating different fault detection and identification (FDI) algorithms were published in the 70s and 80s. A comprehensive review of these methods can be found in [Ho, 1999]. The main idea behind these studies is based on the so-called parity vectors which is the projection of the sensor outputs to the orthogonal complement space of the configuration (sensor observation) matrix [Skoogh et al., 2006]. Once the parity vector is computed, a decision algorithm is used over the magnitude of the parity vector to detect any sensor failure (and isolate them if redundant configuration permits).

A parity vector compensation algorithm was first presented in [Hall, 1982]. In this study, inertial sensor errors (e.g. stability, misalignment etc. which are not considered as failure) are estimated with a Kalman filter which uses the parity vector itself as the observation for the filter. The innovation process of this filter is defined as the compensated parity vector which is processed by the decision algorithms. In this method the Kalman filter is used as a whitening filter for the parity vectors rather than an observer for the systematic sensor errors. Although the proposed Kalman filter estimates the sensor errors implicitly,

these estimated values are not used to correct the computed kinematic variables (acceleration/rotation rates) which are used to drive the navigation algorithms.

In all of these early studies on FDI methods, the main objective was only to detect (and isolate) the failed sensors so that the computed navigation solution are not affected by these failures. Once the healthy sensors are identified with a detection algorithm, the outputs of these healthy units are combined with a simple least square algorithm (weighted with the sensors' additive white noise powers) to compute the body frame referenced 3-axis acceleration/rotation rates (this process is called as data reconstruction in [Ho, 1999]). These computed kinematic variables are then processed by the standard navigation algorithms to form the final navigation solution.

In [Sukkarieh et al., 2000] a partial application of the aforementioned FDI methods was implemented for a low cost MEMS unit (it is a partial application because only a redundant sensor configuration was used without any real fault detection algorithm). In this study, it was shown that it is possible to improve the navigation accuracy of low cost systems by using redundant inertial sensors with proper sensor orientations.

Although the redundant sensor configurations had been used for FDI purposes for a very long time, it was not until [Bar-Itzhack et al., 2002] that such configurations are used to obtain better rotation rate measurement from an SRIMU. In that study it was shown that the raw sensor outputs can be processed as observations in a Kalman filter to estimate the calibration parameter errors of the skew redundant inertial measurement units. However, the proposed method requires the Kalman filter's state vector to be augmented with a model for rotation rates which is derived from the dynamical equation of the (space) vehicle.

The first solution for the problem of the optimal use of redundant sensors during in-motion sensor calibration problem was presented in [Pittelkau 2005a, 2005b, 2005c]. In these studies it is shown that when the navigation equations are executed by the estimated kinematic variables obtained as the weighted average solution of the sensor measurements, the parity vector must be used as the redundancy observation in the navigation Kalman filter. However, in these studies the optimality of such a solution was not defined at all. The reason why the navigation equations are executed with the weighted average solution is described as a practical solution to avoid the use of dynamic motion models of the vehicle in the Kalman filter as suggested in [Bar-Itzhack et al., 2002]. Furthermore, as these studies ([Pittelkau 2005a, 2005b, 2005c]) mainly focused on in-motion sensor calibration problem, no analysis was provided about the possible simplifications of the navigation filters for identical multi inertial sensor systems. Some methods for the determination of the optimal orientation of individual sensors in an SRIMU are also described in the related literature. In [Harrison et al., 1977] and [Sturza, 1988], the comparison of several sensor orientations are provided. Furthermore, in [Sukkarieh et al., 2000] the same problem is also analyzed using the so-called information filter (which is nothing but the inverse covariance form of the standard Kalman filter). As depicted in these studies, the solution of the optimal placement problem can only be solved based on simplified cost function definitions which do not have any direct relation to the optimal navigation solutions. As an example, the well-known polyhedral configurations in [Sturza, 1988] is optimal only if i) all sensors are identical, ii) all sensors are influenced by only additive white noise, iii) navigation errors in all 3-axis propagates identically. Unfortunately, for the MEMS based navigation

systems, none of these assumptions holds in general. Therefore, in this thesis no such special configurations for sensors are pre-assumed in the derivations.

In [Colomina et al., 2003, 2004a, 2004b], [Waegli et al., 2008], [Waegli 2009] and [Bancroft et al., 2008] and [Bancroft 2009, 2010], some examples of multi-INS implementations for redundant inertial sensors are described. However, these studies lack any theoretical background on the subject matter. Some of the reasoning presented in corresponding papers is based on some ambiguous intuitions which seem to lead conflicting conclusions. On the other hand, these studies can still be regarded as valuable for they at least present some application areas for which successful implementations with redundant sensors can provide some accuracy improvements.

1.4 Thesis Outline

In this thesis the entire treatment of the subject is presented in the 3 successive steps.

In the first step (Chapter 2), the most general solution of the mixed stochastic/deterministic estimation problem for the state space models are derived. This general solution is then applied to the sensor fusion problem for SRIMUs. The sensor fusion problem can be defined as the problem of computing the best (with respect to a cost function which will also be defined in Chapter 2) acceleration and rotation rates at time "n" given all the inertial sensor outputs up to and including time "n". The solution of such a fusion problem is important because once the best (optimal) kinematic variables (acceleration and rotation rates) are computed for the SRIMU, the remaining INS algorithms can be executed with these optimal outputs without making any modification in the existing navigation libraries.

In the second step (Chapter 3), the optimal navigation solution for the SRIMU based INSs will be introduced. In this chapter, it will be shown that the solution obtained by running an INS with the optimally fused SRIMU outputs is not theoretically optimal (in this study, this type of solution will be called "pseudo-optimal" for the reasons described in Chapter 3). In order to reach the optimal solution, the navigation states must also be updated with the IMU redundancy observations defined in Chapter 2. Such updates can be implemented either in a single or in a cascaded Kalman filter structure. In Chapter 3, it will be shown that the pseudo-optimal solutions correspond to a form of cascaded Kalman filter implementation in which the redundancy observations are ignored in the 2nd stage filter.

In the final step (Chapter 4), the relationship between the single INS solutions, as described in the Chapter 3, and the multi-INS solutions will be analyzed. In the existing literature the INS design for the redundant sensors are usually handled in the scope multi-INS approach. In this approach, a separate INS solution is computed for only a sufficient number of sensors (i.e. for each set of 3 accelerometers and 3 gyroscopes for 6DoF navigation problem) and then all INS solutions are combined in a single Kalman filter which processes the equivalency of the navigation states as the only form of redundancy observations. Although such an approach is both very problematic in terms of implementation issues and incapable of covering all the possible SRIMU configurations (e.g. the cases for which sensors are skewed or the number of sensors are not integer multiple of number of kinematic axis), it can still be regarded as a valid design method especially for the cases where significant unknown bore-sight exists between different sets of inertial sensors. In Chapter 4, it is shown that when certain conditions are

satisfied, multi-INS implementations become theoretically equivalent to the optimal

single INS implementations with sensor redundancy observations and hence can also be

regarded as optimal.

Chapter 5 concludes this thesis with a summary of important findings and discussion of

future works to which the results of this study can be extended.

The major questions that are listed among thesis objectives (Section 1.2) are categorized

with respect to corresponding chapters in Table 1.1.

Table 1-1 : Questions classified with respect to the chapters

Chapter	*Questions Addressed*
Chapter One	
Chapter Two	(i) – (iv)
Chapter Three	(v) – (viii)
Chapter Four	(ix) – (xii)
Chapter Five	

Chapter Two: **Optimal Sensor Fusion Method For Skew-Redundant Inertial Measurement Units**

2.1 Introduction

There are some navigation applications (e.g. drilling and pipeline mapping) for which the performance of current micro-electro-mechanical-system (MEMS) inertial units are not sufficient to achieve the required navigation accuracies for these applications. For such applications, one of the foreseeable solution is to use abundant number of inertial sensors together (as the size and power constraints permit) to obtain more accurate navigation solution.

On the other hand, the current understanding (practices) do not answer the important questions regarding the optimal use of redundant sensors to achieve improved navigation performance over standard 6-degrees of freedom (6DoF) IMUs. For 6Dof IMUs, the optimal solution can be obtained by forming an extended Kalman filter (EKF) defined for the error model of the navigation states which are linearized around the nominal INS outputs. This Kalman filter is then used to process any external navigation aid to stabilize the navigation errors. However, when a redundant number of sensors exist, the steps in this standard approach become ambiguous. Should only a critical number of sensors (i.e. 3 accelerometers and 3 gyroscopes) be used for a nominal solution or should all the sensors be used? In case of the latter, how will sensor outputs be combined so that the usual navigation equations can be executed? Does the redundancy of sensors provide any additional information other than the redundant raw measurements? If such additional information exists, how can they be represented and processed in an optimal way?

This chapter will address the above questions. In the first part of this chapter, the main framework (the problem formulation and the most general solution of this problem) for the optimal fusion of redundant inertial sensors will be presented. Using this framework, the problem of computing the best acceleration/rotation rates (kinematic variables) on the kinematic axis (the axis for which the navigation equations are defined, i.e. body frame) given all (skew) redundant sensor measurements will be explained.

Once the optimal kinematic variables are estimated from the redundant raw sensor outputs, the usual navigation equations can be executed with the computed accelerations and rotation rates (kinematic variables). In general, as shown in the next chapter, the navigation solution obtained with such an approach is not the optimal navigation solution. Although the computation of this optimal navigation solution depends on exactly the same theoretical framework presented in this chapter, the explicit solution for this specific problem will be derived in Chapter 3.

2.1.1 Scope and content of this chapter

The main objective of this chapter is to answer the following questions:

Let us assume that a redundant number of accelerometers and gyroscopes (e.g. an inertial measurement unit with N≥3 sensors) are placed at the same point (i.e. close enough to ignore any lever arm effects) but arbitrarily oriented in space.

  i. What is the optimal acceleration/rotation rate (kinematic variables defined for the kinematic axis only) that can be obtained from this SRIMU?

  ii. How would the errors on these computed kinematic variables propagate in time?

As seen from these questions, the objective in this chapter is limited to the estimation of the best sensor outputs rather than obtaining the best navigation solution. However, as it is explained in Chapter 3, the results of this chapter can also be used directly to derive the best navigation solution for the SRIMU based navigation systems.

In Section 2.2, the most general problem formulation is presented using the state space representation. The definition of optimality will be explained based on a selected cost function. The equivalence of this selected cost function to the other possible cost function definitions that are frequently used in estimation theory will be provided.

In Section 2.3, the optimal solution of the selected cost function will be derived. The implementation of this optimal solution using Kalman filters will be explained.

The computation of optimal outputs for SRIMUs will be presented in Section 2.4. It will be shown that this problem is in fact just a simplified form of the general problem formulation introduced in Sections 2.2 and 2.3. Using this simplified form, the cases for which the SRIMU contains only identical sensors (or sets of identical sensors) will be examined in greater detail. In this thesis, inertial sensors with identical stochastic error models are referred to as identical sensors. The equivalent error models for the computed (estimated) kinematic variables which are used in the navigation filters will also be derived. Finally, some simulation results which both clarify and verify the theory described in this chapter will be presented in Section 2.4.

2.2 Problem formulation and associated cost functions

A navigation system which uses an SRIMU can be modeled with the following dynamical system representation:

$$x_{k+1} = A_k x_k + N_k u_k + B_k w_k \tag{2.1a}$$

$$y_k = C_k x_k + M_k u_k + v_k \tag{2.1b}$$

$$E\left\{\begin{bmatrix} x_0 \\ w_k \\ v_k \end{bmatrix} \begin{bmatrix} x_0 \\ w_l \\ v_l \\ 1 \end{bmatrix}^T\right\} = \begin{bmatrix} \Pi_0 & 0 & 0 & 0 \\ 0 & Q_k \delta_{kl} & 0 & 0 \\ 0 & 0 & R_k \delta_{kl} & 0 \end{bmatrix}, \quad \forall k,l \tag{2.2}$$

where " x_k " is the state vector of the entire system including both the navigation states

and sensor error states (with an initial covariance matrix Π_0). " u_k " is the vector of the

real kinematic variables (i.e. real acceleration and rotation rates defined on the body

frame) which is assumed to be a deterministic (non-random) unknown." y_k " is the

observation vector which is provided by the inertial sensors (i.e. raw sensor outputs).

Throughout this thesis, the italic type lowercase and uppercase letters are always used to

represent vectors and matrices respectively with appropriate dimensions unless they are

explicitly specified as scalar quantities. An arrow is used over a letter only when the

corresponding vector/matrix is formed by combining some other (lower dimension)

vectors/matrices.

In this chapter, it is assumed that there are no additional observation sources (e.g. GPS)

other than the inertial sensors themselves. Furthermore, it is also assumed that the inertial

sensors are oriented in such a way that all kinematic variables can be observed by the

SRIMU. Thus, M_k is always a full column rank matrix. w_k and v_k denotes the system

disturbance and observation white noises with covariance matrices Q_k and R_k

respectively. In the standard IMU terminology v_k is called as A(V)RW (angle/velocity

random walk) component despite the fact that it is a white noise process. Finally, N_k and C_k are matrices with appropriate dimensions.

The objective is to causally estimate the x_k and u_k given $\{y_l\}_{l=0}^{k}$ $\forall$ k. Due to this causality condition, only filtering solutions will be considered in the rest of this thesis.

As (2.1) consist of both deterministic (i.e. "u_k" which is a non-random unknown) and stochastic (i.e. w_k, v_k, x_0) variables, this is a mixed random/non-random estimation problem. Because of this mix nature, neither random (e.g. Kalman filter (KF), maximum a posteriori estimate (MAP) etc.) nor non-random (e.g. maximum likelihood (ML), minimum variance unbiased (MVU)) estimation methods can be directly used to obtain an immediate answer. Therefore, we first analyze the possible cost functions whose solutions can be used to define the "best" $\{x_k, u_k\}$ estimates.

In Section 2.2.1, the equivalent matrix form of (2.1) is introduced. The solution of the standard ML, MAP, Bayesian and Joint PDF cost functions are derived in Section 2.2.2. It will be shown that all these cost functions have identical solutions. In Section 2.2.3, a quadratic cost function whose optimal solution is also identical to the previous cost functions is defined. In Section 2.3, the main causal (filtering) estimation algorithm will be derived using this final quadratic cost function definition.

2.2.1 Equivalent Matrix Form

Using the linearity property, (2.1) can be rewritten as follows:

$$x_{k+1}^s = A_k x_k^s + B_k w_k$$
$$x_{k+1}^d = A_k x_k^d + N_k u_k \tag{2.3}$$
$$y_k = C_k \left(x_k^s + x_k^d \right) + M_k u_k + v_k$$

$$E\{x_0^s x_0^{sT}\} = \Pi_0$$
$$x_0^d = 0 \tag{2.4}$$

where "x_k^s" represents the purely stochastic part and "x_k^d" is the unknown deterministic

part of the system defined in (2.1). Let us assume $\Phi(k,m) = A_{k-1} \times \ldots \times A_m$. Thus, (2.3)

can be expressed in the following matrix form:

$$
\underbrace{\begin{bmatrix} y_0 \\ y_1 \\ \vdots \\ y_n \end{bmatrix}}_{\vec{y}} = \underbrace{\begin{bmatrix} C_0 & 0 & 0 & & 0 \\ C_1\Phi(1,0) & C_1 B_0 & 0 & \ddots & \vdots \\ C_2\Phi(2,0) & C_2\Phi(2,1)B_0 & C_2 B_1 & & \\ & \vdots & & \ddots & 0 \\ C_n\Phi(n,0) & C_n\Phi(n,1) & \cdots & & C_n B_{n-1} \end{bmatrix}}_{\Phi^s} \underbrace{\begin{bmatrix} x_0^S \\ w_0 \\ w_1 \\ \vdots \\ w_{n-1} \end{bmatrix}}_{\vec{x}^s}
$$

$$
+ \underbrace{\begin{bmatrix} M_0 & 0 & 0 & & 0 \\ C_1 N_0 & M_1 & 0 & \ddots & \vdots \\ C_2\Phi(2,1)N_0 & C_2 N_1 & M_2 & & \\ & \vdots & & \ddots & 0 \\ C_n\Phi(n,1)N_0 & C_n\Phi(n,2)N_1 & \cdots & & M_n \end{bmatrix}}_{\Phi^d} \underbrace{\begin{bmatrix} u_0 \\ u_1 \\ \vdots \\ u_n \end{bmatrix}}_{\vec{x}^d} + \underbrace{\begin{bmatrix} v_0 \\ v_1 \\ \vdots \\ v_n \end{bmatrix}}_{\vec{v}} \tag{2.5}
$$

$$\vec{y} = \Phi^s \vec{x}^s + \Phi^d \vec{x}^d + \vec{v} \tag{2.6}$$

where

$$
E\{\vec{x}^s \vec{x}^{sT}\} = \vec{\Pi} = \begin{bmatrix} \Pi_0 & 0 & & 0 \\ 0 & Q_0 & & \vdots \\ \vdots & & \ddots & 0 \\ 0 & \cdots & 0 & Q_{n-1} \end{bmatrix} \tag{2.7a}
$$

$$
E\{\vec{v}\vec{v}^T\} = \vec{R} = \begin{bmatrix} R_0 & 0 & \cdots & 0 \\ 0 & R_1 & & \vdots \\ \vdots & & \ddots & 0 \\ 0 & \cdots & 0 & R_n \end{bmatrix} \tag{2.7b}
$$

It should be noted that as each M_k in (2.5) is full column rank, so is Φ^d.

As a next step, using a series of linear transformations, (2.6) will be transformed into another form which will be more useful for later derivations. As only linear estimators are considered in this study, these linear transformations have no effect on the final result.

Define a full rank $\hat{T} = \begin{bmatrix} T \\ \overline{T} \end{bmatrix}$ such that

$$Range\left\{\overline{T}^T\right\} = Range\left\{\Phi^d\right\} \tag{2.8a}$$

$$T\Phi^d = 0 \tag{2.8b}$$

(i.e. rows of $\overline{T}$ spans the range space of Φ^d and rows of T is the basis for left null-space of Φ^d. Hence, by construction $\hat{T}$ is a full rank matrix.)

Transform (2.6) using $\hat{T}$:

$$T\vec{y} = T\Phi^s \vec{x}^s + T\vec{v} \tag{2.9a}$$

$$\overline{T}\vec{y} = \overline{T}\Phi^s \vec{x}^s + \overline{T}\Phi^d \vec{x}^d + \overline{T}\vec{v} \tag{2.9b}$$

Define a 2$^{\text{nd}}$ transformation using the LDU decomposition of $E\left\{\hat{T}\vec{v}\left(\vec{v}\hat{T}\right)^T\right\} = \hat{T}\vec{R}\hat{T}^T$.

$$V = \begin{bmatrix} \mathrm{I} & 0 \\ \underbrace{-\overline{T}\vec{R}T^T \left(T\vec{R}T\right)^{-1}}_{-W} & \mathrm{I} \end{bmatrix} \tag{2.10}$$

Pre-multiply both sides of (2.9) (in the matrix form) with (2.10):

$$\underbrace{T\vec{y}}_{\vec{y}_1} = \underbrace{T\Phi^s}_{\vec{A}} \underbrace{\vec{x}^s}_{\vec{x}} + \underbrace{T\vec{v}}_{\vec{v}_1} \tag{2.11a}$$

$$\underbrace{\overline{T}\vec{y} - WT\vec{y}}_{\vec{y}_2} = \underbrace{\left(\overline{T}\Phi^s - WT\Phi^s\right)}_{\vec{B}} \underbrace{\vec{x}^s}_{\vec{x}} + \underbrace{\overline{T}\Phi^d}_{\vec{C}} \underbrace{\vec{x}^d}_{\vec{\theta}} + \underbrace{\left(\overline{T}\vec{v} - WT\vec{v}\right)}_{\vec{v}_2} \tag{2.11b}$$

Where

$$E\left\{\begin{bmatrix} \vec{v}_1 \\ \vec{v}_2 \end{bmatrix}\begin{bmatrix} \vec{v}_1^T & \vec{v}_2^T \end{bmatrix}\right\} = \begin{bmatrix} \vec{R}_1 & 0 \\ 0 & \vec{R}_2 \end{bmatrix}$$

$$= \begin{bmatrix} T\vec{R}T^T & 0 \\ 0 & \overline{T}\vec{R}\overline{T}^T - \overline{T}\vec{R}T^T\left(T\vec{R}T^T\right)^{-1}T\vec{R}\overline{T}^T \end{bmatrix} \qquad (2.12)$$

It should be noted that this final diagonalization of the observation noise covariance is a consequence of the 2nd transformation.

2.2.2 Cost Function Definitions and Their Equivalence

As shown in the previous section, for each dynamical system representation defined by (2.3), there exists an equivalent representation in the following form:

$$\vec{y}_1 = \vec{A}\vec{x} + \vec{v}_1$$
$$\vec{y}_2 = \vec{B}\vec{x} + \vec{C}\vec{\theta} + \vec{v}_2 \qquad (2.13)$$

where $\vec{\theta}$ and $\vec{x}$ represents the non-random and random parameters respectively to be estimated. $\vec{y} = [\vec{y}_1; \vec{y}_2]$ are the observations whose respective noise components ($\vec{v} = [\vec{v}_1; \vec{v}_2]$) are uncorrelated as shown in (2.12). It should be noted that (2.13) is just a simplified representation of (2.11) where $\vec{A}, \vec{B}$ and $\vec{C}$ are explicitly defined as functions of $\overline{T}, T, \Phi^S$ and W which are derived from the state space representation of (2.1). In this section, based on the form of (2.13), several cost function definitions and their solutions will be presented. The objective of this section is to show that, with some modifications, the standard cost functions can still be used over the mixed model defined in (2.13) to estimate $[\vec{\theta}; \vec{x}]$.

Throughout this section, it will be always assumed that all the random vectors (i.e.

$\vec{x}, \vec{v}_1, \vec{v}_2$) have Gaussian distribution.

2.2.2.1 Joint PDF Maximization

The cost function is defined as follows:

$$\max_{\vec{x},\vec{\theta}} \quad pdf\left(\vec{y}, \vec{x}; \vec{\theta}\right) = pdf\left(\vec{y} \mid \vec{x}; \vec{\theta}\right) pdf\left(\vec{x}\right) \tag{2.14}$$

Using the Gaussian distribution assumption and the orthogonality of the observation

noises $\left[\vec{v}_1; \vec{v}_2\right]$, (2.14) can be written as:

$$\min_{\vec{x},\vec{\theta}} \left\|\vec{y}_1 - \vec{A}\vec{x}\right\|^2_{\vec{R}_1^{-1}} + \left\|\vec{y}_2 - \vec{B}\vec{x} - \vec{C}\vec{\theta}\right\|^2_{\vec{R}_2^{-1}} + \left\|\vec{x}\right\|^2_{\vec{\Pi}^{-1}} \tag{2.15}$$

where $\|\ \|^2_{\bullet}$ notation represents the (squared) weighted L2-norm (i.e. $\|x\|^2_Y = x^T Y x$).

By setting the gradient of (2.15) zero, the optimal solution can be found as:

$$\hat{x} = \left(\vec{\Pi}^{-1} + \vec{A}^T \vec{R}_1^{-1} \vec{A}\right)^{-1} \vec{A}^T \vec{R}^{-1} \vec{y}_1 = \vec{\Pi}\vec{A}^T \left(\vec{A}\vec{\Pi}\vec{A}^T + \vec{R}\right)^{-1} \vec{y}_1 \tag{2.16a}$$

$$\hat{\theta} = \vec{C}^{-1}\left(\vec{y}_2 - \vec{B}\hat{x}\right) \tag{2.16b}$$

It should be noted that the optimal solution of $\vec{x}$ is independent of $\vec{y}_2$. Furthermore $\hat{\theta}$

depends on $\vec{y}_1$ only via $\hat{x}$.

2.2.2.2 Maximum Likelihood (ML)

As $\vec{x}$ is a random parameter, standard ML method cannot be used directly for $\vec{x}$

estimation. On the other hand, the ML estimate of $\vec{\theta}$ can be defined as the result of the

following cost function:

$$\hat{\theta}_{ML} = \max_{\theta} pdf\left(\vec{y}_1, \vec{y}_2; \vec{\theta}\right) = \max_{\theta} \int_{\forall \vec{x}} pdf\left(\vec{y}_1, \vec{y}_2 \mid \vec{x}; \vec{\theta}\right) pdf\left(\vec{x}\right) d\vec{x} \qquad (2.17)$$

Using the jointly Gaussian assumption, the probability distribution (pdf) of the observations can be written as:

$$pdf\left(\vec{y}_1, \vec{y}_2; \vec{\theta}\right) = N\left(\begin{bmatrix} 0 \\ \vec{C}\theta \end{bmatrix}, \underbrace{\begin{bmatrix} \vec{A}\vec{\Pi}\vec{A}^T + \vec{R}_1 & \vec{A}\vec{\Pi}\vec{B}^T \\ \vec{B}\vec{\Pi}\vec{A}^T & \vec{B}\vec{\Pi}\vec{B}^T + \vec{R}_2 \end{bmatrix}}_{\vec{R}_{Obs}}\right) \qquad (2.18)$$

where $N(m, C)$ notation represents a Gaussian distribution with mean "m" and variance "C". Hence, the optimum $\vec{\theta}$ estimate in ML sense can be defined as:

$$\hat{\theta}_{ML} = \min_{\theta} \begin{bmatrix} \vec{y}_1 \\ \vec{y}_2 - \vec{C}\theta \end{bmatrix}^T R_{Obs}^{-1} \begin{bmatrix} \vec{y}_1 \\ \vec{y}_2 - \vec{C}\theta \end{bmatrix} \qquad (2.19)$$

The LDU decomposition of $\vec{R}_{Obs}$ is as follows:

$$\vec{R}_{Obs} = \begin{bmatrix} I & 0 \\ \vec{B}\vec{\Pi}\vec{A}^T \left(\vec{A}\vec{\Pi}\vec{A}^T + \vec{R}_1\right)^{-1} & I \end{bmatrix} \begin{bmatrix} \left(\vec{A}\vec{\Pi}\vec{A}^T + \vec{R}_1\right) & 0 \\ 0 & X \end{bmatrix} \begin{bmatrix} I & \left(\vec{A}\vec{\Pi}\vec{A}^T + \vec{R}_1\right)^{-1} \vec{A}\vec{\Pi}\vec{B}^T \\ 0 & I \end{bmatrix} \qquad (2.20)$$

where $X = \vec{B}\vec{\Pi}\vec{B}^T + \vec{R}_2 - \vec{B}\vec{\Pi}\vec{A}^T \left(\vec{A}\vec{\Pi}\vec{A}^T + \vec{R}_1\right)^{-1} \vec{A}\vec{\Pi}\vec{B}^T$ is a positive definite matrix. Using (2.20), (2.19) can be written as follows:

$$\begin{aligned} \hat{\theta}_{ML} &= \min_{\theta} \left\{ \left\|\vec{y}_1\right\|^2_{\left(\vec{A}\vec{\Pi}\vec{A}^T + \vec{R}_1\right)^{-1}} + \left\|\left(\vec{y}_2 - \vec{B}\vec{\Pi}\vec{A}^T \left(\vec{A}\vec{\Pi}\vec{A}^T + \vec{R}_1\right)^{-1} \vec{y}_1 - \vec{C}\theta\right)\right\|^2_{X^{-1}} \right\} \\ &= \vec{C}^{-1}\left(\vec{y}_2 - \vec{B}\left(\vec{\Pi}\vec{A}^T \left(\vec{A}\vec{\Pi}\vec{A}^T + \vec{R}_1\right)^{-1} \vec{y}_1\right)\right) \qquad (2.21) \\ &= \vec{C}^{-1}\left(\vec{y}_2 - \vec{B}\hat{x}\right) \end{aligned}$$

where $\hat{x}$ is as defined in (2.16a). It should be noted that $\vec{C}$ is invertible by construction. As seen from these results, for the ML case although the cost function is defined for only

$\vec{\theta}$, the optimal solution also implicitly depends on the optimal $\hat{x}$ which is defined as the

optimal result of the joint PDF maximization in (2.16a).

2.2.2.3 Maximum aposteriori maximization

The cost function is as follows:

$$\max_{\vec{x},\vec{\theta}} pdf\left(\vec{x} \mid \vec{y};\vec{\theta}\right) = \frac{pdf\left(\vec{y} \mid \vec{x};\vec{\theta}\right) pdf\left(\vec{x}\right)}{pdf\left(\vec{y};\vec{\theta}\right)} \tag{2.22}$$

Although this cost function is similar to the classical MAP cost function definition, it has

one important difference: the denominator depends on $\vec{\theta}$. Therefore it is not apparent

whether or not this maximization is equivalent to the joint-pdf maximization defined in

Section 2.2.2.1.

For a given $\vec{\theta}$, the mean and cross-covariance of random parameters can be written as:

$$E\left\{\begin{bmatrix} \vec{x} \\ \vec{y}_1 \\ \vec{y}_2 \end{bmatrix}\right\} = \begin{bmatrix} 0 \\ 0 \\ \vec{C}\vec{\theta} \end{bmatrix} \tag{2.23a}$$

$$Cov\left\{\begin{bmatrix} \vec{x} \\ \vec{y}_1 \\ \vec{y}_2 \end{bmatrix}\right\} = \begin{bmatrix} \overbrace{\underbrace{\vec{\Pi}}_{}}^{\Sigma_{11}} & \overbrace{\boxed{\vec{\Pi}\vec{A}^T \quad \vec{\Pi}\vec{B}^T}}^{\Sigma_{12}} \\ \underbrace{\boxed{\begin{matrix} \vec{A}\vec{\Pi} \\ \vec{B}\vec{\Pi} \end{matrix}}}_{\Sigma_{21}} & \underbrace{\boxed{\begin{matrix} \vec{A}\vec{\Pi}\vec{A}^T + \vec{R}_1 & \vec{A}\vec{\Pi}\vec{B}^T \\ \vec{B}\vec{\Pi}\vec{A}^T & \vec{B}\vec{\Pi}\vec{B}^T + \vec{R}_2 \end{matrix}}}_{\Sigma_{22}} \end{bmatrix} \tag{2.23b}$$

Therefore, using the notation defined in (2.23b), the conditional Gaussian PDF can be

written as:

$$pdf\left(\vec{x} \mid \vec{y};\vec{\theta}\right) = N\left(\Sigma_{12}\Sigma_{22}^{-1}\begin{bmatrix} \vec{y}_1 \\ \vec{y}_2 - \vec{C}\vec{\theta} \end{bmatrix}, \underbrace{\Sigma_{11} - \Sigma_{12}\Sigma_{22}^{-1}\Sigma_{21}}_{\Sigma_c}\right) \tag{2.24}$$

It should be noted that because of jointly Gaussian property, Σ_c in (2.24) is independent of both $\vec{\theta}$ and $\vec{y}$. Using the logarithm of (2.24), the optimization can be rewritten as follows:

$$\begin{bmatrix} \hat{x}_{MAP} \\ \hat{\theta}_{MAP} \end{bmatrix} = \max_{\bar{\theta},\bar{x}} pdf\left(\vec{x}\mid\vec{y};\vec{\theta}\right) = \min_{\bar{x},\bar{\theta}} \left\| \vec{x} - \Sigma_{12}\Sigma_{22}^{-1}\begin{bmatrix} \vec{y}_1 \\ \vec{y}_2 - \vec{C}\vec{\theta} \end{bmatrix} \right\|_{\Sigma_c^{-1}}^2 \tag{2.25}$$

Using the LDU decomposition of Σ_{22}, the term inside the norm bars of (2.25) can be rearranged as:

$$\vec{x} - \Sigma_{12}\Sigma_{22}^{-1}\begin{bmatrix} \vec{y}_1 \\ \vec{y}_2 - \vec{C}\vec{\theta} \end{bmatrix} = \vec{x} - \vec{\Pi}\vec{A}^T\left(\vec{A}\vec{\Pi}\vec{A}^T + \vec{R}_1\right)^{-1}\vec{y}_1 - X\left(\vec{y}_2 - \vec{C}\vec{\theta} - \vec{B}\vec{\Pi}\vec{A}^T\left(\vec{A}\vec{\Pi}\vec{A}^T + \vec{R}_1\right)^{-1}\vec{y}_1\right) \tag{2.26}$$

where, X is a positive definite matrix whose exact value is not crucial for this discussion. As Σ_c is a positive definite matrix, the minimum of (2.25) is obtained when (2.26) is equal to zero. The $\hat{x}$ and $\hat{\theta}$ values defined in (2.16) sets (2.26) to zero. Therefore, the solution (2.16) is also optimum in terms of MAP sense.

2.2.2.4 Minimum Mean Square Solution

For a given $\vec{\theta}$, the optimum $\vec{x}$ in minimum mean square sense can be defined as:

$$\hat{x}_{MMSE} = \min_{\hat{x}} E\left\{\left[\vec{x} - \hat{x}(\vec{y})\right]\left[\vec{x} - \hat{x}(\vec{y})\right]^T\right\} \tag{2.27}$$

The optimum solution for this cost is:

$$\hat{x}_{MMSE} = E\left\{\vec{x}\mid\vec{y};\vec{\theta}\right\} \tag{2.28}$$

Using (2.24) it can be shown that:

$$\hat{x}_{MMSE} = \Sigma_{12}\Sigma_{22}^{-1} \begin{vmatrix} \vec{y}_1 \\ \vec{y}_2 - \vec{C}\vec{\theta} \end{vmatrix} \qquad (2.29a)$$

$$\text{cov}\left(\vec{x} - \hat{x}_{MMSE}\right) = \Sigma_{11} - \Sigma_{12}\Sigma_{22}^{-1}\Sigma_{12}^{T} \qquad (2.29b)$$

Therefore, such an approach cannot be used to obtain a solution. As soon as $\vec{\theta}$ is

assumed to be an unknown constant, the value of the cost becomes independent of the $\vec{\theta}$,

and hence, no additional constraints can further be imposed on $\vec{\theta}$ for this cost function.

One possible way to obtain a meaningful cost function based on estimation error variance

without any prior knowledge of $\vec{\theta}$ is to assume that $\vec{\theta}$ itself is a stochastic variable with

the following properties:

$$E\{\vec{\theta}\vec{\theta}^{T}\} = \Pi_{\vec{\theta}} = [\infty]$$
$$E\{\vec{x}\vec{\theta}^{T}\} = [0] \qquad (2.30)$$

where $[\infty]$ represents a matrix with infinite variance values. For this $\vec{\theta}$ definition the

optimum solution can be computed as follows:

Let $K = E\{\vec{y}_2\vec{y}_1^{T}\}E\{\vec{y}_1\vec{y}_1^{T}\}^{-1}$ and $\tilde{y}_2 = \vec{y}_2 - K\vec{y}_1 = \left(\vec{A} - K\vec{B}\right)\vec{x} + \vec{C}\vec{\theta} + \vec{v}_2 - K\vec{v}_1$. Then

$E\{\vec{y}_1\tilde{y}_2^{T}\} = [0]$ and $E\{\tilde{y}_2\tilde{y}_2^{T}\} = [\infty]$. Thus the optimum $\vec{x}$ estimate can be found as:

$$\begin{aligned}
\hat{x}_{MMSE} &= E\{\vec{x} \mid \vec{y}_1, \vec{y}_2\} = E\{\vec{x} \mid \vec{y}_1, \tilde{y}_2\} \\
&= E\{\vec{x} \mid \vec{y}_1\} + E\{\vec{x} \mid \tilde{y}_2\} \\
&= \vec{\Pi}\vec{A}^{T}\left(\vec{A}\vec{\Pi}\vec{A}^{T} + \vec{R}\right)^{-1}\vec{y}_1 + \underbrace{E\{\vec{x}\tilde{y}_2^{T}\}E\{\tilde{y}_2\tilde{y}_2^{T}\}^{-1}}_{0}\tilde{y}_2 \qquad (2.31) \\
&= \vec{\Pi}\vec{A}^{T}\left(\vec{A}\vec{\Pi}\vec{A}^{T} + \vec{R}\right)^{-1}\vec{y}_1
\end{aligned}$$

The final step in (2.31) is a consequence of the fact that $E\left\{\tilde{x}\tilde{y}_2^T\right\} = \left(\vec{A} - K\vec{B}\right)\vec{\Pi}\left(\vec{A} - K\vec{B}\right)^T$

has a finite value and $E\left\{\tilde{y}_2\tilde{y}_2^T\right\}$ has infinite covariance.

Furthermore:

$$
\begin{aligned}
\hat{\theta}_{MMSE} &= E\left\{\vec{\theta} \mid \tilde{y}_1, \tilde{y}_2\right\} = E\left\{\vec{\theta} \mid \tilde{y}_2\right\} \\
&= E\left\{\vec{\theta}\tilde{y}_2^T\right\} E\left\{\tilde{y}_2\tilde{y}_2^T\right\}^{-1} \tilde{y}_2 \\
&= \vec{\Pi}_{\vec{\theta}}\vec{C}^T \left(\vec{C}\vec{\Pi}_{\vec{\theta}}\vec{C}^T + Z\right)^{-1} \tilde{y}_2
\end{aligned}
\tag{2.32}
$$

where $Z = E\left\{\left(\tilde{y}_2 - \vec{C}\vec{\theta}\right)^T \left(\tilde{y}_2 - \vec{C}\vec{\theta}\right)\right\}$ is some finite covariance. Therefore, as $\vec{C}$ is an

invertible matrix by construction, the MMSE solution can be derived as follows:

$$
\begin{aligned}
\hat{\theta}_{MMSE} &= \lim_{\vec{\Pi}_{\vec{\theta}} \to \infty} \vec{\Pi}_{\vec{\theta}}\vec{C}^T \left(\vec{C}\vec{\Pi}_{\vec{\theta}}\vec{C}^T + Z\right)^{-1} \tilde{y}_2 \\
&= \vec{C}^{-1}\left(\vec{y}_2 - K\vec{y}_1\right) \\
&= \vec{C}^{-1}\left(\vec{y}_2 - B\hat{x}_{MMSE}\right)
\end{aligned}
\tag{2.33}
$$

The above discussion shows that when $\vec{\theta}$ is assumed to be independent of $\vec{x}$ and has

infinite covariance, the minimum mean square estimation solution becomes identical to

the previous solutions.

2.2.2.5 Quadratic cost function minimization

The quadratic cost function for (2.1) can be defined as follows:

$$
\min_{x_0,\omega_k,u_k} \|x_0\|^2_{\Pi_0^{-1}} + \sum_{k=0}^{n-1}\|\omega_k\|^2_{Q_k^{-1}} + \sum_{k=0}^{n}\|y_k - C_k x_k - M_k u_k\|^2_{R_k^{-1}}
\tag{2.34a}
$$

Subject to:

$$
x_{k+1} = A_k x_k + N_k u_k + B_k \omega_k
\tag{2.34b}
$$

It should be noted that this quadratic cost is equivalent to the logarithm of the joint (Gaussian) PDF defined in (2.14) regardless of the invertibility of B_k. Therefore, the solution of (2.34) is also the solution of the joint PDF maximization problem presented in Section 2.1.1. Hence the solution of (2.34) is also optimal in the sense of ML, MAP, MMSE as described in the previous sections.

The algorithm for causally solving (2.34) for optimum x_k and u_k for each "k" instant is derived in the next section.

2.3 The quadratic cost function

In Sections 2.2.2.1 through 2.2.2.3 several cost functions based on classical estimation methods were introduced and it was shown that all lead to exactly the same solution defined in (2.16) which is based on the equivalent matrix form (2.13). Although this solution has a relatively simple form, in practice it has very little usage. In practical applications the matrix size becomes unmanageable in a very short duration of time which makes (2.16) impossible to be implemented.

From application point of view, an acceptable solution must have a filtering (sequential processing of measurements to obtain the best estimate of only the current state) form rather than the batch form defined in (2.16). In this section such a sequential and causal algorithm is derived using the quadratic cost function defined in (2.34) (Section 2.2.2.4). The proposed solution to this quadratic cost function optimization problem depends on the results presented in [Hassibi et al., 1999 - Chapter 3]. For the sake of completeness the relevant result of [Hassibi et al., 1999 - Chapter 3] is summarized below:

Lemma 1

Let an optimization problem be defined as follow:

$$\min_{x_0, \omega_k} \|x_0\|^2_{\Pi_0^{-1}} + \sum_{k=0}^{n-1} \|w_k\|^2_{Q_k^{-1}} + \sum_{k=0}^{n} \|y_k - C_k x_k\|^2_{R_k^{-1}} \tag{2.35a}$$

Subject to:

$$x_{k+1} = A_k x_k + B_k w_k \tag{2.35b}$$

At time "n", the optimal value of x_n is equivalent to the optimal $\hat{x}_{n|n}$ estimate (x_n estimate given all the observation up to and including y_n) of the Kalman filter for the following system:

$$\begin{aligned} x_{k+1} &= A_k x_k + B_k w_k \\ y_k &= C_k x_k + v_k \end{aligned} \tag{2.36a}$$

$$E\left\{ \begin{bmatrix} x_0 \\ w_k \\ v_k \\ 1 \end{bmatrix} \begin{bmatrix} x_0^T & w_l^T & v_l^T \end{bmatrix} \right\} = \begin{bmatrix} \Pi_0 & 0 & 0 \\ 0 & Q_k \delta_{kl} & 0 \\ 0 & 0 & R_k \delta_{kl} \\ 0 & 0 & 0 \end{bmatrix}, \quad \forall k, l \tag{2.36b}$$

(For the complete proof see, [Hassibi et al., 1999, Lemma 3.2.1, 3.2.2, 3.2.3 & 3.3.1].)

A simpler approach than the one used in [Hassibi et al., 1999] for the derivation of this duality between the Kalman filters and deterministic quadratic optimization problems is also presented in [Kailath et al., 2000 – Chapter 3.5 and 10.7].

It should also be noted that as mentioned in [Kailath et al 2000 – Chapter 10.3 Remark 3], this duality is still valid regardless of the invertibility of $B_k Q_k B_k^T$ as long as Q_k is an invertible matrix.

2.3.1 Optimal solution of the quadratic cost function

The objective is to find $\hat{x}_{k|k}$ and $\hat{u}_{k|k}$ for each instant k which minimizes the cost defined in (2.34).

Unfortunately, Lemma 1 cannot be used directly to obtain this optimal solution because of the existence of non-random parameter u_k in the original cost function definition. Therefore, first of all using a series of linear transformations and change of variables (2.34) must be converted into a form for which Lemma 1 can be applied. Once such a form is obtained, the optimal solution can be derived using the Kalman filter as described in Lemma 1.

First, the following 2 linear transformation are applied to the observation in (2.1b):

Let $\hat{T}_k = \begin{bmatrix} T_k \\ \overline{T}_k \end{bmatrix}$ be a non-singular square matrix such that rows of T_k represents the basis vectors of the left null space of M_k and the rows of $\overline{T}_k$ are the orthogonal complement of the rows of T_k. In other words:

$$T_k M_k = 0 \tag{2.37a}$$

$$Range\{\overline{T}_k^T\} = Range\{M_k\} \tag{2.37b}$$

(This is the same kind of transformation as defined in (2.8). However, in this case the transformation is defined for each "k" instant rather than for the overall matrix notation.)

Thus:

$$y_k^1 = T_k y_k = T_k C_k x_k + T_k v_k \tag{2.38a}$$

$$y_k^2 = \overline{T}_k y_k = \overline{T}_k C_k x_k + \overline{T}_k M_k u_k + \overline{T}_k v_k \tag{2.38b}$$

Furthermore using the LDU decomposition of $\hat{T}_k R_k \hat{T}_k^T$ (where $R_k = E\{v_k v_k^T\}$), a 2nd

transformation is defined as follows:

$$V_k = \begin{bmatrix} I & 0 \\ \underbrace{-\bar{T}_k R_k T_k^T \left(T_k R_k T_k^T\right)^{-1}}_{-\tilde{T}_k} & I \end{bmatrix} \qquad (2.39)$$

Pre-multiplying the both sides of (2.38) with (2.39), the following new set of

observations can be formed:

$$y_k^1 = T_k y_k = T_k C_k X_k + \overbrace{T_k v_k}^{v_k^1} \qquad (2.40a)$$

$$y_k^3 = y_k^2 - \tilde{T}_k y_k^1 = \underbrace{\left(\bar{T}_k - \tilde{T}_k T_k\right)}_{T_k^3} C_k x_k + \underbrace{\bar{T}_k M_k}_{M_k^3} u_k + \underbrace{\left(\bar{T}_k - \tilde{T}_k T_k\right) v_k}_{v_k^3} \qquad (2.40b)$$

It should be noted that M_k^3 is a non-singular matrix. Furthermore, due to the 2nd

transformation v_k^1 and v_k^3 is orthogonal:

$$E\left\{\begin{bmatrix} v_k^1 \\ v_k^3 \end{bmatrix} \begin{bmatrix} v_k^{1T} & v_k^{3T} \end{bmatrix}\right\} = \begin{bmatrix} R_k^1 & 0 \\ 0 & R_k^3 \end{bmatrix} = \begin{bmatrix} T_k R_k T_k^T & 0 \\ 0 & \bar{T}_k R_k \bar{T}_k^T - \bar{T}_k R_k T_k^T \left(T_k R_k T_k^T\right)^{-1} T_k R_k \bar{T}_k^T \end{bmatrix} \qquad (2.41)$$

Using this orthogonality property, the cost function (2.34) can be rewritten for the

transformed observations as follows:

$$\min_{x_0, \omega_k, u_k} \|x_0\|_{\Pi_0^{-1}}^2 + \sum_{k=0}^{n-1} \|\omega_k\|_{Q_k^{-1}}^2 + \sum_{k=0}^{n} \|y_k^1 - T_k C_k x_k\|_{R_k^{1-1}}^2 + \sum_{k=0}^{n} \|y_k^3 - T_k^3 C_k x_k - M_k^3 u_k\|_{R_k^{3-1}}^2 \qquad (2.42a)$$

Subject to:

$$x_{k+1} = A_k x_k + N_k u_k + B_k \omega_k \qquad (2.42b)$$

Now the following change of variables is employed:

$$z_k = y_k^3 - T_k^3 C_k x_k - M_k^3 u_k \qquad (2.43a)$$

Hence:

$$u_k = M_k^{3^{-1}} \left(y_k^3 - T_k^3 C_k x_k - z_k \right) \tag{2.43b}$$

With this change of variables (2.42) becomes:

$$\min_{x_0, \omega_k, z_k} \|x_0\|_{\Pi_0^{-1}}^2 + \sum_{k=0}^{n-1} \|\omega_k\|_{Q_k^{-1}}^2 + \sum_{k=0}^{n} \|y_k^1 - T_k C_k x_k\|_{R_k^{1^{-1}}}^2 + \sum_{k=0}^{n} \|z_k\|_{R_k^{3^{-1}}}^2 \tag{2.44a}$$

Subject to:

$$\begin{aligned}
x_{k+1} &= A_k x_k + N_k \left(M_k^{3^{-1}} \left(y_k^3 - T_k^3 C_k x_k - z_k \right) \right) + B_k \omega_k \\
&= \left(A_k - N_k M_k^{3^{-1}} T_k^3 C_k \right) x_k + B_k \omega_k - N_k M_k^{3^{-1}} z_k + N_k M_k^{3^{-1}} T_k^3 y_k
\end{aligned} \tag{2.45b}$$

In order to get rid of the deterministic input " y_k " from the constraints, the following

dynamical change of variables is introduced:

Let $x_k = x_k^e + x_k^N$ and $y_k^1 = y_k^e + y_k^N$ where:

$$x_{k+1}^N = \left(A_k - N_k M_k^{3^{-1}} T_k^3 C_k \right) x_k^N + N_k M_k^{3^{-1}} T_k^3 y_k \tag{2.46a}$$

$$y_k^N = T_k C_k x_k^N \tag{2.46b}$$

$$x_0^N = 0 \tag{2.46c}$$

Hence an equivalent cost function can be defined in x_k^e and y_k^e as follows:

$$\min_{x_0^e, \omega_k, z_k} \|x_0\|_{\Pi_0^{-1}}^2 + \sum_{k=0}^{n-1} \|\omega_k\|_{Q_k^{-1}}^2 + \sum_{k=0}^{n} \|y_k^e - T_k C_k x_k^e\|_{R_k^{1^{-1}}}^2 + \sum_{k=0}^{n} \|z_k\|_{R_k^{3^{-1}}}^2 \tag{2.47a}$$

Subject to

$$x_{k+1}^e = \left(A_k - N_k M_k^{3^{-1}} T_k^3 C_k \right) x_k^e + B \omega_k - N_k M_k^{3^{-1}} z_k \tag{2.47b}$$

This final form given in (2.47) is equivalent to the form defined in Lemma 1. Therefore,

Lemma 1 can now be used over (2.47) to find the optimal solution for the cost function

defined in (2.34). These results are summarized in Lemma 2.

Lemma 2

> i.   The optimal $\hat{x}_{n|n}^e$ solution for the cost defined in (2.47) is equal to the Kalman
>
>   filter solution of the following system:

$$x_{k+1}^e = \overbrace{\left(A_k - N_k M_k^{3^{-1}} T_k^3 C_k \right)}^{A^\#} x_k^e + \overbrace{\left[B_k \quad -N_k M_k^{3^{-1}} \right]}^{\omega^\#} \begin{bmatrix} \omega_k \\ z_k \end{bmatrix} \tag{2.48a}$$

$$y_k^e = \underbrace{T_k C_k}_{C_k^\#} x_k^e + v_k^1 \tag{2.48b}$$

$$E\left\{ \begin{bmatrix} x_0^e \\ \omega_k \\ z_k \\ v_k^1 \\ 1 \end{bmatrix} \begin{bmatrix} x_0^e \\ \omega_k \\ z_k \\ v_k^1 \end{bmatrix}^T \right\} = \begin{bmatrix} \Pi_0 & 0 & 0 & 0 \\ 0 & Q_k & 0 & 0 \\ 0 & 0 & R_k^3 & 0 \\ 0 & 0 & 0 & R_k^1 \\ 0 & 0 & 0 & 0 \end{bmatrix} \tag{2.48c}$$

Where

$$R_k^3 = E\left\{ z_k z_k^T \right\} = \overline{T}_k R_k \overline{T}_k^T - \overline{T}_k R_k T_k^T \left(T_k R_k T_k^T \right)^{-1} T_k R_k \overline{T}_k^T \tag{2.48d}$$

$$R_k^1 = E\left\{ v_k^1 v_k^{1^T} \right\} = T_k R_k T_k^T \tag{2.48e}$$

> ii.   The optimal $\hat{x}_{n|n}$ (optimal x_n estimate given all the observation up to and
>
>   including y_n) is equal to:

$$\hat{x}_{n|n} = x_n^N + \hat{x}_n^e \tag{2.49}$$

where x_n^N is the state of the deterministic system defined in (2.46).

iii.   As defined in (2.43b), the optimal u_n is $\hat{u}_{n|n} = M_n^{3^{-1}} \left(y_n^3 - T_n^3 C_n \hat{x}_{n|n} - \hat{z}_{n|n} \right)$. The

optimal $\hat{z}_{n|n}$ is always zero as the cost function is independent of z_n. Therefore:

$$\hat{u}_{n|n} = M_n^{3^{-1}} \left(y_n^3 - T_n^3 C_n \hat{x}_{n|n} \right) = M_n^{3^{-1}} T_n^3 \left(y_n - C_n \hat{x}_{n|n} \right) \tag{2.50}$$

2.3.2 Implementation of the optimal Solution

The Lemma 2 might seem rather complicated. However, in this section it will be shown

that it is nothing more than what can be anticipated with the basic engineering intuition.

To this end it will first be proves that the term $M_k^{3^{-1}} T_k^3$ in Lemma 2 is in fact equivalent to

the left (weighted) pseudo inverse of the observations.

Property 1

When R_k is invertible, $M_k^{3^{-1}} T_k^3$ is equal to the weighted pseudo inverse of M_k. In

mathematical terms:

$$
\begin{aligned}
M_k^{3^{-1}} T_k^3 &= \left(\overline{T}_k M_k \right)^{-1} \left(\overline{T}_k - \overline{T}_k R_k T_k^T \left(T_k R_k T_k^T \right)^{-1} T_k \right) \\
&= \left(M_k^T R_k^{-1} M_k \right)^{-1} M_k^T R_k^{-1} \\
&\triangleq M_k^{\#}
\end{aligned}
\tag{2.51}
$$

Proof:

Let $y = Mx + v$ where v has a Gaussian ($N(0,R)$) distribution and M has full column

rank. It is well known that the MVU estimate of x is $\hat{x}_{opt}^1 = \left(M^T R^{-1} M \right)^{-1} M^T R^{-1} y$.

Linear transformations on y do not change the optimal solution. Hence the following 2

transformation can be applied on y without affecting the solution.

i) $\hat{T} = \begin{bmatrix} T \\ \bar{T} \end{bmatrix}$ is a nonsingular matrix where $Range\{\bar{T}^T\} = Range\{M\}$ and $TM = 0$.

ii) $V = \begin{bmatrix} I & 0 \\ \underbrace{-\bar{T}RT^T \left(TRT^T \right)^{-1}}_{-\tilde{T}} & I \end{bmatrix}$

Thus:

$$Ty = Tv$$
$$\left(\bar{T} - \tilde{T}T \right) y = \bar{T}Mx + \left(\bar{T} - \tilde{T}T \right)v \tag{2.52}$$

$\bar{T}M$ is a full rank matrix by construction and Tv is orthogonal to $\left(\bar{T} - \tilde{T}T \right)v$. Therefore

another optimal solution is $\hat{x}^2_{opt} = \left(\bar{T}M \right)^{-1} \left(\bar{T} - \tilde{T}T \right)y$.

As M is assumed to be a full column rank matrix, optimal solution is unique for this

problem. Hence, $\hat{x}^1_{opt} = \hat{x}^2_{opt}$ for all y. Therefore,

$$\left(\bar{T}M \right)^{-1} \left(\bar{T} - \tilde{T}T \right) = \left(M^T R^{-1} M \right)^{-1} M^T R^{-1} = M^{\#}$$ as stated in the Property 1.

Using this equivalence, the results of the Lemma 2 can be rewritten as follows:

Lemma 3

The optimal x_n solution for the cost function defined in (2.34) is equal to the Kalman

filter solution ($\hat{x}_{n|n}$) of the following system:

$$x_{k+1} = \underbrace{\left(A_k - N_k M_k^{\#} C_k \right)}_{A^{\#}} x_k + \underbrace{B_k \omega_k - N_k M_k^{\#} v_k}_{w_k^{\#}} + N_k M_k^{\#} y_k \tag{2.53a}$$

$$y_k^1 = \underbrace{T_k C_k}_{C^{\#}} x_k + \underbrace{T_k v_k}_{v_k^1} \tag{2.53b}.$$

$$E\left\{\begin{bmatrix} x_0 \\ w_k \\ v_k \end{bmatrix}\begin{bmatrix} x_0^T & w_k^T & v_k^T \end{bmatrix}\right\} = \begin{bmatrix} \Pi_0 & 0 & 0 \\ 0 & Q_k & 0 \\ 0 & 0 & R_k \end{bmatrix}, \forall k \qquad (2.53c)$$

Furthermore, the best u_n estimate ($\hat{u}_{n|n}$) given all observations can be computed as:

$$\hat{u}_{n|n} = M^{\#}\left(y_n - C_n\hat{x}_{n|n}\right) \qquad (2.54)$$

It should be noted that the system defined in (2.53) is obtained by adding (2.48) with the nominal system defined in (2.46). Furthermore, the covariance equivalence

$E\{z_k z_k^T\} = E\{v_k^3 v_k^{3^T}\}$ is used to replace z_k with v_k.

In (2.53) $T_k v_k$ is orthogonal to $N_k M_k^{\#} v_k$. Therefore, there is no cross correlation between observation and system driving noises. Hence, any straightforward Kalman filter implementation can be used compute the optimal $\hat{x}_{n|n}$. Such an implementation is presented in Figure 2.1. In this implementation, the pseudo inverse of the observations is used to drive a deterministic system which provides a nominal solution x_k^N around which errors x_k^e are defined. Then, the orthogonal complement of observations (i.e. $T_k y_k$) are used to drive the Kalman filter to compute these error estimates. The optimum solution is then obtained as the sum of the nominal states and estimated error states. The most important property of this implementation is that it defines how a nominal trajectory should be computed when multiple sensors exist.
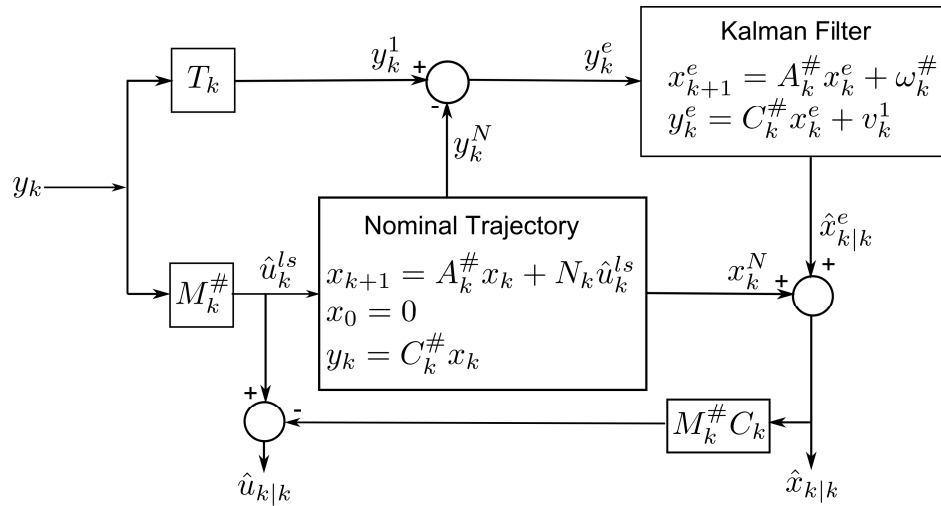
Figure 2-1 : Optimal estimation structure for the cost function defined in (2.34). Kalman filter and nominal trajectory parameters are as defined in (2.48) and (2.53).

In the case when $N_k = 0$ (i.e. when the non-random variables does not affect the propagation of random (stochastic) variables), the form of the optimum solution takes a more simple form as presented in figure 2.2. This form can simply be derived by setting $N_k = 0$ in (2.53).
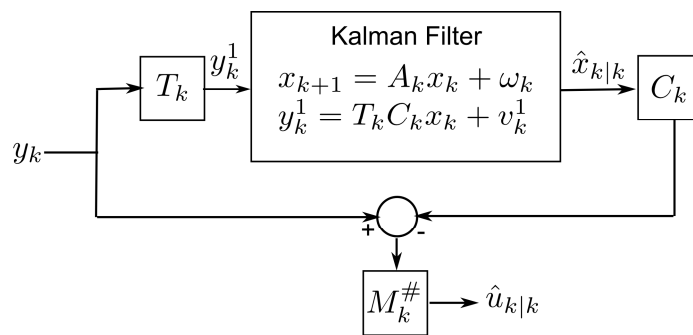
Figure 2-2 : Optimal structure when $N_k = 0$

2.4 Application to Multi-Inertial Sensor Fusion

2.4.1 Solution of Multi Sensor Fusion Problem

In this section, the application of Lemma 3 to the SRIMU problem stated in Section 2.1 is presented.

This problem can be formulated as follows:

Let's assume there exits N sensors (accelerometers and/or gyroscopes) with the following error models and output relations:

$$^{i}x_{k+1} =^{i} A_{k}{}^{i}x_{k} +^{i} B_{k}{}^{i}w_{k} \tag{2.55a}$$

$$^{i}y_{k} =^{i} C_{k}x_{k} +^{i} v_{k} +^{i} Mu_{k} \tag{2.55b}$$

$$E\left\{^{i}x_{0}{}^{i}x_{0}^{T}\right\} =^{i} \Pi_{0}$$
$$E\left\{^{i}v_{k}{}^{i}v_{k}^{T}\right\} =^{i} R_{k} \tag{2.55c}$$
$$E\left\{^{i}w_{k}{}^{i}w_{k}^{T}\right\} =^{i} Q_{k}$$

Where each $\left\{^{i}y_{k}\right\}_{i=1}^{N}$ represents the individual (ith) sensor output, $\left\{^{i}x_{k}\right\}_{i=1}^{N}$ is the corresponding sensor's stability error state (possibly with a dimension greater than 1), $\left\{^{i}v_{k}\right\}_{i=1}^{N}$ is the additive white noise component (i.e. ARV/VRW) and u_{k} is the real kinematic quantity which the sensors are expected to measure (i.e. acceleration/rotation rates on the body frame). $\left\{^{i}M_{k}\right\}_{i=1}^{N}$ is the unit vectors representing the orientation of the sensors in the defined kinematic frame of reference (e.g. body frame). It should be noted that as inertial sensors are multiple input/single output (MISO) systems, each $\left\{^{i}C_{k}\right\}_{i=1}^{N}$

corresponds to a row vector. After combining all the states in a single state vector, (2.55) can be represented in a more compact form as follows:

$$
\begin{aligned}
x_{k+1} &= A_k x_k + B_k w_k \\
y_k &= C_k x_k + M u_k + v_k
\end{aligned}
$$

(2.56)

where $x_k = \begin{bmatrix} {}^1 x_k; & \cdots & ;^N x_k \end{bmatrix}^T$, $y_k = \begin{bmatrix} {}^1 y_k; & \cdots & ;^N y_k \end{bmatrix}^T$, $M = \begin{bmatrix} {}^1 y; & \cdots & ;^N M \end{bmatrix}^T$ and

$E\{v_k v_k^T\} = R_k = diag\left(\begin{bmatrix} {}^1 R_k, \ldots, {}^N R_k \end{bmatrix} \right)$. (2.56) is equal to the (2.1) with $N_k = 0$. Therefore,

Lemma 3 (specifically Figure 2.2) can now be applied to compute the optimal u_k at each

time instant. Thus, $\hat{u}_{k|k} = M^{\#}\left(y_k - C_k \hat{x}_{k|k} \right)$ where $M^{\#} = \left(M^T R_k^{-1} M \right)^{-1} M^T R_k^{-1}$ and $\hat{x}_{k|k}$ is

the optimal solution of the Kalman filter for the following system model:

$$
\begin{aligned}
x_{k+1} &= A_k x_k + B_k w_k \\
T y_k &= T C_k x_k + T v_k
\end{aligned}
$$

(2.57)

where rows of T is the basis for left null space of M (i.e. $TM = 0$ as defined in (2.37)).

A dynamical system representation for the errors on the estimated kinematic variables

$\hat{u}_{k|k}$ is also required for integrated (aided) inertial navigation applications. These error

modes for the $\hat{u}_{k|k}$ can be derived from the individual sensor's error states as follows:

Let $e_k = \hat{u}_{k|k} - u_k$ be the error on the computed (estimated) kinematic variable. Then

$$
\begin{aligned}
e_k &= M^{\#}\left(y_k - C_k \hat{x}_{k|k} \right) - u_k \\
&= M^{\#}\left(C_k \left(x_k - \hat{x}_{k|k} \right) + M u_k + v_k \right) - u_k \\
&= M^{\#} C_k \tilde{x}_{k|k} + M^{\#} v_k
\end{aligned}
$$

(2.58)

Where $\tilde{x}_{k|k}$ represents the error on the output of the Kalman filter for the system (2.57):

$$
\tilde{x}_{k|k} = \left(I - K_k T C_k \right) A_{k-1} \tilde{x}_{k-1|k-1} + \left(I - K_k T C_k \right) B_{k-1} w_{k-1} - K_k T v_k
$$

(2.59)

As a result (2.58) and (2.59) defines the dynamical system representation of the errors on the computed IMU output $\hat{u}_{k|k}$. In this formulation $M^{\#}v_k$ and $\tilde{x}_{k|k}$ represents the effective ARW/VRW component and repeatability/stability errors respectively for the computed kinematic variables that can used to drive navigation equations in an INS. It should be noted that although v_k appears as a part of both the observation noise in (2.58) and system noise in (2.59), there exists no cross-correlation between system and output noises as Tv_k and $M^{\#}v_k$ is orthogonal by construction. Therefore, this final error model can be implemented in any existing integrated navigation application without any complication.

2.4.2 Simulated data results for multi-inertial sensor fusing problem

In this section the results of the method described in the previous section is presented for the simulated system shown in Figure 2.3. This figure represents a skew redundant inertial sensor configuration for a planar navigation application where the IMU consist of 2 gyroscopes on z-axis and 4 accelerometers on the X-Y plane. It is assumed that the sensors have the following error models defined at 1Hz.

Accelerometers (same for all $1 \leq i \leq 4$, defined in m/s^2):

$$^i A^{\text{Acc}} = \begin{bmatrix} 0.99871 & 0 \\ 0 & 1 \end{bmatrix}, {}^i Q^{\text{Acc}} = \begin{bmatrix} 1.2^{-9} & 0 \\ 0 & 1^{-12} \end{bmatrix}$$

$$^i R^{\text{Acc}} = 8.55^{-9}, {}^i \Pi_0^{\text{Acc}} = \begin{bmatrix} 4.9^{-7} & 0 \\ 0 & 1^{-6} \end{bmatrix}, {}^i C^{\text{Acc}} = \begin{bmatrix} 1 & 1 \end{bmatrix} \qquad (2.60a)$$

Gyroscope 1 ($rad/\sec$):

$$^1 A^{\text{Gyro}} = 0.99546, {}^1 Q^{\text{Gyro}} = 5.6^{-9}$$

$$^1 R^{\text{Gyro}} = 4.4^{-10}, {}^1 \Pi_0^{\text{Gyro}} = 6.2^{-7}, {}^1 C^{\text{Gyro}} = 1 \qquad (2.60b)$$

Gyroscope 2 (*rad* / sec):

$$^2 A^{\text{Gyro}} = 0.99773, ^2 Q^{\text{Gyro}} = 4.2^{-10}$$
$$^2 R^{\text{Gyro}} = 3.7^{-7}, ^2 \Pi_0^{\text{Gyro}} = 9.4^{-8}, ^2 C^{\text{Gyro}} = 1$$

(2.60c)

As can be seen from (2.60b) and (2.60c), gyroscope 1 has considerably less additive white noise than gyroscope 2. On the other hand, the stability error characteristic of gyroscope 2 is better than gyroscope 1.
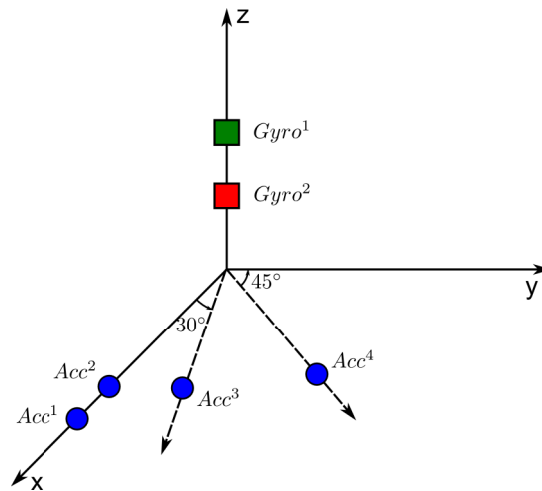
Figure 2-3 : Multi inertial sensor configuration used in the simulation. The configuration matrix corresponding to this orientation is defined in (2.61). The distance between the origin and the sensors are assumed to be negligible.

For this redundant inertial sensor system, the configuration matrix ("M" in (2.56)) relating real kinematic variables (u =[x-Acceleration (a_x), y-Acceleration (a_y), z-Rotation Rate (ω_z)]) with the sensor outputs is as follows:

$$M = \begin{bmatrix} 1 & 0 & 0 \\ 1 & 0 & 0 \\ \cos\left(\dfrac{\pi}{6}\right) & \sin\left(\dfrac{\pi}{6}\right) & 0 \\ \cos\left(\dfrac{\pi}{4}\right) & \sin\left(\dfrac{\pi}{4}\right) & 0 \\ 0 & 0 & 1 \\ 0 & 0 & 1 \end{bmatrix} \tag{2.61}$$

Thus, each individual sensor output can be represented as:

$$y = \begin{bmatrix} Acc^1 \\ Acc^2 \\ Acc^3 \\ Acc^4 \\ Gyro^1 \\ Gyro^2 \end{bmatrix} = \underbrace{\begin{bmatrix} {}^1C^{Acc} & 0 & \cdots & & & \\ 0 & {}^2C^{Acc} & 0 & \cdots & & \\ & 0 & {}^3C^{Acc} & 0 & \cdots & \\ & \cdots & 0 & {}^4C^{Acc} & 0 & \\ & & \cdots & 0 & 1 & 0 \\ & & & \cdots & 0 & 1 \end{bmatrix}}_{C} \underbrace{\begin{bmatrix} {}^1x_k^{Acc} \\ {}^2x_k^{Acc} \\ {}^3x_k^{Acc} \\ {}^4x_k^{Acc} \\ {}^1x_k^{Gyro} \\ {}^2x_k^{Gyro} \end{bmatrix}}_{x} + M\underbrace{\begin{bmatrix} a_x \\ a_y \\ \omega_z \end{bmatrix}}_{u} + \begin{bmatrix} {}^1v_k^{Acc} \\ {}^2v_k^{Acc} \\ {}^3v_k^{Acc} \\ {}^4v_k^{Acc} \\ {}^1v_k^{Gyro} \\ {}^2v_k^{Gyro} \end{bmatrix} \tag{2.62}$$

where "$ {}^ix^{Acc,Gyro}$" denotes the error states of each individual sensor.

Using the error and configuration definitions given in (2.60)-(2.62), 100 minutes of stationary sensor output was generated using Matlab at 1Hz. Then, the generated outputs were processed as described in Section 2.4.1 to obtain the best kinematic variable estimates $\hat{u}_{n|n} = \left[\hat{a}_x; \hat{a}_y; \hat{\omega}_z\right]^T$.

The comparison of individual raw gyro outputs ($Gyro^1$ and $Gyro^2$) is shown in figure 2.4. In figure 2.5, the comparison of 2 different z-rotation rate estimates ($\hat{\omega}_z$) which are derived from these raw gyro outputs are presented. The first "$\hat{\omega}_z$" estimate (blue curve in Figure 2.5) is the optimal solution which is computed using the structure shown in the figure 2.2 ($\hat{u}_{n|n}^{opt} = M^{\#}\left(y_n - C\hat{x}_{n|n}\right)$). The second estimate (red curve in Figure 2.5) is the

simple weighted least square solution ($\hat{u}_n^{wls} = M^{\#}y$). From these figures the following observations can be made:

1. As seen from Figure 2.4 (and error definitions given in (2.60)), the 2 gyroscopes have complimentary characteristics: $Gyro^2$ has relatively big additive white noise (ARW) but small stability errors, whereas $Gyro^1$ has low "ARW" but a bigger stability error.

2. As the WLS solution ($\hat{\omega}_z^{wls}$) only considers the ARW values to form an average, this solution is mainly characterized by $Gyro^1$. Therefore, as seen in Figure 2.5, it also suffers from the large stability errors.

3. On the other hand, the optimal solution ($\hat{\omega}_z^{opt}$) in Figure 2.5 combines (fuse) both gyroscope outputs in such a way that the optimal result has both small additive white noise (as inherited from $Gyro^1$) and small stability errors (as inherited from $Gyro^2$). As these figures suggest, the optimal solution has the property of blending the best characteristics of individual sensors which is a clear advantage over WLS type solutions when the underlying sensors have different (but complimentary) characteristics.
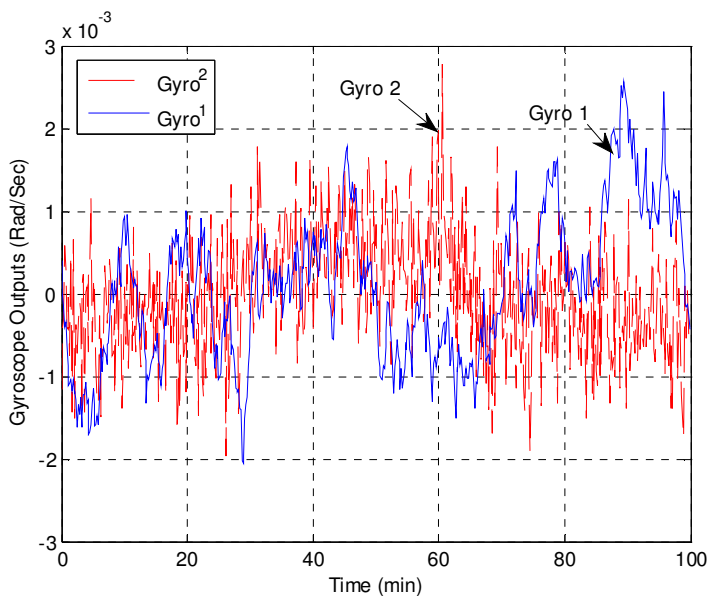
Figure 2-4 : Comparison of simulated raw gyroscopes outputs on z axis.
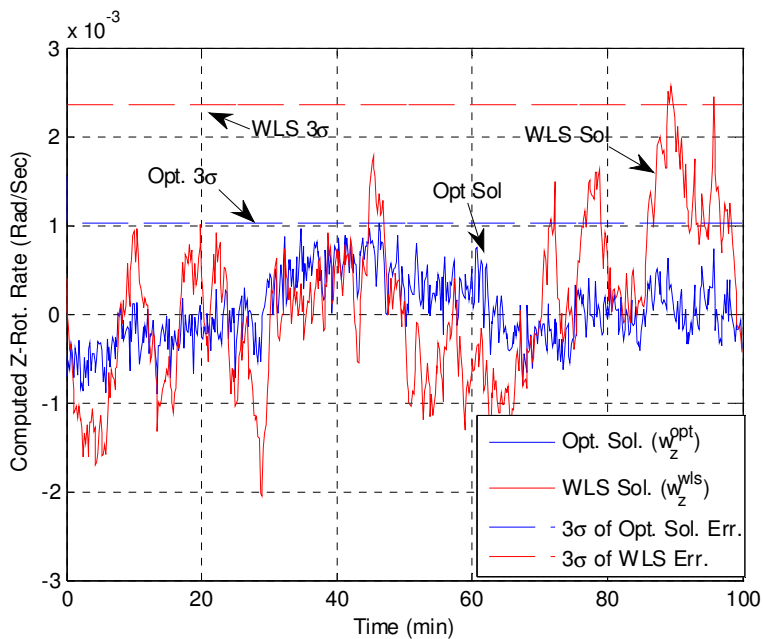
Figure 2-5 : Comparison of optimal ($\hat{\omega}_z^{opt}$) and WLS ($\hat{\omega}_z^{wls}$) solutions for estimated z-axis rotation rate ($\hat{\omega}_z$). The dashed lines correspond to the standard deviation (3σ) values of the corresponding solutions.

In figure 2.6, a similar kind of comparison for the computed (estimated) y-axis accelerations ($\hat{a}_y$) are provided. In this figure, 3 different results are compared. These are: i)the optimal solution ($\hat{a}_y^{opt}$), ii)WLS solution ($\hat{a}_y^{wls}$) and iii)Partial WLS solution computed only with Acc^3 and Acc^4 ($\hat{a}_y^{ls} = -3.8637\left(\sin\left(\pi/4\right)Acc^3 - \cos\left(\pi/6\right)Acc^4\right)$).

From this figure, the following observations can be made:

1. Although only Acc^3 and Acc^4 are directly affected by the y-axis acceleration, the combined solution of all 4 accelerometers ($\hat{a}_y^{wls}$) is significantly less erroneous than $\hat{a}_y^{ls}$ as expected.

2. Optimal Solution and WLS solutions ($\hat{a}_y^{opt}, \hat{a}_y^{wls}$) are exactly the same (they are represented by a single (red) curve in Figure 2.6).

This second observation is important because it suggests that under certain conditions the Kalman filter in the optimum solution has no use at all, and hence, can be completely eliminated.

The theoretical reason and useful consequences of this final observation is further described in the next section.
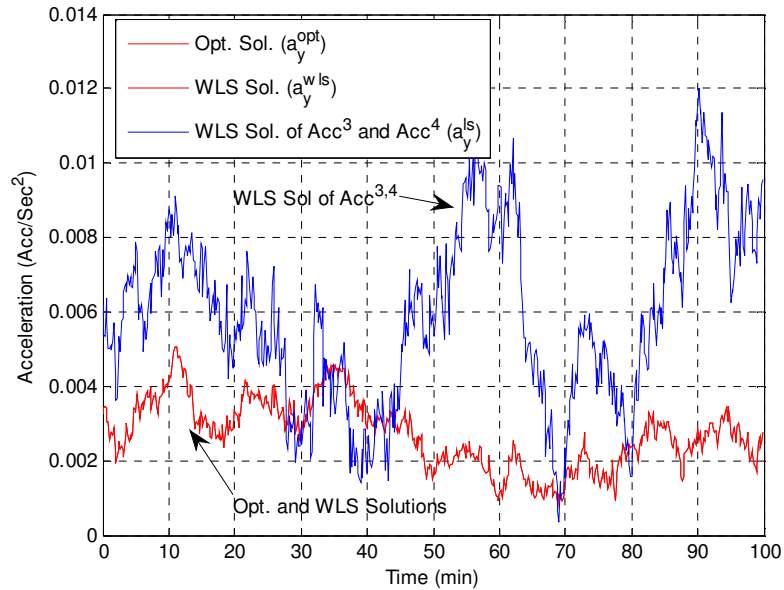
Figure 2-6 : Comparison of optimal ($\hat{a}_y^{opt}$), WLS ($\hat{a}_y^{wls}$) and partial WLS ($\hat{a}_y^{ls}$)

solutions for the computed y-axis acceleration. The Optimal and WLS solutions

exactly overlap, and hence seem as a single curve.

2.4.3 Optimal sensor fusion results for the case of identical inertial units

When an SRIMU contains only inertial sensors which have identical stochastic error

models (or at least contains sets of sensors that have identical models) then the optimal

solution for the inertial sensor fusing problem reduces to more simple forms.

Furthermore, for such systems the number of states in the equivalent error models can be

greatly reduced. In this section these properties of optimal solutions are analyzed.

2.4.3.1 Case I: Identical Inertial Sensors

In this section, it will be proved that when i) all the inertial sensors in an SRIMU have

exactly the same error model parameters (same $^{i}A, {}^{i}B, {}^{i}C, {}^{i}\Pi_0, {}^{i}R, {}^{i}Q$ in (2.55)) and ii)

the sensor error characteristics are independent (no cross correlation between sensor errors), then regardless of the sensor orientations (M), the optimum solution is $\hat{u}_{k|k}^{opt} = M^{\#} y_k$. In other words, for such systems $M^{\#} C_k \hat{x}_{k|k} = 0$ for $\forall k$ in (2.54).

To prove this, it will be shown that required linear combination of error states $M^{\#} C_k x_k$ is always orthogonal to the redundancy observations $T y_k$ (i.e. $E\{M^{\#} C_k x_k y_l^T T^T\} = 0, \forall k,l$) when the sensors are identical as stated above.

First, it should be noted that as the sensors are independent and identical $R_k = r_k I$ is a diagonal matrix where r_k is the power (scalar) of the additive white noise of the individual sensors. Thus:

$$
\begin{aligned}
M^{\#} T^T &= \left(M^T R^{-1} M\right)^{-1} M^T R^{-1} T^T \\
&= \left(M^T M\right)^{-1} M^T T^T \\
&= 0
\end{aligned}
\tag{2.63}
$$

The final step is the direct consequence of the fact that rows of T is orthogonal to the columns of M by construction.

The cross covariance between the redundancy observations and combination of error states is equal to:

$$
E\{M^{\#} C_k x_k y_l^T T^T\} = M^{\#} C_k \underbrace{E\{x_k x_l^T\}}_{\Pi_{kl}} C_k^T T^T
\tag{2.64}
$$

Assuming there exist "n" sensors, $\Pi_{kl} = diag\left({}^1\Pi_{kl} \quad \ldots \quad {}^n\Pi_{kl}\right)$ is itself a block diagonal matrix with identical block diagonal elements (as each unit is assumed to be identical and independent). Therefore:

$$
C_k \Pi_{kl} C_l^T = \gamma_{kl} I
\tag{2.65}
$$

where γ_{kl} is a scalar. Thus, combining (2.65) with (2.63):

$$M^{\#}C_k\Pi_{kl}C_k^TT^T = \gamma_{kl}M^{\#}T^T = 0 \qquad (2.66)$$

This shows that observations are always orthogonal to the required linear combination of states. Therefore, $M^{\#}C_k\hat{x}_{k|k} = 0, \forall k$ as claimed.

Under these conditions, the error model of the computed optimal outputs ($\hat{u}_{k|k}^{opt} = \hat{u}_{k|k}^{wls}$) also has a relatively simple form as shown below:

Let $e_k = u_k - \hat{u}_{k|k}^{opt}$, then:

$$\begin{aligned} e_k &= M^{\#}y_k - u_k \\ &= M^{\#}\left(Mu_k + C_kx_k + v_k\right) - u_k \\ &= M^{\#}C_kx_k + M^{\#}v_k \end{aligned} \qquad (2.67)$$

The correlation structure of e_k can be represented as:

$$\begin{aligned} E\left\{e_ke_l^T\right\} = P_{kl} &= M^{\#}C_l\Pi_{kl}C_l^TM^{\#^T} + M^{\#}R_kM^{\#^T}\delta[k-l] \\ &= \gamma_{kl}\left(M^TM\right)^{-1} + r_k\left(M^TM\right)^{-1}\delta[k-l] \end{aligned} \qquad (2.68)$$

For the Kalman filtering point of view, any dynamical system representation (DSR) which has this correlation structure is equivalent (because Kalman filters use only 2$^{\text{nd}}$ order stochastic properties). Therefore, instead of the real sensor error model (for which (#states)=(#sensor)*(#states per each sensor)) any other DSR which has the same correlation as in (2.68) can be implemented in the navigation Kalman filter. (It should be noted that the equivalent error models is only required by the navigation Kalman filters, not by the optimal sensor fusion filters).

In figure 2.7, an alternative structure which can be used to generate the same correlation as (2.68) but with possibly less number of states is presented. This structure assumes that

regardless of how many inertial sensors are used in the real system, each kinematic axis

contains only one (virtual) independent sensor whose output error correlation is equal to "

$\gamma_{kl} + r_k \delta[k-l]$". Therefore, the error model assigned for each axis is identical to the

single individual sensor error model.

As an example, using the alternative structure in figure 2.7, an equivalent representation

of the errors on the computed acceleration values ($e_k = [a_x; a_y] - [\hat{a}_x^{opt}; \hat{a}_y^{opt}]^T$) for the 2D

SRIMU shown in figure 2.3 (where all accelerometers have identical error models) can

be derived as follows:

Let $\bar{M}$ be the first 4 rows of the M matrix defined in (2.61). Then:

$$\begin{bmatrix} {}^1 x_{k+1}^{eq} \\ {}^2 x_{k+1}^{eq} \end{bmatrix} = \begin{bmatrix} A_k^{\text{Acc}} & 0 \\ 0 & A_k^{\text{Acc}} \end{bmatrix} \begin{bmatrix} {}^1 x_k^{eq} \\ {}^2 x_k^{eq} \end{bmatrix} + \begin{bmatrix} {}^1 \omega_k \\ {}^2 \omega_k \end{bmatrix} \tag{2.69a}$$

$$e_k = \begin{bmatrix} e_k^{Acc_x} \\ e_k^{Acc_y} \end{bmatrix} = \underbrace{\sqrt{\left(\bar{M}^T \bar{M}\right)^{-1}} \begin{bmatrix} C_k^{\text{Acc}} & 0 \\ 0 & C_k^{\text{Acc}} \end{bmatrix}}_{C_k^{eq}} \begin{bmatrix} {}^1 x_k^{eq} \\ {}^2 x_k^{eq} \end{bmatrix} + \underbrace{\sqrt{\left(\bar{M}^T \bar{M}\right)^{-1}} \begin{bmatrix} {}^1 v_k \\ {}^2 v_k \end{bmatrix}}_{v_k^{eq}} \tag{2.69b}$$

where $E\left\{ \begin{bmatrix} {}^1 x_0^{eq} \\ {}^2 x_0^{eq} \end{bmatrix} \begin{bmatrix} {}^1 x_0^{eq} \\ {}^2 x_0^{eq} \end{bmatrix}^T \right\} = diag\left(\Pi_0^{\text{Acc}}, \Pi_0^{\text{Acc}}\right)$, $E\left\{ \begin{bmatrix} {}^1 \omega_k \\ {}^2 \omega_k \end{bmatrix} \begin{bmatrix} {}^1 \omega_k \\ {}^2 \omega_k \end{bmatrix}^T \right\} = diag\left(Q^{\text{Acc}}, Q^{\text{Acc}}\right)$,

$E\left\{ \begin{bmatrix} {}^1 v_k \\ {}^2 v_k \end{bmatrix} \begin{bmatrix} {}^1 v_k \\ {}^2 v_k \end{bmatrix}^T \right\} = diag\left(R^{\text{Acc}}, R^{\text{Acc}}\right)$. Furthermore, $A_k^{\text{Acc}}, C_k^{\text{Acc}}, \Pi_0^{\text{Acc}}, Q^{\text{Acc}}, R^{\text{Acc}}$ are

exactly the same as defined in (2.60a).

It should be noted that in this equivalent representation only 4 states are used to represent

the errors on the computed acceleration values whereas in the real system there exists 8

states (2 for each 4 accelerometers). Furthermore, even if the system defined in figure 2.3

had 100 identical accelerometers on the x-y plane, still only 4 states would be sufficient

for the equivalent representation. As this example suggests, these equivalent

representations provide a great convenience for the navigation Kalman filter designs

when there exists abundant number of sensors in an SRIMU.
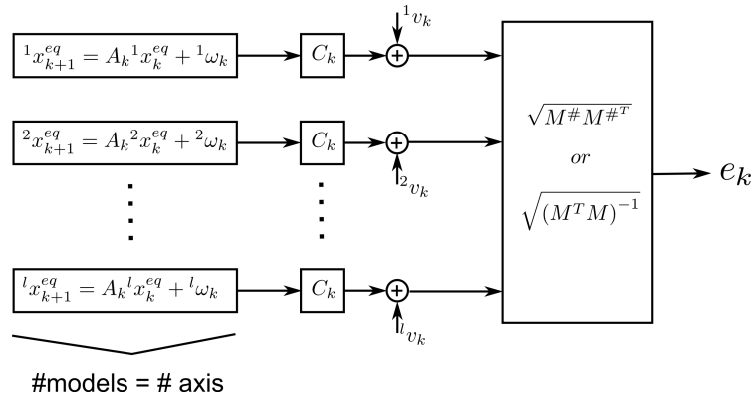
Figure 2-7 : Equivalent error model for the errors on the (optimal) computed

kinematic variables when all the sensors are identical. The number of models used is

equal to the number of kinematic axis (i.e. size of u_k).

2.4.3.2 Case II: Sets of identical sensors

In this section the ideas presented in the previous section are extended to the case in

which there exist L sets of inertial sensors and each set consist of $\left\{{}^{i}N\right\}_{i=1}^{L}$ number or of

identical sensors. For such a case the entire observation equations can be represented as

follows:

$$
\begin{aligned}
{}^{1}y_k &= {}^{1}Mu_k + {}^{1}C_k \, {}^{1}x_k + {}^{1}v_k \\
&\;\;\vdots \\
{}^{L}y_k &= {}^{L}Mu_k + {}^{L}C_k \, {}^{L}x_k + {}^{L}v_k
\end{aligned}
\tag{2.70}
$$

It should be noted that in the previous section left-superscripts were used to represent the individual sensors. However, in this section they are used to represent all the sensors in the individual sets. Furthermore, to avoid unnecessary complexity in the notation it is assumed that all $\left\{ {^i M} \right\}_{i=1}^{L}$ matrices are full column rank.

Using the same linear transformations as described in (2.37) (but with specifically selecting $^i\overline{T} = {^i M}^T$), the observation equations (2.70) can be rewritten as:

$$^1 M^{\#\,1} y_k = u_k + {^1 M}^{\#1} C_k^{\,1} x_k + {^1 M}^{\#1} v_k$$
$$\vdots \tag{2.71a}$$
$$^L M^{\#\,L} y_k = u_k + {^L M}^{\#L} C_k^{\,L} x_k + {^L M}^{\#L} v_k$$

$$^1 T y_k = {^1 T} C_k^{\,1} x_k + {^1 T} v_k$$
$$\vdots \tag{2.71b}$$
$$^L T y_k = {^L T}^{\,L} C_k^{\,L} x_k + {^L T}^{\,L} v_k$$

where

$$^i M^{\#} = \left({^i M}^T \, {^i R_k^{-1}} \, {^i M} \right)^{-1} {^i M}^T \, {^i R_k^{-1}} = \left({^i M}^T \, {^i M} \right)^{-1} {^i M}^T \tag{2.72}$$

Again using the similar linear transformations, the first set of equation in (2.71a) can be decomposed into 2 sub-sets one of which does not contain non-random parameter u_k as follows:

Let $\hat{S} = \begin{bmatrix} S \\ \overline{S} \end{bmatrix}$ be a non singular matrix where the row space of S is the orthogonal complement of the row space of $\overline{S}$ and $S = \underbrace{\begin{bmatrix} I & \cdots & I \end{bmatrix}}_{\#L}$ contains only L identity matrices.

Thus, (2.71a) can be rewritten as:

$$\frac{{}^1M^{\#1}y_k + \ldots + {}^L M^{\#L}y_k}{L} = u_k + \frac{\left({}^1M^{\#1}C_k{}^1x_k + \ldots + {}^LM^{\#L}C_k{}^Lx_k\right)}{L}$$
$$+ \frac{\left({}^1M^{\#1}v_k + \ldots + {}^LM^{\#L}v_k\right)}{L} \tag{2.73a}$$

$$\overline{S}\begin{bmatrix} {}^1M^{\#1}y_k \\ \vdots \\ {}^LM^{\#L}y_k \end{bmatrix} = \overline{S}\begin{bmatrix} {}^1M^{\#1}C_k{}^1x_k \\ \vdots \\ {}^LM^{\#L}C_k{}^Lx_k \end{bmatrix} + \overline{S}\begin{bmatrix} {}^1M^{\#1}v_k \\ \vdots \\ {}^LM^{\#L}v_k \end{bmatrix} \tag{2.73b}$$

As (2.71b) and (2.73b) does not contain "u_k" and (2.73a) does not contain any further

redundancy, the Kalman filter to estimate the best $\left| {}^1\hat{x}_{k|k} \quad \ldots \quad {}^1\hat{x}_{L|L} \right|$ requires only (2.71b)

and (2.73b) as the sensor redundancy observations.

Furthermore, as each set of sensors is assumed to be independent, the optimal solution

can be algebraically expressed as the combination of 2 consecutive WLS steps as

follows:

$$\hat{u}_{k|k} = M^{\#}\begin{bmatrix} {}^1y_k - {}^1C_k{}^1\hat{x}_{k|k} \\ \vdots \\ {}^Ly_k - {}^LC_k{}^L\hat{x}_{k|k} \end{bmatrix} = M_B^{\#}\begin{bmatrix} {}^1M^{\#1}y_k - {}^1M^{\#1}C_k{}^1\hat{x}_{k|k} \\ \vdots \\ {}^LM^{\#L}y_k - {}^LM^{\#L}C_k{}^L\hat{x}_{k|k} \end{bmatrix} \tag{2.74}$$

where:

$$M = \begin{bmatrix} {}^1M \\ \vdots \\ {}^LM \end{bmatrix}, R_k = \begin{bmatrix} {}^1R_k & 0 & \vdots \\ 0 & \ddots & 0 \\ \ldots & 0 & {}^LR_k \end{bmatrix}, M^{\#} = \left(M^T R_k^{-1} M\right)^{-1} M^T R_k^{-1} \tag{2.75}$$

$$\overline{R}_k^{-1} = \begin{bmatrix} \left({}^1M\right)^T\left({}^1R_k^{-1}\right)\left({}^1M\right) & & 0 \\ & \ddots & \\ 0 & & \left({}^LM\right)^T\left({}^LR_k^{-1}\right)\left({}^LM\right) \end{bmatrix} \tag{2.76a}$$

$$M_B^{\#} = \left(\begin{bmatrix} I & \cdots & I \end{bmatrix} \bar{R}_k^{-1} \begin{bmatrix} I \\ \vdots \\ I \end{bmatrix} \right)^{-1} \begin{bmatrix} I & \cdots & I \end{bmatrix} \bar{R}_k^{-1} \qquad (2.76b)$$

$$\underbrace{\phantom{\begin{bmatrix} I & \cdots & I \end{bmatrix}}}_{\#L}$$

and $^i\hat{x}_{k|k}$ is the solution of the Kalman filter with the observation models presented in

(2.71b) and (2.73b) and with the following state transition model:

$$\begin{bmatrix} ^1 x_{k+1} \\ \vdots \\ ^L x_{k+1} \end{bmatrix} = \begin{bmatrix} ^1 A_k & & 0 \\ & \ddots & \\ 0 & & ^2 A_k \end{bmatrix} \begin{bmatrix} ^1 x_k \\ \vdots \\ ^L x_k \end{bmatrix} + \begin{bmatrix} ^1 \omega_k \\ \vdots \\ ^L \omega_k \end{bmatrix} \qquad (2.77)$$

On the other hand, as seen in (2.74), the optimal $\hat{u}_{k|k}$ estimate depends only on the "

$^i M^{\#i} C_k{}^i x_k$ " term. However, as proved in the previous section all the observations defined

in (2.71b) is orthogonal to this linear combination of states as all sensors in a single set is

identical. Therefore, these observations can be completely ignored and the Kalman filter

for the system (2.77) can be run only with the observations defined in (2.73b).

Furthermore, as explained in the previous section, when the sensors are identical, each

$^i M^{\#i} C_k{}^i x_k$ term can be represented with another equivalent model which usually has less

number of states than the actual error model for the corresponding set. Therefore, instead

of (2.77), the Kalman filter can be defined using these reduced order alternative models

for each set. As $\hat{u}_{k|k}$ only requires the best estimate for $^i M^{\#i} C_k{}^i x_k$ (rather than $^i x_k$), the

use of such reduced order error models in the Kalman filter does not affect the optimal

solution at all.

As a result, the above discussion shows that when there are L sets of identical inertial

sensors, the optimal solution of inertial sensor fusion problem can be solved with the

following steps:

i.   Consider each set of identical sensors as a single (multidimensional) sensor whose output is equal to $^{i}\overline{y}_{k} = \left(^{i}M^{\#}\right)\left(^{i}y_{k}\right)$.

ii. For each set, derive the reduced order alternative error models for the $\left\{^{i}\overline{y}_{k}\right\}_{i=1}^{L}$ as described in Section 2.4.3.1.

iii. The optimal solution can then be obtained by applying the optimal sensor fusion algorithm described in Section 2.4.1 over these virtual (multidimensional) sensor outputs ($\left\{^{i}\overline{y}_{k}\right\}_{i=1}^{L}$) with the reduced order error models derived in step ii. In this case the fusion algorithm uses (2.73b) as the only source of redundancy observations.

In the next section, the application of this method for the SRIMU systems is described (clarified) using simulated data examples.

2.4.3.3 Simulated Data results for SRIMU systems with Identical Sensors

In this section, the results of the optimal inertial sensor fusion algorithm for the multi sensor configuration shown in Figure 2.8 are presented. As seen from this figure, the SRIMU under consideration contains 2 sets of accelerometers placed in the x-y plane and 1 set of gyroscope on the z-axis (this is an SRIMU configuration for a 2D planar navigation application). Each accelerometer sets contains 5 identical accelerometers, and the gyroscope set contains 2 identical gyroscopes. The error model parameters for the set 1 accelerometers ($Acc^{1,2,3,4,5}$) and the gyroscope set ($Gyro^{1,2}$) are as defined in (2.60a) and (2.60b) respectively. For the accelerometers in set 2 ($Acc^{6,7,8,9,10}$), the following error model parameters (defined for 1Hz) were used:

Accelerometers Set 2 ($6 \leq i \leq 10$):

$$^{i} A^{\text{Acc}} = 1, ^{i} Q^{\text{Acc}} = 1^{-12}, ^{i} R^{\text{Acc}} = 8.55^{-9}, ^{i} \Pi_{0}^{\text{Acc}} = 1.3^{-5}, ^{i} C^{\text{Acc}} = 1 \qquad (2.78)$$

By comparing (2.60a) and (2.78) it can be seen that the accelerometers in Set 2 have better stability characteristics than Set 1. However the initial covariance of stability errors for Set 2 is much worse. The two sets of accelerometers have the same additive white noise powers.
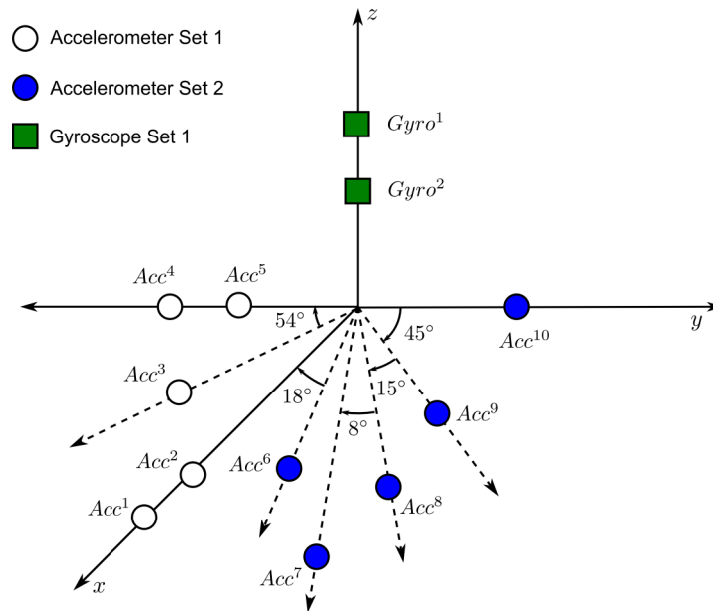
Figure 2-8 : Sensor configurations for the 3D SRIMU containing 2 sets of accelerometers on the x-y plane and 1 set of gyroscope on the z-axis. The distance between the sensors and the origin is assumed to be negligible.

The configuration matrices for each set of sensors are as follows:

$$^{A1}M = \begin{bmatrix} 1 & 0 \\ 1 & 0 \\ \cos(-pi/5) & \sin(-pi/5) \\ \cos(-pi/2) & \sin(-pi/2) \\ \cos(-pi/2) & \sin(-pi/2) \end{bmatrix}$$ (2.79a)

$$^{A2}M = \begin{bmatrix} \cos(pi/10) & \sin(pi/10) \\ \cos(pi/8) & \sin(pi/8) \\ \cos(pi/6) & \sin(pi/6) \\ \cos(pi/4) & \sin(pi/4) \\ \cos(pi/2) & \sin(pi/2) \end{bmatrix}$$ (2.79b)

$$^{G1}M = \begin{bmatrix} 1 \\ 1 \end{bmatrix}$$ (2.79c)

As described in the previous section, instead of using this real system, the optimum solution can be derived using "virtual" sensor equivalents for each set of identical sensors. For each time instant the output of each (multi-dimensional) virtual sensor is computed as follows:

$$Acc_k^{EQ1} = \begin{bmatrix} {}^1a_k^x \\ {}^1a_k^y \end{bmatrix} = \left(\left({}^{A1}M \right)^T \left({}^{A1}M \right) \right)^{-1} \left({}^{A1}M \right)^T \begin{bmatrix} Acc_k^1 \\ Acc_k^2 \\ Acc_k^3 \\ Acc_k^4 \\ Acc_k^5 \end{bmatrix}$$ (2.80a)

$$Acc_k^{EQ2} = \begin{bmatrix} {}^2a_k^x \\ {}^2a_k^y \end{bmatrix} = \left(\left({}^{A2}M \right)^T \left({}^{A2}M \right) \right)^{-1} \left({}^{A2}M \right)^T \begin{bmatrix} Acc_k^6 \\ Acc_k^7 \\ Acc_k^8 \\ Acc_k^9 \\ Acc_k^{10} \end{bmatrix}$$ (2.80b)

$$Gyro_k^{EQ} = \omega_k^z = \frac{Gyro_k^1 + Gyro_k^2}{2}$$ (2.80c)

The new configuration corresponding to these virtual sensors is presented in Figure 2.9.
As seen from this figure, in the new configuration it is assumed that each axis contains
only one sensor for each type. As explained in Section 2.4.3.1, the overall observation
and error model for this virtual configuration can be represented as follows:

$$
\underbrace{\begin{bmatrix} Acc_k^{EQ1} \\ Acc_k^{EQ2} \\ Gyro_k^{EQ} \end{bmatrix}}_{y^{eq}} = \begin{bmatrix} {}^1a_k^x \\ {}^1a_k^y \\ {}^2a_k^x \\ {}^2a_k^y \\ {}^1g_k^z \end{bmatrix} = \underbrace{\begin{bmatrix} \mathbf{I}_{2\times2} & 0_{2\times1} \\ \mathbf{I}_{2\times2} & 0_{2\times1} \\ 0_{1\times2} & 1 \end{bmatrix}}_{M^{eq}} \underbrace{\begin{bmatrix} a_k^x \\ a_k^y \\ \omega_k^z \end{bmatrix}}_{u_k} + \underbrace{\begin{bmatrix} C_{2\times4}^{A1} & 0_{2\times2} & 0_{2\times1} \\ 0_{2\times4} & C_{2\times2}^{A2} & 0_{2\times1} \\ 0_{1\times4} & 0_{1\times2} & C_{1\times1}^{G1} \end{bmatrix}}_{C^{eq}} \underbrace{\begin{bmatrix} x_k^{eq1} \\ x_k^{eq2} \\ x_k^{eq3} \\ x_k^{eq4} \\ x_k^{eq5} \end{bmatrix}}_{x_k^{eq}} + \underbrace{\begin{bmatrix} {}^1v_k^{eq} \\ {}^2v_k^{eq} \\ {}^3v_k^{eq} \end{bmatrix}}_{v_k^{eq}} \tag{2.81a}
$$

$$
\begin{bmatrix} x_{k+1}^{eq1} \\ x_{k+1}^{eq2} \\ x_{k+1}^{eq3} \\ x_{k+1}^{eq4} \\ x_{k+1}^{eq5} \end{bmatrix} = diag \begin{pmatrix} {}^1A_{2\times2}^{Acc} \\ {}^1A_{2\times2}^{Acc} \\ {}^6A_{2\times1}^{Acc} \\ {}^6A_{2\times1}^{Acc} \\ {}^1A_{1\times1}^{Gyro} \end{pmatrix} \begin{bmatrix} x_k^{eq1} \\ x_k^{eq2} \\ x_k^{eq3} \\ x_k^{eq4} \\ x_k^{eq5} \end{bmatrix} + \omega_k^{eq} \tag{2.81b}
$$

where

$$
C_{2\times4}^{A1} = \sqrt{\left(\left({}^{A1}M \right)^T \left({}^{A1}M \right) \right)^{-1}} \begin{bmatrix} 1 & 1 & 0 & 0 \\ 0 & 0 & 1 & 1 \end{bmatrix} \tag{2.82a}
$$

$$
C_{2\times2}^{A1} = \sqrt{\left(\left({}^{A2}M \right)^T \left({}^{A2}M \right) \right)^{-1}} \begin{bmatrix} 1 & 0 \\ 0 & 1 \end{bmatrix} \tag{2.82b}
$$

$$
C_{1\times1}^{G1} = \frac{1}{\sqrt{2}} \tag{2.82c}
$$

$$
E\left\{ v_k^{eq} v_k^{eq^T} \right\} = diag \begin{pmatrix} \left({}^1R^{Acc} \right) \left(\left({}^{A1}M \right)^T \left({}^{A1}M \right) \right)^{-1} \\ \left({}^6R^{Acc} \right) \left(\left({}^{A2}M \right)^T \left({}^{A2}M \right) \right)^{-1} \\ \dfrac{{}^1R^{Gyro}}{2} \end{pmatrix} \tag{2.82d}
$$

$$E\left\{\omega_k^{eq}\omega_k^{eq^T}\right\} = diag\left({}^1Q^{Acc},{}^1Q^{Acc},{}^6Q^{Acc},{}^6Q^{Acc},{}^1Q^{Acc},{}^1Q^{Gyro}\right) \tag{2.82e}$$

$$E\left\{x_0^{eq}x_0^{eq^T}\right\} = diag\left({}^1\Pi_0^{Acc},{}^1\Pi_0^{Acc},{}^6\Pi_0^{Acc},{}^6\Pi_0^{Acc},{}^1\Pi_0^{Acc},\Pi_0^{Gyro}\right) \tag{2.82f}$$

As can be seen from (2.81b), in this equivalent representation only 7 states are used to define the errors whereas the real system contains 17 states.
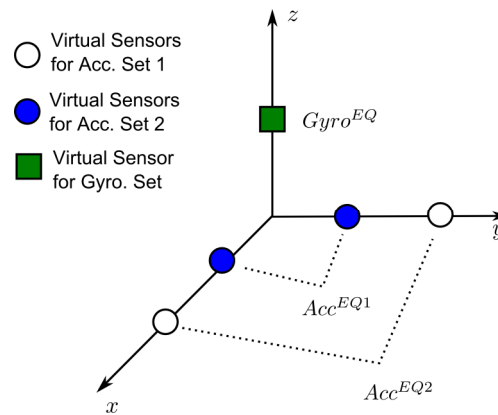
Figure 2-9 : Configuration of virtual sensors used to compute the optimal sensor fusion solution. The outputs of these virtual sensors are as defined in (2.80) and the corresponding error model for these outputs is defined in (2.81).

In figure 2.10 and 2.11, the comparison of 5 different x and y acceleration estimation results are presented. The compared results are as follows:

i.   The optimal acceleration estimate ($\hat{u}^{opt}$): Optimally fused outputs were computed using the real system and observation model. (This result was computed using a 17 states Kalman filter which processes 9 redundancy observations at each update interval.)

ii.   The optimal acceleration estimate ($\hat{u}^{red}$): The optimal outputs were computed using the reduced order system and observation models presented in (2.80) and

(2.81). (In this reduced order case, the number of states of the Kalman filter was only 7 and the Kalman filter processed only 2 redundancy observations).

iii.   The WLS acceleration estimate ($\hat{u}^{wls}$): The combined outputs were computed as the weighted (with VRW coefficients) least square solution of all sensors.

iv.   The optimal acceleration estimate for only set-1 accelerometers ($\hat{u}^{A1}$): Only set-1 accelerometers were optimally fused to form the combined output (the set-2 accelerometers were completely ignored in this solution.). As all accelerometers are identical in set 1, this result was computed using the WLS algorithm.

v.   The optimal acceleration estimate for only set-2 accelerometers ($\hat{u}^{A2}$): Similar to "$\hat{u}_k^{A1}$" solution, only set-2 accelerometers were optimally fused with WLS algorithm to form the combined output. (In this case, set-1 accelerometers were ignored.)

The key observations regarding to the figures 2.10 and 2.11 are summarized below:

1.   Both of the optimal results ($\hat{u}^{opt}$, $\hat{u}^{red}$) and the error standard deviation of these optimal results are exactly identical as anticipated.

2.   As the set 2 accelerometers have large initial bias errors, the $\hat{u}^{A2}$ result also suffer from these initial biases. However, (except these initial bias errors) $\hat{u}^{A2}$ results are more stable than $\hat{u}^{A1}$ results.

3. $\hat{u}^{wls}$ is equivalent to simple weighted combination of $\hat{u}^{A1}$ and $\hat{u}^{A2}$ (This fact can be observed from (2.74) by setting $\hat{x}_{k|k} = 0$). Therefore, $\hat{u}^{wls}$ is also affected by both the initial bias errors of set 2 and large stability errors of set 1 accelerometers.

4. Due to the Kalman filter in the optimal sensor fusing algorithm, the optimal result (both $\hat{u}^{opt}$ and $\hat{u}^{red}$) blends the best characteristics of both sets of accelerometers: it has the initial bias characteristics of set 1 and the stability characteristics of set 2.
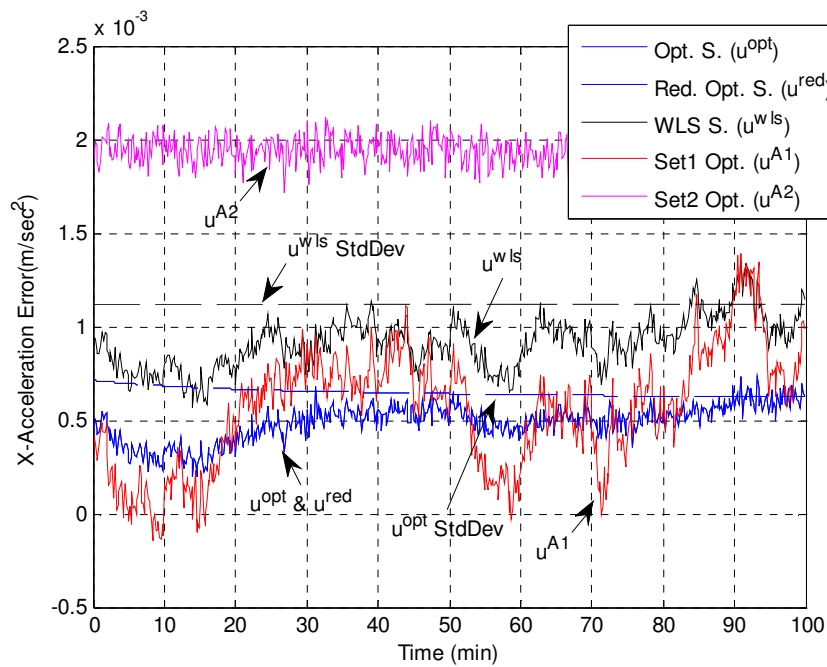
Figure 2-10 : Comparison of several x-axis acceleration estimation results. Solid lines represent the combined outputs whereas dashed lines represent the error standard deviations of the corresponding solutions.
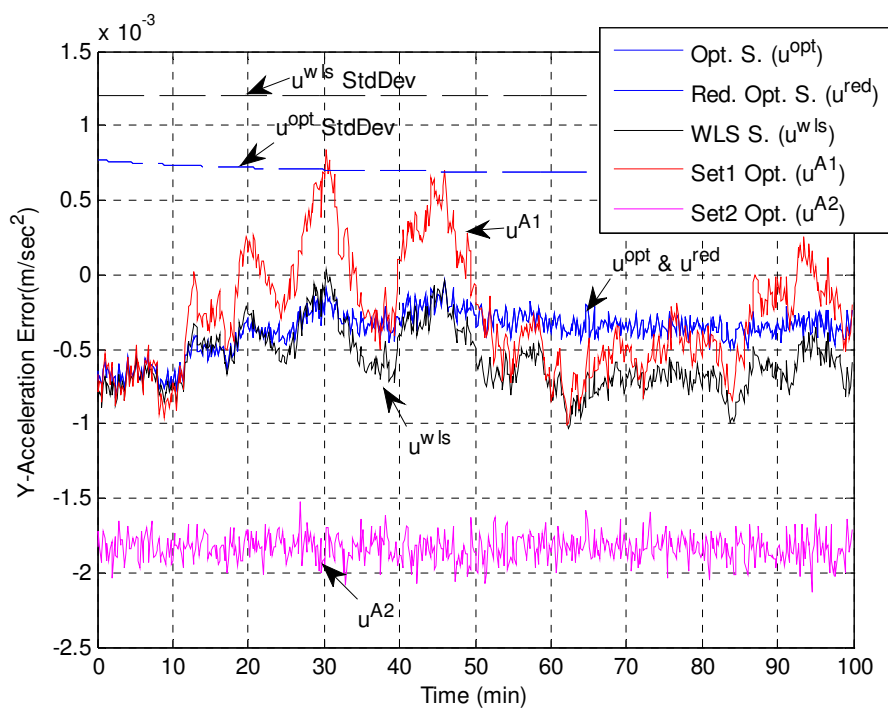
Figure 2-11 : Comparison of several y-axis acceleration estimation results. Solid lines represent the combined outputs whereas dashed lines represent the error standard deviations of the corresponding solutions

Chapter Three: **Design of Inertial Navigation Systems Using Skew Redundant Inertial Measurement Units**

3.1 Introduction

In this chapter, the INS designs with SRIMUs are analyzed using the general framework presented in Chapter 2. In the previous chapter, the algorithm for optimally estimating the system states and unknown deterministic inputs for the system model defined in (2.1) was derived. Furthermore, a method for optimally fusing redundant inertial sensor data was described based on this algorithm.

Although the kinematic variables (i.e. acceleration and rotation rates defined on the body frame) can be optimally estimated with the algorithm presented in Chapter 2, the INS outputs which are driven by only these optimal kinematic variable estimates ($\hat{u}_{k|k}$) are not in general the optimal navigation solution. As it will be explained later in this chapter, it only constitutes a pseudo-optimal solution in which some observations provided by the redundancy of the sensors are ignored in the estimation of navigation states. Hence, the problem of computing the optimal navigation solution for skew redundant multi inertial measurement units (SRIMU) has yet to be answered.

In this chapter, the derivation and implementation of this optimal navigation solution will be presented. Based on the results of the previous chapter, the optimal navigation structure for the SRIMUs is derived in Section 3.3. In this section, it will be shown that the optimal solution can theoretically be implemented as a cascade of 2 Kalman filters. The first Kalman filter is used for the (SR)IMU errors and the second one is used for the navigation errors. The relationship between the optimal solution and the pseudo-optimal

solutions (the navigation solution which is computed using only $\hat{u}_{k|k}$) will also be explained in this section.

Section 3.4 deals with the pseudo-optimal and suboptimal navigation structures for SRIMUs. In this section it will be shown that when the identical sensors are used in an SRIMU, the 1st stage IMU Kalman filter in the optimal solution can be removed without affecting the optimality of the results.

Some simulated data results will be presented in Section 3.5 to clarify the implementation issues for SRIMU based INSs.

The steady state (SS) performance of the SRIMU Kalman filter will be explained in Section 3.6. When a steady state Kalman gain is used for the 1st stage SRIMU Kalman filter, the equivalent sensor error models used in the navigation filters also become time invariant. For such cases, it is usually more feasible to re-derive these equivalent error models empirically from the computed $\hat{u}_{k|k}$ rather than to define it theoretically based on individual sensor error models. In a recent paper [Yuksel et al., 2010], a new modeling method that can be used to model stability errors based on these combined outputs ($\hat{u}_{k|k}$) for SRIMU systems has been developed. In Section 3.6, the application of this new error modeling method for the 1st stage steady state SRIMU Kalman filter will be presented.

In this thesis the comparison of several proposed structures is performed using an INS simulation environment. Therefore, before describing the main SRIMU concepts, this simulation environment will be introduced in Section 3.2 first. The preferred INS mechanization equations and corresponding error propagation models for this mechanization will also be derived in this section.

3.2 The INS mechanization equations and the simulation environment

In the first part of this section, the body frame mechanization equations and the

corresponding linear error propagation models for a 6DOF navigation system will be

introduced. In the second part (Section 3.2.2), the mechanization equations and

simulation environment for a 2D (3DoF) navigation system defined on a non-rotating

planar navigation frame of reference is described. In the rest of this chapter, all the

SRIMU simulations will be performed using this simplified 2D navigation system and

corresponding simulation environment.

3.2.1 Body Frame Mechanization Equations

The mechanization equation for which the velocity (with respect to earth) "v^b" is defined

in body frame and the attitude C_b^n is defined from body to navigation frame of reference

is as follows:

$$\dot{v}^b = a^b - \left(\omega_{ie}^b + \omega^b\right) \times v^b - C_n^b g^n \tag{3.1a}$$

$$\dot{C}_b^n = C_b^n S\left(\omega^b\right) - S\left(\omega_{in}^n\right) C_b^n \tag{3.1b}$$

$$\dot{p} = R C_b^n v^b \tag{3.1c}$$

where position "p" is defined as latitude/longitude/height $[L, l, h]$ (

$R = diag\left(\dfrac{1}{R_n + h}, \dfrac{1}{R_e + h}, -1\right)$ is derived from the radius of the earth). a^b and ω^b is the

acceleration and rotation rate defined in the body frame, g^n is the gravity vector (in NED

frame). $S(\ )$ is the operator which transforms a vector into the skew-symmetric matrix.

w_{ie}^b is the Earth's rotation defined in the body frame and ω_{in}^n is the transport rate of the

navigation (e.g. local geodetic) frame. The detailed derivation of these equations are explained in standard INS books such as [Titterton, 2004 – Chapter 3].

Although these body frame mechanization equations have not in general been popular in traditional INS designs, we observed that this type of mechanization is more suitable for low-cost INSs of ground vehicles for which the main source of external observation is odometer outputs defined in the body frame. With the body frame mechanizations, the initial covariance errors do not lead to erroneous heading angle estimations under holonomic constraints. Furthermore, different error models can be associated to the odometer based velocity and position observations. This provides more flexibility during the design of the navigation Kalman filters.

For the mechanization equations in (3.1) the navigation errors ($\phi, \delta v, \delta p$) with respect to any nominal trajectory ($\tilde{v}^b, \tilde{C}_b^n, \tilde{p}$) are defined as follows:

$$\tilde{C}_b^n = \left[I - S(\phi) \right] C_b^n \tag{3.2a}$$

$$\delta v = \tilde{v}^b - v^b \tag{3.2b}$$

$$\delta p = \tilde{p} - p \tag{3.2c}$$

Furthermore, the sensor errors are defined as:

$$\delta a = \tilde{a}^b - a^b \tag{3.3a}$$

$$\delta \omega = \tilde{\omega}^b - \omega^b \tag{3.3b}$$

where $\tilde{a}^b$ and $\tilde{\omega}^b$ are the observed (computed) kinematic variables. In the literature (3.2a) is called as phi-angle formulation for attitude errors (e.g. [Arshal 1987]).

For any nominal trajectory that satisfies (3.1), the simplified error propagation equations can be expressed as follows:

$$\dot{\phi} = -\tilde{C}_b^n \delta\omega + \delta\omega_{in}^n - S\left(\tilde{\omega}_{in}^n\right)\phi \tag{3.4a}$$

$$\delta\dot{v} = \delta a - \left(\delta\omega_{ie}^b + \delta\omega\right)\times\tilde{v}^b - \left(\tilde{\omega}_{ie}^b + \tilde{\omega}^b\right)\times\delta v + \tilde{C}_n^b S\left(g^n\right)\phi \tag{3.4b}$$

$$\delta\dot{p} = \tilde{R}\left(\tilde{C}_b^n \delta v + S\left(\tilde{C}_b^n \tilde{v}^b\right)\phi\right) + \delta R \tilde{C}_b^n \tilde{v}^b \tag{3.4c}$$

Where ϕ, δv and δp corresponds to the attitude, velocity and position errors respectively. $\delta\omega_{in}^n$ and $\delta\omega_{ie}^b$ are the errors in earth and transport rate. These equations are obtained as a result of the perturbation of (3.2) with respect to navigation and IMU error states. Such perturbation techniques are described extensively in books on inertial navigation such as [Titterton et al., 2004] and [Savage 2000a]. Although only navigation frame error propagation equations are explicitly derived in these references, as the derivation of (3.4) is almost identical to the NED frame case, these derivations are not repeated here.

For the body frame mechanizations, definition of $\delta\omega_{in}^n$ and $\delta\omega_{ie}^b$ in terms of $\phi, \delta v, \delta p$ is more complicated than the corresponding variables in NED frame. On the other hand, for the low cost INS designs the effect of these variables on the overall error growth are completely negligible with respect to the sensor errors. Therefore, these variables can be completely ignored in (3.4). However, for the sake of completeness, the expressions for these variables are also given below:

$$\delta O_1 = \begin{bmatrix} -\Omega^{Earth}\sin\left(\tilde{L}\right)\delta L \\ 0 \\ -\Omega^{Earth}\cos\left(\tilde{L}\right)\delta L \end{bmatrix} \tag{3.5a}$$

$$O_2 = \begin{bmatrix} 0 & \dfrac{1}{R_e + \tilde{h}} & 0 \\ -\dfrac{1}{R_n + \tilde{h}} & 0 & 0 \\ 0 & -\dfrac{\tan(\tilde{L})}{R_e + \tilde{h}} & 0 \end{bmatrix} \qquad (3.5b)$$

$$\delta O_3 = O_2 \left(\tilde{C}_b^n \delta v + S\left(\tilde{C}_b^n \tilde{v}^b \right) \phi \right) \qquad (3.5c)$$

$$\delta \omega_{in}^n = \delta O_1 + \delta O_3 \qquad (3.5d)$$

$$\delta \omega_{ie}^b = \tilde{C}_n^b \left(\delta O_1 - S\left(\tilde{\omega}_{ie}^n \right) \phi \right) \qquad (3.5e)$$

It should be noted that, the perturbation of (3.5b) with respect to position errors are ignored in (3.5d).

3.2.2 2D navigation equations and the simulation environment

In this study, all simulations were performed based on a 2D navigation system defined on a planar surface. For this system, the navigation frame is assumed to be fixed (non-rotating, non-moving) in the position where the simulation starts. Furthermore, the gravity is also assumed to be constant (not position dependent). The position of the system is defined in this (Cartesian) navigation frame.

The 2D (3DoF) navigation equations for this set-up can be derived from (3.1) by setting $\omega_{ie}^e = 0$ and $\omega_{en}^n = 0$ as follows:

$$\dot{v}^b = a^b - S\left(\omega^b \right) v^b - C_n^b g^n \qquad (3.6a)$$

$$\dot{C}_b^n = C_b^n S\left(\omega^b \right) \qquad (3.6b)$$

$$\dot{p} = C_b^n v^b \tag{3.6c}$$

The most important property of this set of equations is that when $a_z^b = \omega_x^b = \omega_y^b = 0$ (assuming that the initial tilt angles are also 0), roll, pitch, z velocity and position becomes algebraically decoupled from the rest of the navigation states. Therefore (3.6) can be directly used for 2D navigation on planar surfaces.

Similar to (3.4), the error propagation equations for (3.6) are as follows:

$$\dot{\phi} = -\tilde{C}_b^n \delta\omega \tag{3.7a}$$

$$\delta\dot{v} = \delta a + S\left(\tilde{v}^b\right)\delta\omega - S\left(\tilde{\omega}^b\right)\delta v + \tilde{C}_n^b S\left(g^n\right)\phi \tag{3.7b}$$

$$\delta\dot{p} = \tilde{C}_b^n \delta v + S\left(\tilde{C}_b^n \tilde{v}^b\right)\phi \tag{3.7c}$$

For the 2D case, as the unused navigation states are algebraically uncoupled, the error propagation equations can be obtained from (3.7) by directly removing the corresponding states. Thus, the 2D error propagation equations can be represented in matrix form as follows:

$$\underbrace{\begin{bmatrix} \delta\dot{p}_x \\ \delta\dot{p}_y \\ \delta\dot{v}_x \\ \delta\dot{v}_y \\ \dot{\psi} \end{bmatrix}}_{\dot{x}^{\text{nav}}} = \underbrace{\begin{bmatrix} 0 & 0 & C_{11} & C_{12} & \tilde{v}_y^n \\ 0 & 0 & C_{21} & C_{22} & -\tilde{v}_x^n \\ 0 & 0 & 0 & \omega_z^b & 0 \\ 0 & 0 & -\omega_z^b & 0 & 0 \\ 0 & 0 & 0 & 0 & 0 \end{bmatrix}}_{A^{\text{nav}}} \underbrace{\begin{bmatrix} \delta p_x \\ \delta p_y \\ \delta v_x \\ \delta v_y \\ \psi \end{bmatrix}}_{x^{\text{nav}}} + \underbrace{\begin{bmatrix} 0 & 0 & 0 \\ 0 & 0 & 0 \\ 1 & 0 & \tilde{v}_y^n \\ 0 & 1 & -\tilde{v}_x^n \\ 0 & 0 & C_{33} \end{bmatrix}}_{N} \underbrace{\begin{bmatrix} \delta a_x \\ \delta a_y \\ \delta\omega_x \end{bmatrix}}_{\tilde{u}} \tag{3.8a}$$

$$E\left\{x_0^{\text{nav}} x_0^{\text{nav}^T}\right\} = \Pi_0^{\text{nav}} \tag{3.8b}$$

where ψ is the heading angle error and C_{kl} is the corresponding element of $\tilde{C}_b^n$.

Because of the nature of the kinematic equations, (3.8a) is derived in continuous time. However, in navigation applications discrete time Kalman filters are always preferred [Maybeck 1982]. Therefore, in practice (3.8) is converted into discrete time using any of the approximate discretization methods (e.g. 1st order Euler approximation). After discretization, (3.8) can be expressed as follows:

$$x_{k+1}^{nav} = A_k^{nav} x_k^{nav} + N_k \tilde{u}_k \tag{3.9a}$$

$$\tilde{u}_k = \begin{bmatrix} \delta a_x \\ \delta a_y \\ \delta \omega_x \end{bmatrix}_k = C_k x_k^{imu} + v_k^{imu} \tag{3.9b}$$

where, A_k^{nav} and N_k are the discrete counterparts of A^{nav} and N in (3.8a) and

$\tilde{u}_k = \begin{bmatrix} \delta a_x; \delta a_y; \delta \omega_z \end{bmatrix}$ are the sensor errors defined in discrete time. "v_k^{imu}" corresponds to the sensor additive white noise which is also called as ARW/VRW in the standard error modeling literature. It is assumed that x_k^{imu} has the following model whose parameters are determined as a result of inertial sensor modeling tests.

$$x_{k+1}^{imu} = A_k^{imu} x_k^{imu} + w_k^{imu} \tag{3.9c}$$

$$E\left\{ w_k^{imu} w_k^{imu^T} \right\} = Q_k^{imu} \tag{3.9d}$$

$$E\left\{ x_0^{imu} x_0^{imu^T} \right\} = \Pi_0^{imu} \tag{3.9e}$$

In order to both compare several proposed navigation structures and verify the results of the related derivations, an inertial navigation simulation environment was developed for SRIMU based systems. The same approach described in [Savage 2000b – Chapter 17] was implemented for the trajectory simulator. In this approach, the trajectory simulator is

composed of a trajectory shaping function and a trajectory generation function. The trajectory shaping function is responsible for generating the body accelerations and the derivatives of Euler angles for a user defined motion. The outputs of the shaping function are then converted into the required kinematic variables (e.g. acceleration, rotation rates and PVA) by the trajectory generator part.

In this chapter, the 2D trajectory presented in Figure 3.1 was used in the simulations. A trajectory shaping function for ground vehicles which can only accelerate/decelerate along only the x-axis of its body frame was implemented to drive the trajectory generator. As the trajectory was generated on a plane, the simulated ω_x^b, ω_y^b and a_z^b were 0 for the entire simulation. Therefore, the error propagation equation for this simulated trajectory is as defined in (3.8).

The generated conditions and the steps followed during the simulation analysis can be summarized as follows:

1. Using the trajectory generator, the kinematic variables defined for the centre of the IMU are computed for the specified trajectory shape.

2. For a given SRIMU structure, the true outputs of each sensor unit are computed by transforming the kinematic variables generated in the previous step for the centre point to the individual sensor locations and orientations. In this thesis, as all the sensors are assumed to be placed at the central point, no lever arm effect was considered. Therefore, the transformation of variables was mainly performed based on only the sensor orientations (i.e. configuration matrix).

3. Sensor errors are added to the computed true kinematic values to simulate the realistic (and erroneous) sensor outputs. In this thesis, sensor errors were always characterized by state space representations as defined in (3.9). Although the effect of scale factor and temperature dependent errors can also be handled in this state space forms, in this thesis only the sensor stability and repeatability errors (including the random biases) were considered as a part of the simulated sensor errors. During the simulations, all noise components (i.e. w_k^{imu} and v_k^{imu} in (3.9)) were generated as a Gaussian distribution. The numerical values of the state space models (i.e. A_k^{imu}, C_k, Q_k^{imu} and Π_0^{imu} in (3.9)) used in each simulation analysis are specified in the sections where the corresponding simulation results are presented. In general, the values used in the simulations are selected to reflect the low-end MEMS sensors characteristics. However, in some cases, the selected error model parameters are modified to a certain degree to emphasize the differences between the proposed structures more clearly.

4. The initial navigation states of the INSs which are used to process the simulated sensor outputs are generated by adding noise on the initial PVA output of the trajectory generator. In this thesis, these initialization errors were simulated as a Gaussian distribution with the following covariance values:

$$\Pi_0^{nav} = diag\left(0,0,0.05m/s,0.05m/s,0.1rad\right)^2 \qquad (3.10)$$

where the first two elements represents initial position error covariance, the 3rd and 4th elements represents the initial velocity error covariance and the final element represents the initial heading angle error covariance value.

After the erroneous SRIMU outputs and initial navigation state values are generated as described above, the simulated data set is processed using different structures which are described throughout this thesis. The outputs of such simulation analysis are presented in Sections 3.5, 3.6, 4.3 and 4.5.
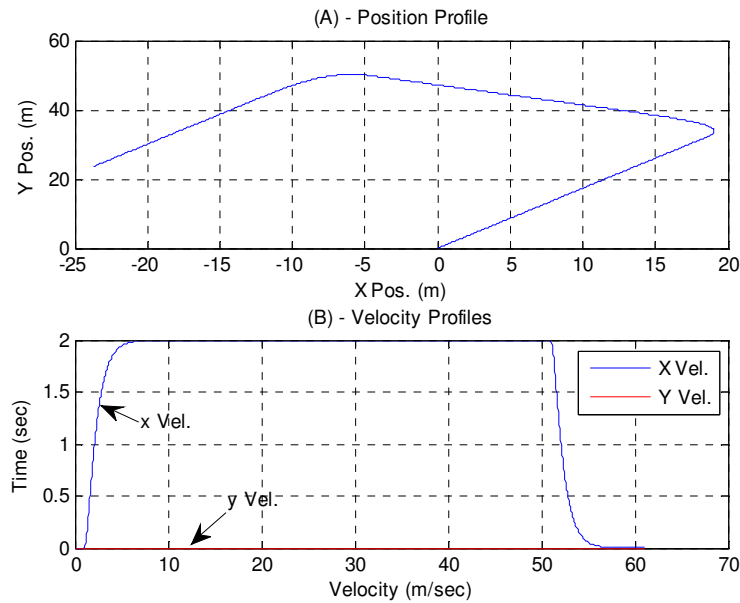
Figure 3-1 : Simulated trajectory. A) Simulated position profile on x-y plane. B) Velocity profiles of the body frame x & y axis.

3.3 The optimal navigation solution for SRIMU systems

As presented in Chapter 2, one possible way of obtaining optimal state estimates for linear systems defined in (2.1) is to define a Kalman filter for only the stochastic part of the system which is defined as the difference between the system state and the nominal trajectory generated by the deterministic (and known) input $M_k^\#\left(y_k - C\hat{x}_k\right)$ where y_k

represents the (skew redundant) sensor outputs, $\hat{x}_k$ is the nominal state value and "

$$M_k^\# = \left(M_k^T R_k^{-1} M_k \right)^{-1} M_k^T R_k^{-1} \text{''}$$ (Chapter 2 - Lemma 2 & 3).

This approach can be directly extended to the non-linear INS equations to obtain so-called optimal solution for the SRIMU based INSs. In this method, the Kalman filter is defined for the difference between the true navigation states and the nominal solution generated by the INS which is driven by the (combined) weighted least square solution of the inertial sensor outputs. Theoretically, this difference between the true navigation states and the nominal solution is characterized by non-linear differential equations for which a Kalman filter cannot be employed. On the other hand, these differential equations of errors are in general not sensitive to the variations of the nonlinear coefficients. Therefore, they can be safely linearized around the nominal INS outputs without inducing significant approximation errors (as long as the nominal INS output errors are guaranteed to be kept within certain limits). In practice, these linearization errors are almost completely negligible with respect to other type errors (e.g. sensor modeling errors for low-cost MEMS units). Hence, in general, they are completely ignored during the design phase and the Kalman filter based solutions are referred to as optimal solutions.

Ignoring such approximation errors due to the linearization, the system model of the Kalman filter can be derived as described below.

The inertial sensor outputs can be represented as:

$$y_k^{\text{imu}} = M_k u_k + C_k x_k^{\text{imu}} + v_k^{\text{imu}}$$ (3.11)

where u_k is the vector of true kinematic variables (i.e. $u_k = [a_k^b, \omega_k^b]$), v_k^{imu} is the additive white noise of the sensors (ARW/VRW components) and the x_k^{imu} denotes the stability errors of the sensors as defined in (3.9c). M_k is the configuration matrix, each row of which is the unit vector representing the orientation of the individual sensors in the body frame of reference. The weighted least square estimate of kinematic variables for this model can be defined as:

$$\hat{u}_k^{wls} = \underbrace{\left(M_k^T R_k^{-1} M_k \right)^{-1} M_k^T R_k^{-1}}_{M_k^{\#}} y_k^{imu} \tag{3.12}$$

where $R_k = E\left\{ v_k^{imu} v_k^{imu^T} \right\}$.

As described in Chapter 2, the nominal trajectory for the optimal solution should be generated with $\hat{u}_k^{wls} = M_k^{\#} \left(y_k^{imu} - C_k \hat{x}_k^{imu} \right)$. However, due to the IMU calibration processes, it is always assumed that the nominal IMU errors ($\hat{x}_k^{imu}$) are 0. Therefore, for the SRIMU based INS case, the nominal trajectory can be assumed to be generated by $\hat{u}_k^{wls} = M_k^{\#} y_k^{imu}$ rather than $\hat{u}_k^{wls} = M_k^{\#} \left(y_k^{imu} - C_k \hat{x}_k^{imu} \right)$.

Let the difference between the true navigation solution and the nominal INS outputs be represented as:

$$x_k^{nav} = \begin{bmatrix} \tilde{p} \\ \tilde{v} \\ \tilde{C} \end{bmatrix} - \begin{bmatrix} p \\ v \\ C \end{bmatrix} \tag{3.13}$$

where p, v, C are the true position, velocity and the attitude (DCM matrix) respectively.

Also, the variables with tilde represent the INS outputs for the corresponding variables.

The time propagation of x_k^{nav} can be defined as:

$$\dot{x}^{\text{nav}} = f\left(\tilde{p}, \tilde{v}, \tilde{C}, M^{\#}y\right) - f\left(p, v, C, u\right) \tag{3.14a}$$

$$\dot{x}^{\text{nav}} \cong \frac{\partial f}{\partial\left(\tilde{p}, \tilde{v}, \tilde{C}\right)} x^{\text{nav}} - \frac{\partial f}{\partial\left(\hat{u}^{wls}\right)} \underbrace{\left(M^{\#}y - u\right)}_{\tilde{u}} \tag{3.14b}$$

where f is the kinematic equation of motion such as (3.1) and (3.14b) is obtained as a

result of linearization of (3.14a) around $\tilde{p}, \tilde{v}, \tilde{C}$. By discretizing (3.14b) the following

form of the propagation model can be obtained:

$$x_{k+1}^{\text{nav}} = A_k x_k^{\text{nav}} + N_k \tilde{u}_k \tag{3.14c}$$

Using (3.11), $\tilde{u}_k$ in (3.14c) can be expressed as follows:

$$\tilde{u}_k = M^{\#}y_k - u_k = M^{\#}C_k x_k^{\text{imu}} + M^{\#}v_k^{\text{imu}} \tag{3.15}$$

Therefore, by combining (3.9c), (3.14) and (3.15) the overall system model can be

represented as follows:

$$\begin{bmatrix} x_{k+1}^{\text{nav}} \\ x_{k+1}^{\text{imu}} \end{bmatrix} = \begin{bmatrix} A_k^{\text{nav}} & N_k M_k^{\#} C_k \\ 0 & A_k^{imu} \end{bmatrix} \begin{bmatrix} x_k^{\text{nav}} \\ x_k^{\text{imu}} \end{bmatrix} + \begin{bmatrix} N_k M_k^{\#} v_k^{\text{imu}} \\ w_k \end{bmatrix} \tag{3.16}$$

As an example, for the body frame mechanization defined in Section 3.2, the linear error

propagation model parameters (A_k^{nav} and N_k) of a 2D planar navigation system is the

discrete time counterparts of (3.8). By comparing (3.8) with (3.16) it can be seen that the

only difference between the SRIMU and IMU systems is that C_k and v_k^{imu} is replaced by

their combined equivalents $M^{\#}C_k$ and $M^{\#}v_k^{\text{imu}}$.

In an SRIMU based navigation system 2 types of observation can be identified: i) observations generated by the redundancy of the inertial sensors, ii) observations generated by the external navigation aids (e.g. GPS, odometer etc). As described in Chapter 2, all sensor redundancy based observations can be represented as the projection of sensor outputs (3.11) to the left null space of M_k. Denoting this projection operator as T_k, the redundancy based observations can be represented as follows:

$$\underbrace{T_k y_k^{imu}}_{y_k^l} = \underbrace{T_k C_k}_{H_k^{imu}} x_k^{imu} + T_k v_k^{imu} \tag{3.17a}$$

For the 2nd type of observation (external navigation observations), the measurement model can be expressed as:

$$y_k^{nav} = H_k^{nav} x_k^{nav} + v_k^{nav} \tag{3.17b}$$

It should be noted that although both the system noise in (3.16) and observation noise in (3.17a) contains v_k^{imu}, the system and observation noises are orthogonal (i.e.

$E\left\{ M^{\#} v_k^{imu} v_k^{imu^T} T_k^T \right\} = M^{\#} R_k T_k^T = 0$). Therefore, standard Kalman filter recursions can be directly applied to (3.16) and (3.17) without any modification.

In Figure 3.2, the general structure of the optimal navigation solution for SRIMU systems is presented. In this figure the Kalman filter is run in closed loop form where the best estimates are fed back to the INS and IMU subsystems. Thanks to this closed loop structure, no additional system implementation is required inside the Kalman filter block to generate the innovation process (i.e. $y_k - H_k \hat{x}_k$).

In this structure, for each IMU output cycle, the Kalman filter has to be run to process $T_k y_k^{imu}$ observations. The estimated IMU error parameters are fed back and subtracted

from $\hat{u}_k^{wls}$. Therefore, implicitly, the INS subsystem is not driven by the $\hat{u}_k^{wls}$ but rather

by the best kinematic variable estimate $\hat{u}_{k|k} = \hat{u}_k^{wls} - M_k^{\#} C_k \hat{x}_{k|k}^{\text{imu}}$. Whenever an external

navigation aid is available, these external observations are also processed by the Kalman

filter and the results are again fed back to the INS and IMU subsystems exactly in the

same manner as it is done in single IMU implementations.
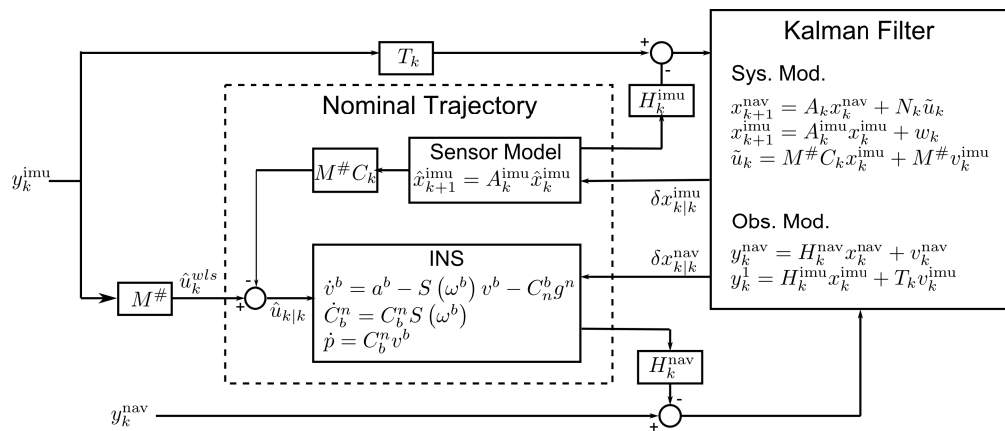
Figure 3-2 : The optimal structure for the SRIMU based navigation system. The

Kalman filter processes both the external and the redundancy based observations.

The system and observation models are as defined in (3.16) and (3.17)

As can be seen from (3.16) the system model for INS errors have an upper diagonal

matrix form. Furthermore, the IMU redundancy observations are only related with the

sensor error states. Therefore, using a similar approach employed in Schmidt-Kalman

form [Brown 1996 – Chapter 9.2], the optimal Kalman filter can be implemented as

shown in Figure 3.3. As seen in this figure, the redundancy observations $T_k y_k^{\text{imu}}$ are first

processed by a 1$^{\text{st}}$ stage IMU Kalman Filter to form "$\hat{u}_{k|k}$", and then the INS is run by

using these $\hat{u}_{k|k}$ estimates.
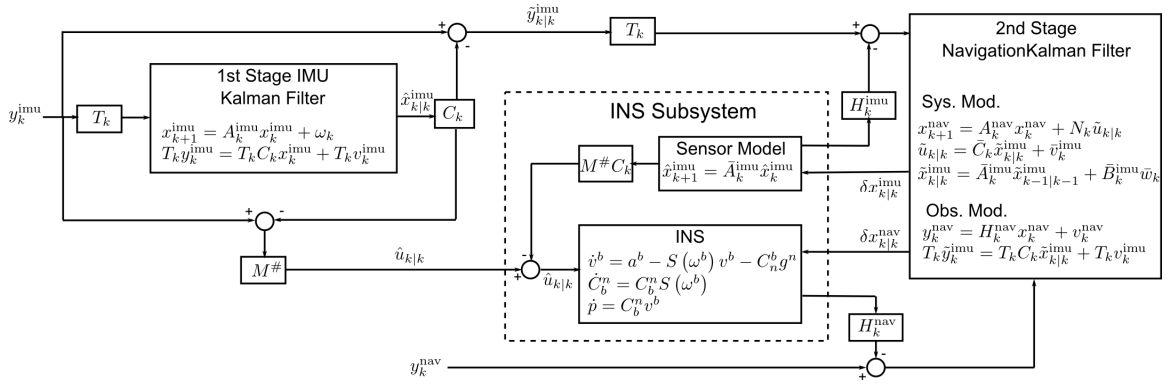
Figure 3-3 : Optimal structure for the SRIMU based navigation system using 2 separate Kalman filters. The 1st stage filter is in the open loop form, whereas the 2nd filter is in the closed loop form. The system model for the 1st filter is defined in (3.9c) and (3.17a), and for the 2nd filter in (3.20).

In this structure, the equivalent IMU error model in the 2nd stage navigation Kalman filter is replaced by the error propagation model of the 1st stage SRIMU Kalman filter. This error model can be represented as follows:

$$
\begin{aligned}
\tilde{u}_{k|k} &= \hat{u}_{k|k} - u_k \\
&= \underbrace{M^\# C_k}_{\bar{C}_k} \underbrace{\left(\hat{x}_{k|k}^{\text{imu}} - x_k^{\text{imu}} \right)}_{\tilde{x}_{k|k}^{\text{imu}}} + \underbrace{M^\# v_k^{\text{imu}}}_{\bar{v}_k^{\text{imu}}}
\end{aligned}
\tag{3.18a}
$$

$$
\begin{aligned}
\tilde{x}_{k+1|k+1}^{\text{imu}} &= A_k^{\text{imu}} \hat{x}_{k|k}^{\text{imu}} + K_{k+1} T_{k+1} \left(y_{k+1} - C_{k+1} A_k^{\text{imu}} \hat{x}_{k|k}^{\text{imu}} \right) - A_k^{\text{imu}} x_k^{\text{imu}} - w_k \\
&= \underbrace{\left(\mathrm{I} - K_{k+1}^{\text{imu}} T_{k+1} C_{k+1} \right) A_k^{\text{imu}}}_{\bar{A}_k^{\text{imu}}} \tilde{x}_{k|k}^{\text{imu}} + \underbrace{\left[\mathrm{I} - K_{k+1}^{\text{imu}} T_{k+1} C_{k+1} \quad -K_{k+1}^{\text{imu}} T_{k+1} \right]}_{\bar{B}_k^{\text{imu}}} \underbrace{\begin{vmatrix} w_k \\ v_{k+1}^{\text{imu}} \end{vmatrix}}_{\bar{w}_k}
\end{aligned}
\tag{3.18b}
$$

where K_{k+1}^{imu} corresponds to the Kalman gain of the 1st stage IMU Kalman filter.

As can be seen in Figure 3.3, the redundancy observations must be processed both in the 1st stage IMU Kalman filter and the 2nd stage navigation Kalman filter to preserve the optimality. The reason for this is that the navigation states in the 2nd stage filter are still

correlated with the redundancy observations, even though the nominal INS outputs are generated with the optimally fused sensor outputs $\hat{u}_{k|k}$. On the other hand, it must be noted that the sensor states in the 2nd stage, whose models are defined in (3.18), are always orthogonal these redundancy measurements. Hence, these measurements do not generate any additional estimate for the sensor states in the 2nd stage filter. They only affect the navigation states.

The new measurement model of the redundancy observations for the 2nd stage filter can be defined based on the innovation processes of the 1st stage IMU KF as follows:

$$T_k \tilde{y}_k^{\text{imu}} = T_k \left(y_k^{\text{imu}} - \hat{y}_{k|k}^{\text{imu}} \right) = -T_k C_k \tilde{x}_k^{\text{imu}} + T_k v_k^{\text{imu}} \tag{3.19}$$

Finally, by combining (3.14c), (3.17b), (3.18) and (3.19), the overall system and observation model of the 2nd stage navigation Kalman Filter can be written as follows:

System model:

$$\begin{bmatrix} x_{k+1}^{\text{nav}} \\ \tilde{x}_{k+1|k+1}^{\text{imu}} \end{bmatrix} = \begin{bmatrix} A_k^{\text{nav}} & N_k M^{\#} C_k \\ 0 & \text{I} - K_{k+1}^{\text{imu}} T_{k+1} C_{k+1} \end{bmatrix} \begin{bmatrix} x_k^{\text{nav}} \\ \tilde{x}_{k|k}^{\text{imu}} \end{bmatrix} + \begin{bmatrix} N_k M^{\#} v_k^{\text{imu}} \\ \left(\text{I} - K_{k+1}^{\text{imu}} T_{k+1} C_{k+1} \right) w_k - K_{k+1}^{\text{imu}} T_{k+1} v_{k+1}^{\text{imu}} \end{bmatrix} \tag{3.20a}$$

Observation Model

$$\begin{bmatrix} y_k^{\text{nav}} \\ T_k \tilde{y}_k^{\text{imu}} \end{bmatrix} = \begin{bmatrix} H_k^{\text{nav}} & 0 \\ 0 & -T_k C_k \end{bmatrix} \begin{bmatrix} x_k^{\text{nav}} \\ \tilde{x}_{k|k}^{\text{imu}} \end{bmatrix} + \begin{bmatrix} v_k^{\text{nav}} \\ T_k v_k^{\text{imu}} \end{bmatrix} \tag{3.20b}$$

It must be noted that (3.20) is not compatible with the standard Kalman filter system model definition. The reason for this is that the observation noise "$T_k v_k^{\text{imu}}$" is correlated with the system noise "$K_{k+1}^{\text{imu}} T_{k+1} v_{k+1}^{\text{imu}}$" in an unusual manner. Therefore, standard Kalman filter recursions cannot be applied to this system definition. On the other hand this form

of the optimal structure is useful for this study as it relates the optimal solution to the

pseudo-optimal solutions which is described in the next section.

Although, in this thesis the structure shown in figure 3.3 is not used for the optimal

estimation at all, for the sake of completeness, the modified form of the Kalman update

equations which can be applied to this system (when there is no external navigation aid)

is presented in Appendix A.

3.4 Suboptimal Solutions

3.4.1 Pseudo – Optimal Solution

In this thesis, the pseudo-optimal solution denotes the case where the redundancy

observations are used only to estimate the optimal kinematic variables that run the INS

algorithm. In this type of solution, the redundancy observations are not used to estimate

the navigation errors as it is done in the optimal configurations.

The system configuration which realizes this pseudo-optimal solution is shown in Figure

3.4. As proved in Chapter 2, the output of the first stage Kalman filter is equivalent to the

optimal kinematic variable estimate "$\hat{u}_{k|k}$" for the SRIMU. The INS is run by these

optimal "$\hat{u}_{k|k}$" estimates. Therefore, the errors on $\hat{u}_{k|k}$, which are derived in (3.18), are

augmented to the navigation error states in the navigation Kalman filter. Thus, the overall

system model of the navigation filter is the same as (3.20a). However, as the redundancy

based observations are completely ignored in the navigation filter, the filter observation

model for the 2nd Kalman filter only constitutes (3.17b).

As can be seen from Figure 3.3 and 3.4, apart from the use of redundancy based observations for the navigation state estimation, the optimal and pseudo-optimal solutions are exactly the same.
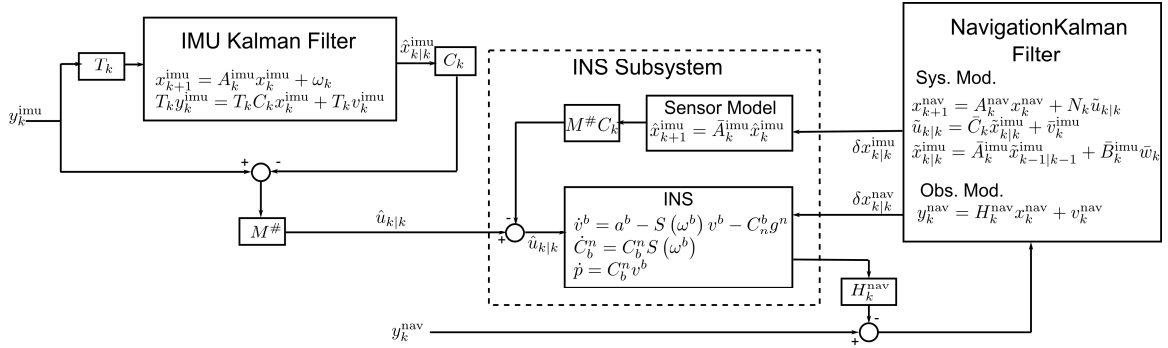
Figure 3-4 : Pseudo-optimal structure for the SRIMU based navigation system. The navigation Kalman Filter only processes external navigation observations.

3.4.2 WLS Based Solutions

In the existing literature about FDI methods (such as [Ho, 1999], [Sukkarieh et al., 2000]), the structure shown in Figure 3.5 is used for the navigation systems. In this configuration, all sensor outputs (after they are verified by the FDI methods), are combined using a simple weighted least square algorithm and the INS is run by this combined output $\hat{u}_k^{wls} = M^{\#} y_k^{\text{imu}}$ as defined in (3.12).

In the navigation Kalman filter, the errors on $\hat{u}_k^{wls}$ are augmented to the navigation error states. The model for these combined sensor errors are as defined in (3.15). Hence, the overall system model of the navigation filter of the WLS based solution becomes equal to (3.16).

By comparing Figures 3.5 and 3.2, it can be seen that the only difference between the

optimal and WLS based configuration is that the redundancy based observation are not

used in the navigation Kalman filter. However, this does not mean that WLS based

solutions are equivalent to the pseudo-optimal solutions. In the pseudo-optimal

configurations the 1st stage IMU Kalman filter still uses the redundancy observation to

compute the optimal $\hat{u}_{k|k}$, whereas in the WLS based solutions the redundancy

observations are completely ignored in all levels.

Figure 3-5 : System configuration for WLS based solution for SRIMU navigation

systems.

3.4.3 System Configuration for identical inertial sensors

3.4.3.1 Case I: All sensors are identical

When all the inertial sensors in an SRIMU are identical, the navigation solution of all 3

configurations (optimal, pseudo-optimal, WLS) becomes theoretically identical. As

proved in Section 2.4.3.1, when all the sensors are identical, the redundancy observations

(Ty_k^{imu}) become orthogonal to $M^{\#}C_k x_k^{\text{imu}}$. Therefore, the 1st stage IMU Kalman filter

becomes completely functionless in both the optimal and pseudo-optimal solutions and

hence for this case $\hat{u}_{k|k} = \hat{u}_k^{wls}$.

Furthermore, as shown in (3.14c) and (3.15), the navigation errors are only affected by

$\tilde{u}_k^{wls} = M^{\#}C_k x_k^{imu} + M^{\#}v_k^{imu}$. As $T_k y_k^{imu}$ is orthogonal to both $M^{\#}C_k x_k^{imu}$ and $M^{\#}v_k^{imu}$, the

navigation errors also become orthogonal to the redundancy observations. Hence, the

redundancy observations in the navigation filter of the optimal solution also become

functionless. Therefore, the optimal navigation solution becomes equivalent to the

solution computed by the structure shown in Figure 3.5.

On the other hand, it should be noted that the equivalency is only valid for the navigation

states. Because of the 1st stage IMU Kalman filter, some combination of sensor errors can

still be estimated even for the identical IMU case. Therefore, the pseudo-optimal and

optimal solutions can still be used for the IMU calibration purposes. However, as these

combinations of sensor error states do not affect the combined output $\hat{u}_{k|k} = \hat{u}_k^{wls}$, the

navigation errors are invariant to the redundancy observations.

As showed in Section 2.4.3, when identical sensors are used, the errors on the combined

outputs ($\tilde{u}_k^{wls} = \hat{u}_k^{wls} - u_k$) can be remodeled with less number of states using a different

system representation which has the same 2nd order characteristics (Chapter 2, Figure

2.7). As the optimal navigation solution only depends on $\tilde{u}_k^{wls}$, these equivalent

representations can also be used in the navigation filters without affecting the optimality.

Such a model order reduction provides a great flexibility on the filter design when

abundant number of identical sensors is used in the system.

3.4.3.2 Case II: Sets of identical Sensors

As described in Section 2.4.3.2 when sets of identical sensors are used, each set can be

represented by an equivalent (virtual) IMU configuration which contains only critical

number of sensors (i.e. one sensor per each kinematic axis). In these virtual

configurations, each virtual sensor set corresponds to the weighted least square solution "

$^{i}\hat{u}_{k}^{wls}$ " of the real ith sensor set. Furthermore, the redundancy observations can now be

defined using only the outputs $^{i}\hat{u}_{k}^{wls}$ of these virtual sensor sets as the remaining

observation are orthogonal to the $M^{\#}C_{k}x_{k}^{imu}$. Similar to the case described in the previous

section, when the INS is run by the combination of these virtual sensor outputs, the

navigation error estimates are also not affected by the replacement of real sensor models

with the equivalent models of these virtual sensors.

In the next section the application of these virtual sensor concepts to the SRIMU based

navigation systems will be clarified based on simulated data examples.

3.5 Simulated Data Examples

In this section, using the simulation environment introduced in Section 3.2, the

performance comparison of several structures described in the Section 3.4 is presented.

Furthermore, some implementation issues regarding the identical sensors are clarified

using simplified examples.

3.5.1 Example I

The sensor configuration simulated for this 2D navigation example is shown in Figure

3.6. As seen from this figure, the simulated SRIMU contains 5 accelerometers placed on

the x-y plane to sense the x & y accelerations. Furthermore, it has 3 gyroscopes on the z-axis to sense the yaw rate.

For this SRIMU configuration the trajectory shown in Figure 3.1 was simulated as described in Section 3.2. It was assumed that only a single external position observation become available at the 50th seconds of the trajectory. The 2D navigation equations and the corresponding linear error propagation model for this system are as presented in (3.6) and (3.8).
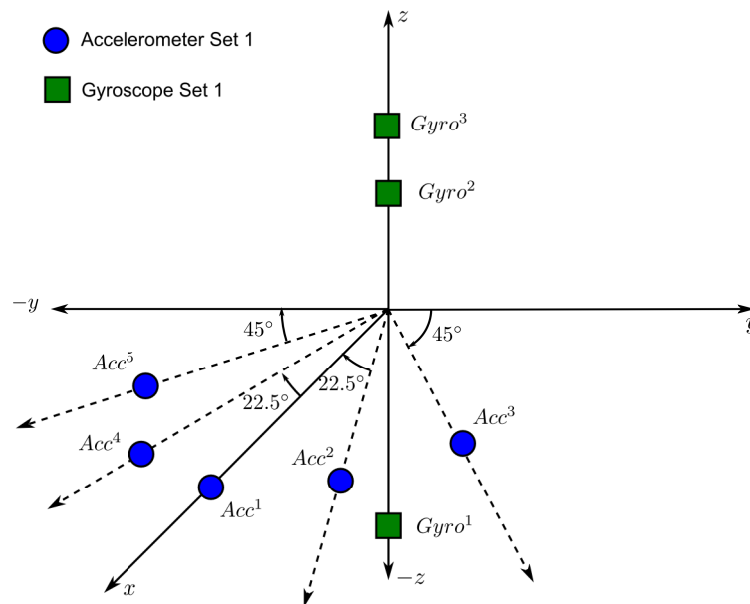
Figure 3-6 : Inertial Sensor Configuration for Example I. All accelerometers are placed on the x-y plane and gyroscopes are on the z-axis. The distances between the sensors and the origin are assumed to be negligible.

The sensor observation model for the specified configuration is as follows:

$$
y_k^{\text{imu}} = \begin{bmatrix} Acc^1 \\ Acc^2 \\ Acc^3 \\ Acc^4 \\ Acc^5 \\ Gyro^1 \\ Gyro^2 \\ Gyro^3 \end{bmatrix} = \underbrace{\begin{bmatrix} \cos(0) & \sin(0) & 0 \\ \cos(\pi/8) & \sin(\pi/8) & 0 \\ \cos(\pi/4) & \sin(\pi/4) & 0 \\ \cos(-\pi/8) & \sin(-\pi/8) & 0 \\ \cos(-\pi/4) & \sin(-\pi/4) & 0 \\ 0 & 0 & -1 \\ 0 & 0 & 1 \\ 0 & 0 & 1 \end{bmatrix}}_{M} \underbrace{\begin{bmatrix} a_x \\ a_y \\ \omega_z \end{bmatrix}_k}_{u_k} + C_k \underbrace{\begin{bmatrix} {}^1 x_k^{\text{acc}} \\ {}^2 x_k^{\text{acc}} \\ {}^3 x_k^{\text{acc}} \\ {}^4 x_k^{\text{acc}} \\ {}^5 x_k^{\text{acc}} \\ {}^1 x_k^{\text{gyro}} \\ {}^2 x_k^{\text{gyro}} \\ {}^3 x_k^{\text{gyro}} \end{bmatrix}}_{x_k^{\text{imu}}} + \underbrace{\begin{bmatrix} v_k^{\text{acc}} \\ v_k^{\text{gyro}} \end{bmatrix}}_{v_k^{\text{imu}}} \quad (3.21)
$$

where y_k^{imu} is the sensor outputs, u_k is the kinematic variables to be estimated. x_k^{imu} and v_k^{imu} represents the sensor stability errors and ARW/VRW components respectively for which $R_k^{\text{imu}} = E\left\{ v_k^{\text{imu}} v_k^{\text{imu}^T} \right\}$ and $\Pi_o^{\text{imu}} = E\left\{ x_k^{\text{imu}} x_k^{\text{imu}^T} \right\}$.

For this example, It was assumed that all 3 gyroscopes and 5 accelerometers have the following identical stochastic error parameters defined at 25Hz:

Accelerometers Stability Errors (i=1..5):

$$
{}^i x_{k+1}^{\text{acc}} = {}^i x_k^{\text{acc}} + 1.1^{-4} w_k^{\text{acc}}
$$
$$
E\left\{ {}^i x_0^{\text{acc}} \, {}^i x_0^{\text{acc}^T} \right\} = 1^{-4} \left(m/\sec^2 \right)^2 \quad (3.22a)
$$
$$
E\left\{ {}^i v_k^{\text{acc}} \, {}^i v_k^{\text{acc}^T} \right\} = 7.5^{-5} \left(m/\sec^2 \right)^2
$$

Gyroscope Stability Errors (i=1..3):

$$
{}^i x_{k+1}^{\text{gyro}} = {}^i x_k^{\text{gyro}} + 1.8^{-4} w_k^{\text{gyro}}
$$
$$
E\left\{ {}^i x_0^{\text{gyro}} \, {}^i x_0^{\text{gyro}^T} \right\} = 6^{-9} \left(rad/\sec \right)^2 \quad (3.22b)
$$
$$
E\left\{ {}^i v_k^{\text{gyro}} \, {}^i v_k^{\text{gyro}^T} \right\} = 6.25^{-6} \left(rad/\sec \right)^2
$$

In (3.22), $v_k^{\text{acc,gyro}}$ represents the V/ARW components of the sensors. It is assumed that each inertial sensor has a stability error component ($x_k^{\text{acc,gyro}}$) in the form of 1$^{\text{st}}$ order

Markov processes all of which are independent of each other. It should be noted that as each sensor has only one stability error state, C_k is an 8×8 identity matrix.

As all the sensors in this configuration have identical error parameters, the optimal navigation solution can be computed using the equivalent virtual sensor configuration with reduced order sensor models. Using the method described in Section 2.4.3, the virtual configuration and the associated error models can be derived as follows:

Let $M^{\#}_{\text{acc/gyro}} = \left(M^T_{\text{acc/gyro}} R^{-1}_{\text{acc/gyro}} M_{\text{acc/gyro}} \right)^{-1} M^T_{\text{acc/gyro}} R^{-1}_{\text{acc/gyro}}$, where "acc" denotes nonzero columns of the first 5 rows of M and R^{imu}_k, and "gyro" denotes the non-zero columns on the last 3 rows. Hence:

$$y^{\text{acc}_{\text{eq}}}_k = M^{\#}_{\text{acc}} y^{\text{acc}}_k = \begin{bmatrix} a_x \\ a_y \end{bmatrix}_k + \underbrace{\sqrt{\left(M^T_{\text{acc}} M_{\text{acc}} \right)^{-1}}}_{C^{\text{acc}_{\text{eq}}}} \begin{bmatrix} {}^1 x^{\text{acc}}_k \\ {}^2 x^{\text{acc}}_k \end{bmatrix} + \underbrace{\sqrt{\left(M^T_{\text{acc}} M_{\text{acc}} \right)^{-1}} \begin{bmatrix} {}^1 v^{\text{acc}}_k \\ {}^2 v^{\text{acc}}_k \end{bmatrix}}_{v^{\text{acc}_{\text{eq}}}_k} \quad (3.23a)$$

$$y^{\text{gyro}_{\text{eq}}}_k = M^{\#}_{\text{gyro}} y^{\text{gyro}}_k$$
$$= \omega_{z_k} + \underbrace{\sqrt{\left(M^T_{\text{gyro}} M_{\text{gyro}} \right)^{-1}}}_{C^{\text{gyro}_{\text{eq}}}} \left({}^1 x^{\text{gyro}}_k \right) + \underbrace{\sqrt{\left(M^T_{\text{gyro}} M_{\text{gyro}} \right)^{-1}} \left({}^1 v^{\text{gyro}}_k \right)}_{v^{\text{gyro}_{\text{eq}}}_k} \quad (3.23b)$$

where the numerical values of the corresponding matrices are equal to:

$$C^{\text{acc}_{\text{eq}}} = \begin{vmatrix} 0.5194 & 0 \\ 0 & 0.8795 \end{vmatrix} \quad (3.23c)$$

$$E\left\{ v^{\text{acc}_{\text{eq}}} v^{\text{acc}^T_{\text{eq}}} \right\} = \begin{vmatrix} 2^{-5} & 0 \\ 0 & 5.8^{-5} \end{vmatrix} \quad (3.23d)$$

$$C^{\text{gyro}_{\text{eq}}} = 0.5774 \quad (3.23e)$$

$$E\left\{ v^{\text{gyro}_{\text{eq}}} v^{\text{gyro}^T_{\text{eq}}} \right\} = 2.08^{-6} \quad (3.23f)$$

As seen from (3.23), in the virtual configuration there is only one sensor per each kinematics axis (i.e. 1 accelerometer on x and y axis and 1 gyroscope on z axis). Furthermore only 3 states are used to represent the stability errors of this virtual configuration. Also, for this configuration, the stochastic error models turn out to be independent for each axis (the off diagonal elements in (3.23c-d) are zero). This independence of error model for each virtual axis comes from the fact that all the accelerometers in Figure 3.6 are placed symmetrically around x-axis. As a result of this independence, the error model of the virtual configuration can be handled as if it is the error model of a standard orthogonal single IMU system. Hence, this form can be implemented in any existing navigation software without any modification at all. For this example, the following 3 different navigation solutions were defined and implemented:

i.   Optimal Solution:

In this solution, the structure shown in Figure 3.2 was implemented. The IMU observation model shown in (3.21) was used in the system models of the Kalman filter (No reduction of system model was considered for this implementation). Therefore, for this solution the main filter consisted of 13 states (8 states for the sensor errors, and 5 states for the navigation errors defined in (3.8)). A single Kalman filter was used to process both sensor redundancy observations which are derived from (3.21) and the single external navigation observation at the 50th second.

ii.   Reduced order WLS solution:

This solution was obtained with the structure shown in Figure 3.5. However, the entire implementation was derived based on the virtual sensor configuration defined in (3.23).

Therefore, the navigation filter for this solution contained only 8 states (5 for navigation errors and 3 for virtual sensor errors).

iii.   Pseudo-Optimal Solution:

This solution was obtained with the structure presented in Figure 3.4. The design was derived based on the real configuration defined in (3.21).

During the simulations, the navigation Kalman filter was used to process only one external position observation which occurred at the 50th second. In Figure 3.7, the position results of all 3 solutions are presented. As can be seen from this figure the position solutions are exactly the same for all implementation as explained in the previous sections. This figure verifies the fact that when identical sensors are used in an SRIMU system, the equivalent virtual sensor configuration can be used for the design of the entire system without affecting the optimality. This property provides great convenience when abundant number of sensors is used in a SRIMU system. It should be noted that even if 1000 accelerometers were used in the original configuration, only 3 states would still be sufficient to model all of these sensors in the navigation filter. Furthermore, this figure also verifies that when only 1 type of sensor is used in a SRIMU, no 1st stage IMU Kalman filter is required for the optimal solution. The optimal navigation solution can be obtained simply by running the INS algorithm with the WLS solution $\hat{u}_k^{wls} = M^{\#} y_k^{imu}$ as shown in Figure 3.5.
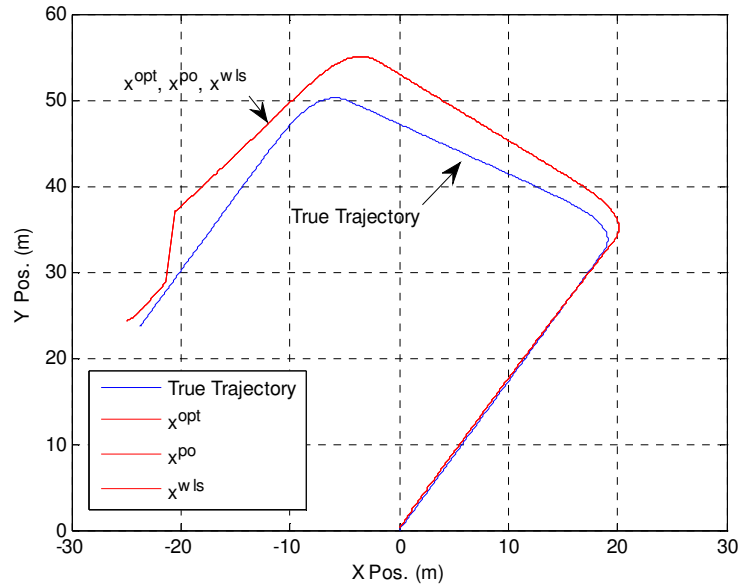
Figure 3-7 : Comparison of position solution of all 3 solutions. x^{opt} **,** x^{po} **and** x^{wls} **is the solutions of the optimal, pseudo-optimal and reduced order WLS implementations respectively**

In Figure 3.8, the accelerometer bias estimate for the Acc^1 is shown for the optimal and pseudo-optimal solutions. As seen from this figure, with the redundancy observations (Ty_k^{imu}), it is possible to obtain a bias estimate for each individual sensor even if all sensors are identical. Therefore, if for some reason, the primary objective is to estimate sensor errors rather than to obtain optimal navigation solution, then the optimal and pseudo-optimal structures should be used instead of WLS based configurations. On the other hand, as explained in Section 3.4.3, these individual bias estimates have no effect on the optimal navigation solution. The reason for this can be seen from Figure 3.9. In this figure, the " $M^{\#}C_k x_k^{imu}$ " estimates for the x-axis are presented for the optimal and reduced order WLS configurations. These estimates correspond to the effective bias

estimates on the "$\hat{u}_{k|k}$" which runs the INS. Therefore, INS is only affected by this value rather than the individual sensor error estimates such as the one presented in Figure 3.8. As shown in Figure 3.9, the optimal estimate for "$M^{\#}C_{k}x_{k}^{\text{imu}}$" is exactly zero under the redundancy observations. (The change in the 50th second is due to the external position observation processed by the navigation Kalman filter.). This figure verifies the fact that when identical sensors are used, "$M^{\#}C_{k}x_{k}^{\text{imu}}$" is always orthogonal to the redundancy observations (Ty_{k}^{imu}).
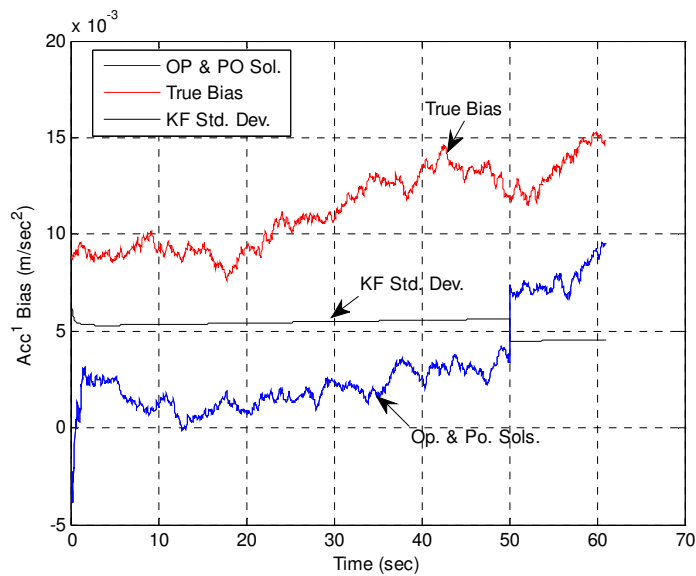
Figure 3-8 : The Acc^{1} bias estimate computed in optimal and pseudo-optimal configurations.
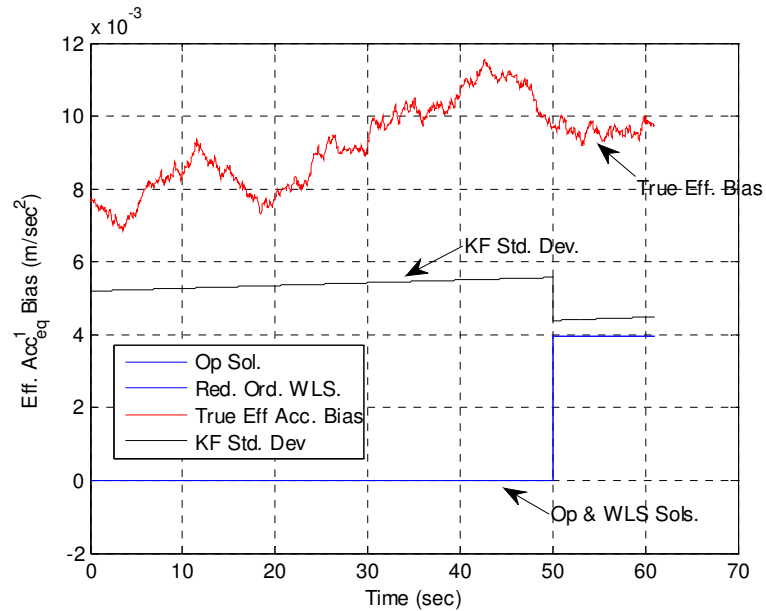
Figure 3-9 : The effective bias estimates on x-axis. The jump in the solution at the 50th second is due to the effect of external position observation.

3.5.2 Example II

In this example, 3 more accelerometers were added to the sensor configuration used in Section 3.5.1. The new sensor configuration is shown in Figure 3.10. These 3 accelerometers are identical with each other but have different error model parameters than the remaining 5 accelerometers. The model parameters (at 25Hz) for the new accelerometers are as follows:

Accelerometer Set 2 (i=6..8)

$$^{i}x_{k+1}^{acc} = 0.9999464\,^{i}x_{k}^{acc} + 2.6^{-6}w_{k}^{acc}$$
$$E\left\{^{i}x_{0}^{acc}\,^{i}x_{0}^{acc^{T}}\right\} = 2.5^{-7}(m/\sec^{2})^{2}$$
$$E\left\{^{i}v_{k}^{acc}\,^{i}v_{k}^{acc^{T}}\right\} = 2.5^{-5}(m/\sec^{2})^{2}$$

$$(3.24)$$

Where v_{k}^{acc} and x_{k}^{acc} represents the VRW and stability error components respectively.
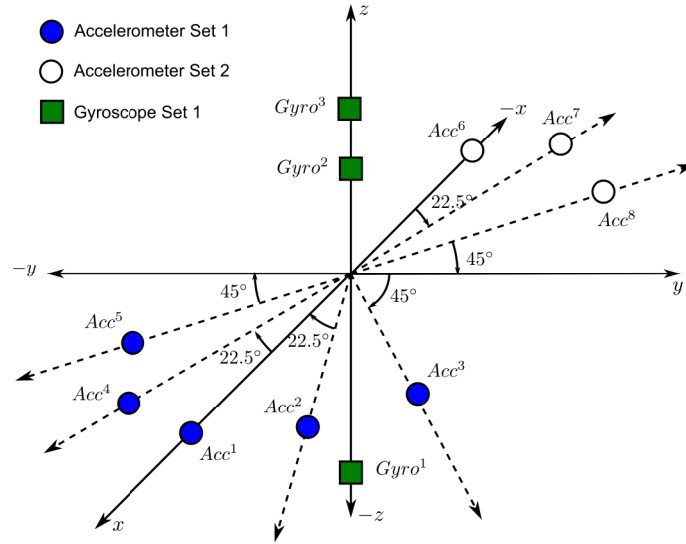
Figure 3-10 : Inertial Sensor configuration for Example II. All accelerometers are on the x-y plane and the gyroscopes are on z-axis. The sensor lever-arms are assumed to be negligible.

The overall sensor observation model for this system can be represented as follows:

$$
y_k^{\text{imu}} = \underbrace{\begin{bmatrix} {}^{S1}M_{acc} & 0_{5\times1} \\ {}^{S2}M_{acc} & 0_{3\times1} \\ 0_{3\times2} & {}^{S1}M_{gyro} \end{bmatrix}}_{M} \underbrace{\begin{bmatrix} a_x \\ a_y \\ \omega_z \end{bmatrix}_k}_{u_k} + \underbrace{\begin{bmatrix} {}^{1}x_k^{\text{acc}} \\ \vdots \\ {}^{8}x_k^{\text{acc}} \\ {}^{1}x_k^{\text{gyro}} \\ \vdots \\ {}^{3}x_k^{\text{gyro}} \end{bmatrix}}_{x_k^{\text{imu}}} + \begin{bmatrix} {}^{S1}v_k^{\text{acc}} \\ {}^{S2}v_k^{\text{acc}} \\ {}^{S1}v_k^{\text{gyro}} \end{bmatrix}
\tag{3.25a}
$$

Where ${}^{S1}M_{acc}$ is the corresponding columns of the first 5 rows of (3.21), ${}^{S1}M_{gyro}$ is the corresponding columns of last 3 rows of (3.21) and ${}^{S2}M_{acc}$ is equal to:

$$
{}^{S1}M_{acc} = \begin{bmatrix} \cos(\pi) & \sin(\pi) \\ \cos(7\pi/8) & \sin(7\pi/8) \\ \cos(6\pi/8) & \sin(6\pi/8) \end{bmatrix}
\tag{3.25b}
$$

Furthermore:

$$^{S1}R_{acc} = E\left\{ ^{S1}v_k^{acc}\,^{S1}v_k^{acc^T} \right\} = 7.5^{-5}\,\mathrm{I}_{5\times5} \qquad (3.25c)$$

$$^{S2}R_{acc} = E\left\{ ^{S2}v_k^{acc}\,^{S2}v_k^{acc^T} \right\} = 2.5^{-5}\,\mathrm{I}_{3\times3} \qquad (3.25d)$$

$$^{S1}R_{gyro} = E\left\{ ^{S1}v_k^{gyro}\,^{S1}v_k^{gyro^T} \right\} = 6.25^{-6}\,\mathrm{I}_{5\times5}. \qquad (3.25e)$$

As the system in Figure 3.10 consists of 3 sets of identical sensors, an equivalent virtual configuration can be generated using the method described in Section 2.4.3.2. This virtual equivalent configuration is shown in Figure 3.11. As seen from this figure, in this virtual configuration there are only 4 accelerometers and 1 gyroscope all of which are placed on the body frame axes. As each x and y axis contains 2 accelerometers, there are still redundancy observations that must be processed to reach the optimum solution. The overall sensor observation model for this virtual equivalent system can be defined as follows:

Let:

$$^{S1}M_{acc}^{\#} = \left(^{S1}M_{acc}^{T}\,^{S1}R_{acc}^{-1}\,^{S1}M_{acc} \right)^{-1}\,^{S1}M_{acc}^{T}\,^{S1}R_{acc}^{-1} \qquad (3.26a)$$

$$^{S2}M_{acc}^{\#} = \left(^{S2}M_{acc}^{T}\,^{S2}R_{acc}^{-1}\,^{S2}M_{acc} \right)^{-1}\,^{S2}M_{acc}^{T}\,^{S2}R_{acc}^{-1} \qquad (3.26b)$$

$$^{S1}M_{gyro}^{\#} = \left(^{S1}M_{gyro}^{T}\,^{S1}R_{gyro}^{-1}\,^{S1}M_{gyro} \right)^{-1}\,^{S1}M_{gyro}^{T}\,^{S1}R_{gyro}^{-1} \qquad (3.26c)$$

$$\overline{M} = \begin{bmatrix} ^{S1}M_{acc}^{\#} & 0 & 0 \\ 0 & ^{S2}M_{acc}^{\#} & 0 \\ 0 & 0 & ^{S1}M_{gyro}^{\#} \end{bmatrix} \qquad (3.26d)$$

$$C^{eq} = \begin{bmatrix} \sqrt{\left({}^{S1}M_{acc}^{T}\,{}^{S1}M_{acc} \right)^{-1}} & 0 & 0 \\ 0 & \sqrt{\left({}^{S2}M_{acc}^{T}\,{}^{S2}M_{acc} \right)^{-1}} & 0 \\ 0 & 0 & \sqrt{\left({}^{S1}M_{gyro}^{T}\,{}^{S1}M_{gyro} \right)^{-1}} \end{bmatrix}$$ (3.26e)

Then:

$$y_k^{imu_{eq}} = \begin{bmatrix} Acc_{eq}^1 \\ Acc_{eq}^2 \\ Acc_{eq}^3 \\ Acc_{eq}^4 \\ Gyro_{eq}^1 \end{bmatrix} = \bar{M}y_k^{imu} = \underbrace{\begin{bmatrix} 1 & 0 & 0 \\ 0 & 1 & 0 \\ 1 & 0 & 0 \\ 0 & 1 & 0 \\ 0 & 0 & 1 \end{bmatrix}}_{M^{eq}} \begin{bmatrix} a_x \\ a_y \\ \omega_z \end{bmatrix}_k + C^{eq}\begin{bmatrix} {}^1x_k^{acc} \\ {}^2x_k^{acc} \\ {}^6x_k^{acc} \\ {}^7x_k^{acc} \\ {}^1x_k^{gyro} \end{bmatrix} + C^{eq}\begin{bmatrix} {}^1v_k^{acc} \\ {}^2v_k^{acc} \\ {}^6v_k^{acc} \\ {}^7v_k^{acc} \\ {}^1v_k^{gyro} \end{bmatrix}$$ (3.27)

It should be noted that the redundancy observation for this equivalent configuration can now be defined using the left null space of M^{eq}.
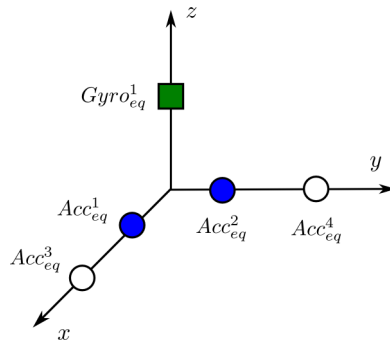
Figure 3-11 : Equivalent virtual configuration for example II

For this example, 4 different methods were identified and implemented:

i.   Optimal Solution:

The structure shown in Figure 3.2 was implemented for this solution. The complete sensor model was used in the Kalman filter and the redundancy observations were derived from (3.25). (The total number of Kalman filter states was 16 for this solution.)

ii.   Reduced order optimal solution:

In this solution the structure shown in Figure 3.2 was implemented using the equivalent

virtual sensor configuration defined in (3.27) and Figure 3.11. (The total number of

Kalman filter states was 10 for this solution)

iii.   Reduced order WLS solution:

The structure presented in Figure 3.5 was implemented using the equivalent virtual

sensor configuration defined in (3.27).

iv.   Pseudo-optimal Solution:

For this solution, the structure shown in Figure 3.4 was implemented using the complete

sensor error and observation models.

These configurations were run using the simulation environment described in Section 3.2.

During the simulations only 1 external position observation at 40th second was processed

by the navigation Kalman filter. In Figure 3.12 and 3.13, the position and x-velocity

solutions of all 4 configurations are presented. From these figures the following

observations can be made:

I.   The optimal and reduced order optimal solutions are exactly the same as

explained in Section 3.4.3.2.

II.   The optimal and pseudo-optimal solutions are almost the same. This shows that

the navigation state aiding provided by redundancy observations is not significant.

III.   WLS solution is not as accurate as optimal and pseudo-optimal solutions. This is

an expected result as the redundancy observations are completely ignored in the

WLS based solution.
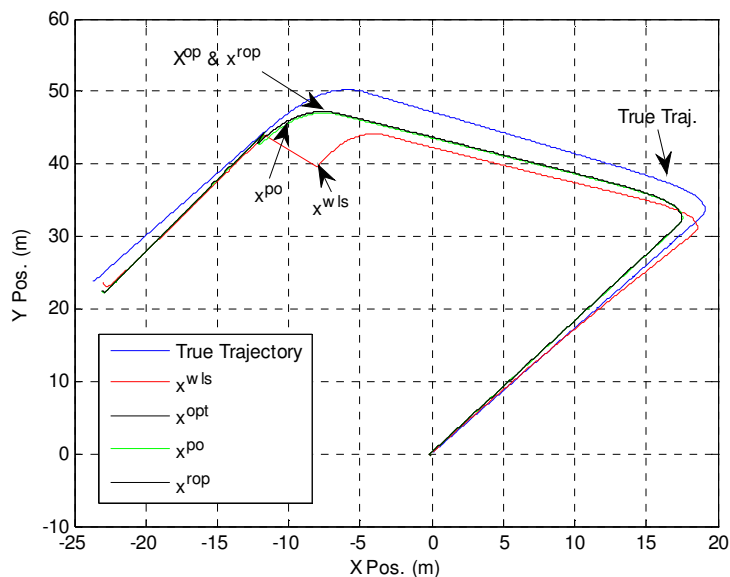
Figure 3-12 : Comparison of position solutions. x^{op} **is the optimal solution (i),** x^{rop} **is the reduced order optimal solution (ii),** x^{wls} **is the WLS based solution (iii) and** x^{po} **is the pseudo-optimal solution (iv)**
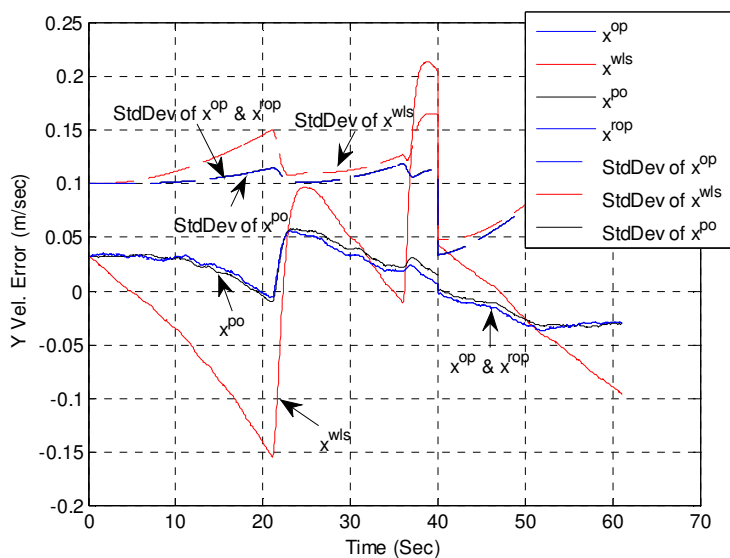
Figure 3-13 : Comparison of x-axis velocity solutions for optimal (x^{op} **), reduced order optimal (** x^{rop} **), WLS (** x^{wls} **) and pseudo-optimal (** x^{po} **) solutions.**

3.5.3 Example III

In this example the same configuration used in Section 3.5.2 (Figure 3.10) was used.

However, in this section it was assumed that all the accelerometers have the same error

model defined in (3.24) except the initial covariance of the accelerometers in set 1

(accelerometers 1-5 in Figure 3.10) which were set to $E\left\{ {}^{i}x_{0}^{\text{acc}}\,{}^{i}x_{0}^{\text{acc}^{T}} \right\}_{i=1}^{5} = 4^{-4}$.

In Figure 3.14, the y-axis velocity errors of 3 different solutions are presented. These

solutions are i)optimal solution (Figure 3.2), ii) pseudo-optimal solution (Figure 3.4) and

iii)WLS based solution (Figure 3.5). As seen from these figures, optimal and pseudo-

optimal solutions are almost the same. However, although all sensor error parameters

except the initial covariance are the same, the WLS and optimal solutions turned out to be

very different. The reason for this difference can be seen from Figure 3.15. In this figure

the effective y-axis accelerometer bias estimation errors ($M^{\#}C_{k}\left(x_{k}^{\text{imu}} - \hat{x}_{k}^{\text{imu}} \right)$) is

presented for the optimal and WLS solutions. As redundancy observations are completely

ignored in WLS solutions, the bias could not be estimated until the external position aid

was processed at the 40th second. On the other hand, as the set 2 accelerometers had

lower initial bias error, the bias errors of set 1 accelerometers could be quickly estimated

in the optimal (and pseudo-optimal) solutions. Hence navigation solution was not

affected by the relatively large bias errors of set 1 in the optimal solution.
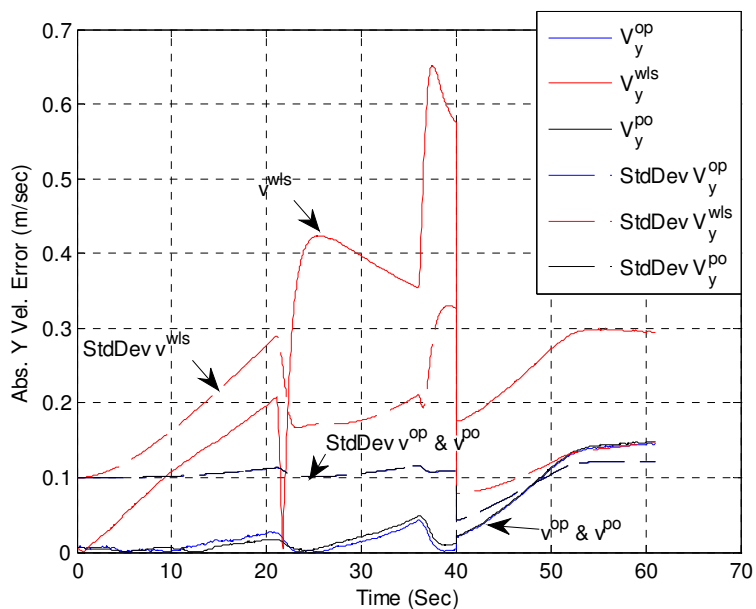
Figure 3-14 : Comparison of y-axis velocity errors for optimal (x^{op}), pseudo-optimal (x^{po}) and WLS (x^{wls}) solutions.
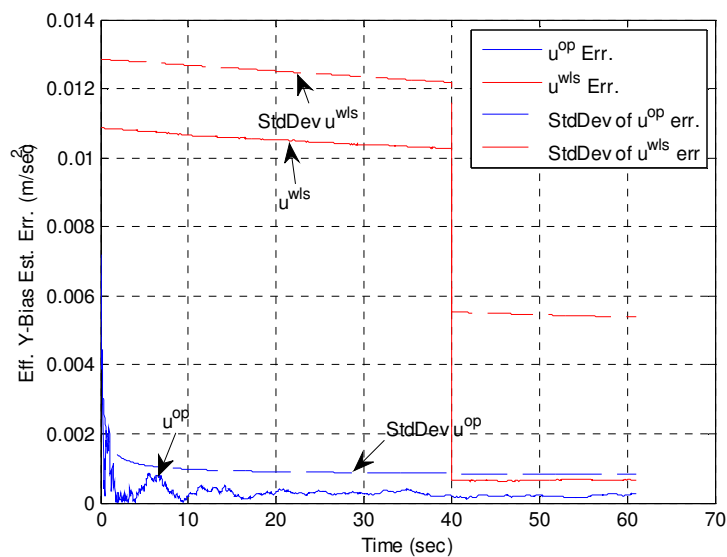
Figure 3-15 : Comparison of the effective y-axis acceleration bias estimation errors for optimal ($\hat{u}^{op}$) and WLS $\hat{u}^{wls}$ solutions.

3.6 Steady State Solution and Effective Sensor Modeling for Pseudo-Optimal Structures

In the pseudo-optimal solutions, the system model of the navigation Kalman filter must

consist of the output error model of the 1st stage IMU Kalman filter. As shown in (3.18),

these error models can theoretically be defined using the error model of each sensor and

the parameters of the 1st stage IMU Kalman filter (e.g. K_k, T_k). However, when an

abundant number of non-identical sensors is used, this approach becomes impractical

because of the increased number of states in the navigation Kalman filter. It should be

noted that, as described in Section 3.4.3, this is not a problem for the identical sensor

case.

On the other hand, for the navigation Kalman filter, the use of exact models as in (3.18) is

not essential. Any error model which approximates the 2nd order stochastic characteristics

of (3.18) can be used in the navigation Kalman filter without compromising the accuracy

too much. Such approximate models can be computed from i) the theoretical

autocorrelation of (3.18) or ii) directly from a test data. In this second test based

approach, the combined output of the SRIMU (after corrected by the IMU Kalman filter)

is collected for sufficiently long time under stationary conditions in the laboratory

environment and the error models are extracted from this combined data ($\hat{u}_{k|k}$) using the

inertial sensor modeling methods.

Although the first approach theoretically seems more accurate, in practice more useful

results can be obtained with the 2nd test based approach, especially for the low cost units.

The reason for this is that as explained in [Yuksel et al., 2010] the low cost sensor errors

are mainly characterized by the external conditions which usually cannot be modeled by

dynamical system representations. Hence, the error models associated with the individual sensors are just a rough approximation of observed characteristics. Therefore, instead of theoretically re-approximating (3.18), which is itself based on approximate models, re-modeling the real combined SRIMU output data using the inertial sensor modeling methods is usually both more practical and more accurate.

On the other hand, the Allan variance method, which is the most accepted sensor modeling method, cannot be used to model combined SRIMU outputs "$\hat{u}_{k|k}$". Allan variance procedure is defined for only single axis data and it completely ignores any cross correlation between the errors on different axis. However, depending on the sensor configuration, the errors on the IMU KF outputs can be highly correlated for each kinematic axis.

In a recent paper [Yuksel et al., 2010], a new sensor error modeling method which is also capable of modeling the cross-correlations between axes has been introduced. In this section the application of this modeling method for the combined SRIMU outputs (output of the 1st stage IMU KF) of the pseudo-optimal solutions is described. As the modeling method assumes that the sensor errors are stationary, first a discussion about the steady state characteristics of the IMU Kalman filters will be presented in Section 3.6.1. Then in Section 3.6.2, modeling the steady state IMU Kalman filter output errors will be explained using simulated data examples.

3.6.1 Steady State IMU Kalman Filters

When the individual sensor errors do not contain any time varying component (such as the scale factor and temperature dependent bias errors), the time-varying (and optimal)

gain of the 1st stage IMU Kalman filter in the pseudo-optimal solution can be replaced by a steady state Kalman gain to eliminate the need for any Kalman filter recursion. In general as the associated Ricatti equation for the IMU Kalman filter does not have a unique solution (because in almost all cases the SRIMU system models are not detectable and stabilizable), these steady gains can only be defined as the solution to which the Newton iterations converge. Although those converged solutions depend on the initial covariance, in practice such deviations from real steady state gains do not lead to significant difference.

The adverse effect of using constant gain becomes apparent when the individual sensors have strong random constant type repeatability errors. Regardless of whether such states are observable or not, the Kalman gain corresponding to these states becomes 0 in the steady state conditions. When these random constant type states are indeed observable, the optimal (time-varying) Kalman filter can estimate these states whereas in the suboptimal filters with constant steady state gains these states are not estimated at all. On the other hand, in practice the use of optimal (time-varying) Kalman filters does not always mean better results for these repeatability errors. As explained in [Yuksel et. al. 2010], the determination of initial covariance values for the repeatability errors is generally very difficult. Hence, usually some approximate covariance values are used in the Kalman filters. Therefore, even if the optimal Kalman filters are used, in most cases the estimation results for these repeatability errors are far from being optimal due to these initial covariance mismatches.

In the next section, simulated data results comparing steady state and (time-varying) Kalman filter outputs will be presented.

3.6.2 Simulated data results for Steady State IMU Kalman Filters and output modeling

In this section the sensor configuration presented in Figure 3.16 was used in the simulations. As seen from this figure, the SRIMU unit contains 5 accelerometers on the x-y plane and 2 gyroscopes on the z-axis. The overall output model for this configuration is as follows:

$$
x_{k+1}^{imu} = \mathrm{diag}\begin{pmatrix} 0.9998666 \\ 0.9999047 \\ 0.9999166 \\ 0.9999333 \\ 0.9999444 \\ 0.9998888 \\ 0.9999333 \end{pmatrix} x_k^{imu} + \mathrm{diag}\begin{pmatrix} 2.59^{-6} \\ 2.59^{-6} \\ 3.67^{-6} \\ 3.67^{-6} \\ 4.5^{-6} \\ 1.99^{-6} \\ 2.82^{-6} \end{pmatrix}\begin{bmatrix} {}^1 w_k \\ \vdots \\ {}^7 w_k \end{bmatrix} \tag{3.28a}
$$

$$
E\left\{ x_0^{imu} x_0^{imu^T} \right\} = \mathrm{diag}\begin{pmatrix} 1.25^{-6} \\ 1^{-6} \\ 7.5^{-7} \\ 5^{-7} \\ 2.5^{-7} \\ 6^{-5} \\ 6^{-9} \end{pmatrix} \tag{3.28b}
$$

$$
y_k^{imu} = \begin{bmatrix} Acc^1 \\ \vdots \\ Acc^5 \\ Gyro^1 \\ Gyro^2 \end{bmatrix} = \underbrace{\begin{bmatrix} \cos(0) & \sin(0) & 0 \\ \cos(2\pi/16) & \sin(2\pi/16) & 0 \\ \cos(4\pi/16) & \sin(4\pi/16) & 0 \\ \cos(6\pi/16) & \sin(6\pi/16) & 0 \\ \cos(8\pi/16) & \sin(8\pi/16) & 0 \\ 0 & 0 & -1 \\ 0 & 0 & 1 \end{bmatrix}}_{M}\begin{bmatrix} a_x \\ a_y \\ \omega_z \end{bmatrix}_k + x_k^{imu} + v_k^{imu} \tag{3.28c}
$$

$$
E\left\{ v_k^{imu} v_k^{imu^T} \right\} = \begin{bmatrix} 2.5^{-5}I_{5\times5} & 0 \\ 0 & 6.25^{-6}I_{2\times2} \end{bmatrix} \tag{3.28d}
$$

In (3.28) x_k^{imu} represents the stability error states for the entire SRIMU. It is assumed that all sensors have stability errors in the form of 1st order Markov processes which are also time-invariant. As seen from (3.28b), significantly different initial error covariance values are used for each sensor. However, as shown in (3.28d), it was assumed that all accelerometers and gyroscopes have identical random walk (additive white noise) components.

The same navigation mechanization equations and trajectory described in Section 3.2 was used in all simulations. In addition to inertial data, an external velocity observation is generated for the navigation Kalman filter to process at 0.1Hz.

For this simulation 3 different solutions were implemented:

i) Pseudo-optimal solution with optimal gain

ii) Pseudo-optimal solution with constant steady state gain

iii) Pseudo-optimal solution with constant steady state gain and approximate sensor error models
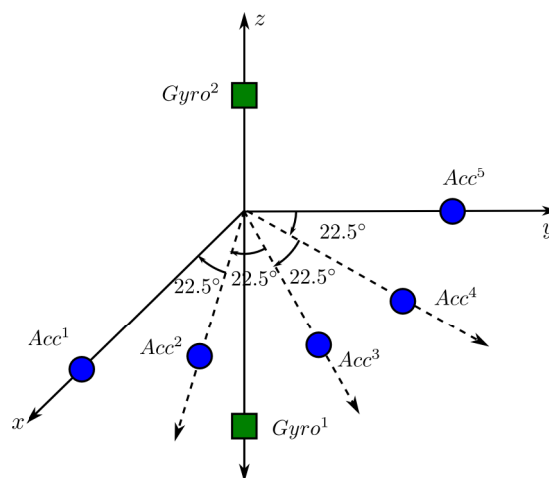
Figure 3-16 : Sensor configuration. All accelerometer are placed on the 1st quadrant of the x-y plane

The solution "i" was the direct implementation of Figure 3.4. (3.28) was used as the sensor error model in IMU Kalman filter and (3.18) was used the equivalent sensor error model in the navigation Kalman filter.

In the solution "ii", the IMU KF was executed with the steady state Kalman gain instead of the optimal time varying gain. This steady state gain was computed using Newton iterations over corresponding Ricatti equation starting from the initial covariance defined in (3.28b). The sensor error models in the navigation Kalman filter were derived using (3.18), but with the computed steady state gain.

The solution "iii" is similar to the solution "ii". However in this solution, the sensor error models in the navigation Kalman filter were derived from a simulated test data. For this purpose, 8 hours of stationary data for the system in Figure 3.16 was generated. This data is then processed by only the IMU Kalman filter with the constant steady state gain to

obtain the kinematic variable estimates ($\hat{u}_{k|k}$). Then the sensor error modeling method

described in [Yuksel et al., 2010] was applied to these $\hat{u}_{k|k}$ estimates.

The computed autocorrelation curves and fitted exponentials to these curves for the x and

y accelerations are presented in Figure 3.17. These curves were obtained at the 10th

filtering level (the filtering and exponential curve fitting operations are explained in

[Yuksel et. al. 2010]). From the fitted exponentials (including the exponential for the z-

gyroscope which is not shown in Figure 3.17), the following approximate error model

was extracted as described in [Yuksel 2010 et al.]:

$$x_{k+1}^{imu_{apx}} = \begin{bmatrix} 0.999899 & 0 & 0 \\ 0 & 0.999921 & 0 \\ 0 & 0 & 0.999871 \end{bmatrix} x_{k+1}^{imu_{apx}} + w_k^{apx} \tag{3.29a}$$

$$E\left\{w_k^{apx} w_k^{apx^T}\right\} = \begin{bmatrix} 4.18^{-12} & -3.59^{-12} & 0 \\ -3.59^{-12} & 1.05^{-11} & 0 \\ 0 & 0 & 3.9^{-12} \end{bmatrix} \tag{3.29b}$$

$$\tilde{u}_{k|k}^{apx} = x_k^{imu_{apx}} + v_k^{imu_{apx}} \tag{3.29c}$$

$$E\left\{v_k^{imu_{apx}} v_k^{imu_{apx}^T}\right\} = \begin{bmatrix} 1.304^{-5} & -6.27^{-6} & 0 \\ -6.27^{-6} & 1.303^{-5} & 0 \\ 0 & 0 & 3.11^{-6} \end{bmatrix} \tag{3.29d}$$

where $\tilde{u}_{k|k}^{apx}$ represents the errors on the $\hat{u}_{k|k}$ which is computed as a result of the IMU

Kalman filter. As seen from (3.29a) and (3.29d) the errors on the x and y axis

accelerations are strongly correlated with each other. If the Allan variance method had

been used to model $\hat{u}_{k|k}$ sequence, these cross-correlation effects could not be modeled at

all.
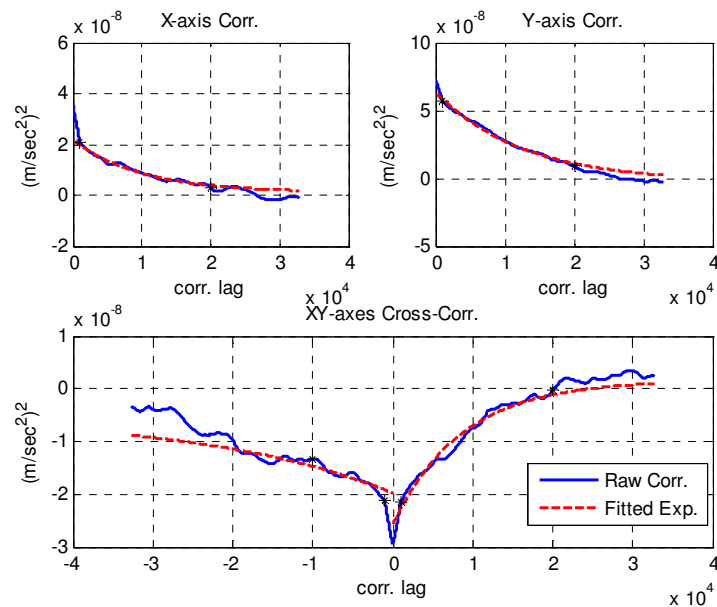
Figure 3-17 : Computed correlation of simulated (generated) $\hat{u}_{k|k}$ sequence for the x and y accelerations. The solid blue curves represent the computed correlation of raw data. Dashed red curves represent the fitted exponential functions for the corresponding correlations.

In Figure 3.18, the theoretical autocorrelation of (3.29ac) is compared with the theoretical autocorrelation of the output of steady state IMU Kalman filter (which was derived based on (3.28) and the steady state Kalman gain). As can be seen from this figure, although only 3 states are used in the approximate model of (3.29), the final 2nd order characteristics of the both models (stability parts for the approximate model of (3.29) and the true model of (3.18)) are very similar. This figure verifies the fact that the new error modeling method described in [Yuksel et. al. 2010] can be used to obtain approximate error models with less number of states for SRIMU systems.
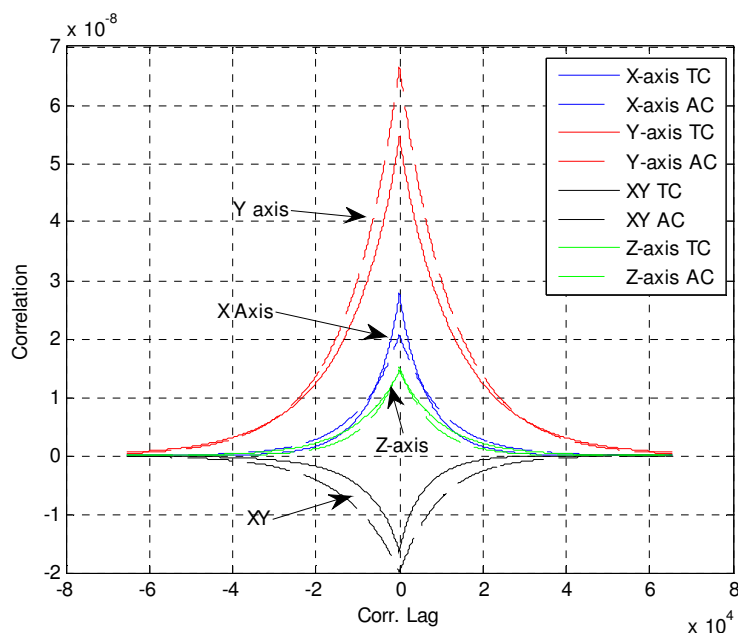
Figure 3-18 : Comparison of theoretical autocorrelation of (stability part of) approximate model (3.29) and true model (3.18) (which is derived from (3.28)). Solid curves represent the true model's autocorrelation whereas dashed curves represent the approximate model's autocorrelation.

The position results of the 3 types of solutions described above are presented in Figure 3.19. As shown in this figure, there is no significant difference between the navigation results obtained with the theoretical error model of (3.18) with the steady state gain and the reduced order approximate model of (3.29). The navigation filters which use these error models (solutions "ii" and "iii") produced almost exactly the same position solution. However, as can be seen from the same figure, the results of the configurations which use the steady state IMU filters (solutions "ii" and "iii") are slightly worse than the configuration which uses the optimal Kalman gain in the IMU filter (solution "i"). The main reason for this difference lies in the initial stability error covariance values of the 2

107

gyroscopes. As can be seen from the last two elements of (3.28b) the initial covariance of

$Gyro^1$ is 10^4 times bigger than $Gyro^2$. As the steady state Kalman filter does not

consider this difference, the heading angle computed using the results of the steady state

IMU Kalman filter is also corrupted by these initial gyroscope biases.
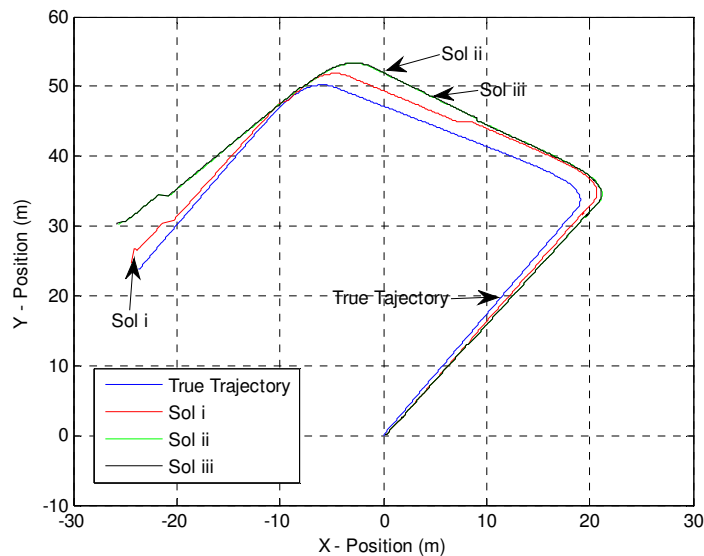
Figure 3-19 : Comparison of position results for 3 implementations. "Sol i" is the pseudo-optimal solution, "Sol ii" is the pseudo-optimal solution with steady state IMU Kalman filter and "Sol iii" is the pseudo-optimal solution with steady state gain and approximate error models.

The heading angle estimation errors for all 3 types of implementation are presented in

Figure 3.20. As seen from this figure, the IMU Kalman filter with the optimal gain can

quickly estimate the initial bias error of gyroscope 1 using the outputs of gyroscope 2,

and hence leads to better heading angle results. This figure also verifies that when

different sensors have very large initial bias errors and when these biases are correctly

modeled in the IMU Kalman filter, the optimal gain can lead to better navigation

solutions than the IMU Kalman filter with steady state gains. However, it should be noted

that for real sensors these initial bias differences are usually not as much as it was used

for this simulation. Therefore, in most practical cases, the IMU Kalman filters with

steady state gains also provide similar navigation solutions with the optimal gains.
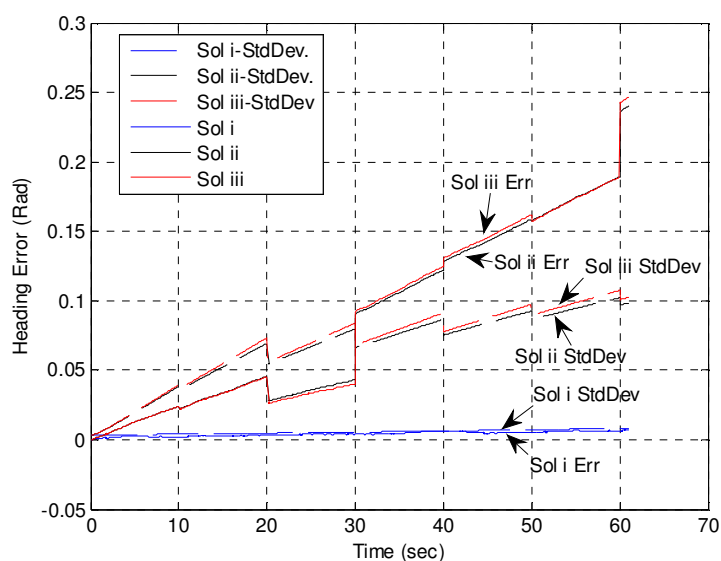
Figure 3-20 : Comparison of heading angle error for 3 types of solutions. Solid lines represent the errors and dashed lines represent the standard deviation estimates of navigation Kalman Filter. Sol i, ii and iii are as described in Section 3.6.3.

Chapter Four: **Comparison of Multi-INS and Single-INS Solutions for the Skew Redundant Inertial Measurement Unit based Inertial Navigation systems**

4.1 Introduction

The optimal navigation solution for the SRIMU based INSs has been introduced in Chapter 2 and 3. The optimal solution described in these chapters leads to the following SRIMU based strapdown implementation steps (the symbols are defined in Section 3.3):

i.   Compute $\hat{u}_k^{wls} = M^{\#} y_k^{\mathrm{imu}}$ (the weighted least square estimate of kinematic variables)

ii. Run a single strapdown implementation using $\hat{u}_k^{wls}$

iii. Generate Kalman filter observations as the projection of y_k^{imu} into left null space of configuration matrix M.

iv. Run a Kalman filter with these redundancy observations and correct the navigation and sensor error states.

As seen from these steps, this optimal approach uses only a single strapdown implementation. On the other hand, in the existing literature there exists another type of solution which utilizes multiple strapdown implementations for SRIMU systems. Such multi-INS based methods are presented in [Colomina et al., 2004], [Waegli et al., 2008] and [Bancroft 2009]. Although these studies are generally ambiguous and contain some inconsistent points, they can still be regarded as important because they present some field test results with real redundant sensors. The main structure of the proposed methods in these studies can be summarized as follows:

i.   For each complete sensor set (e.g. 3 accelerometers and gyroscopes for 6DoF navigation) a separate INS is implemented (the existing studies do not consider the case in which the number of sensors are not suitable for such exact grouping).

ii.   Kalman filter observations are generated in the form of the equivalence of the navigation states of different INSs (i.e. PVA of INS1=PVA of INS2 etc)

iii.   A Kalman filter is run with these equivalency observations and each individual strapdown INS and IMU error states are corrected with the filtered estimates.

Although the aforementioned studies ([Colomina et al., 2004], [Waegli et al., 2008], [Bancroft 2009]) can successfully explain the general structure of multi-INS configurations for SRIMUs, all these 3 studies lack the theoretical background and contain some errors which render their conclusions unreliable. For instance, the two methods ("synthetic mechanization" and "extended mechanization") described in [Colomina et al., 2004] and [Waegli et al., 2008] as different methods are theoretically identical. Therefore, in contrast to what was claimed in the corresponding studies, the outputs of these methods must be the same. Also, in [Bancroft 2009], the external observations are processed as if they are independent for each INS which is not a correct way of using these external measurements.

In this chapter, the theory that is presented in the previous chapters based on single INS implementations is extended to cover multi-INS implementations.

In Section 4.2, it is shown that the multi-INS implementation is just a reformulation of single INS implementation with redundant number of navigation states.

In Section 4.3, the relation between 2 types of observations (i.e. observations based on equivalence of navigation states in multi-INS implementations and observations based on

the projection of sensor outputs to the left null space of configuration matrix) are described. It is proved that these 2 types of observation are equivalent under some conditions.

Section 4.4 describes the processing of external PVA type observations in multi-INS systems. For single INS implementations the processing of external measurements with the standard navigation Kalman filter is trivial. However, for multi-INS systems there exist several different ways of processing these measurements. Although all of these alternatives are theoretically equivalent to each other, in practice the selected approach can have some effects on the overall system stability. These differences will be presented in Section 4.5 using some simulated data examples.

The effect of unknown and time-varying boresight between inertial sensors on the final navigation solution is also analyzed in Section 4.5. Using simulations, it is shown that multi-INS implementation can be better modified to reduce the effect of the unknown bore-sight factors in SRIMU based navigation systems.

4.2 Optimal Processing of SRIMU outputs using Multi-INS implementations

In Chapter 2, it was shown that the optimal x_k estimate ($\hat{x}_{k|k}$) for:

$$x_{k+1} = A_k x_k + N_k u_k + B_k w_k \tag{4.1a}$$

$$y_k = C_k x_k + M_k u_k + v_k \tag{4.1b}$$

is equal to the Kalman filter output for the following system:

$$x_{k+1} = A_k x_k + N_k M_k^{\#}\left(y_k - C_k x_k\right) + B_k w_k - N_k M_k^{\#} v_k \tag{4.2a}$$

$$T_k y_k = T_k C_k x_k + T_k v_k \tag{4.2b}$$

where $E\{v_k v_k^T\} = R_k$, $E\{w_k w_k^T\} = Q_k$, $M_k^{\#} = \left(M_k^T R_k^{-1} M_k\right)^{-1} M_k^T R_k^{-1}$ and T_k is the basis

matrix for the left null space of M_k (i.e. $T_k M_k = 0$). (The rest of the parameters are

defined in Chapter 2 – Lemma 3.)

In this section, it is shown that the Kalman filter output for the system in (4.2) is also

equivalent to the Kalman filter output for the following system:

$$x_{k+1} = A_k x_k + N_k M_k^* \left(y_k - C_k x_k\right) + B_k w_k - N_k M_k^* v_k \qquad (4.3a)$$

$$T_k y_k = T_k C_k x_k + T_k v_k \qquad (4.3b)$$

where M_k^* is any matrix (not necessarily $M_k^{\#}$) such that $M_k^* M_k = I$.

First of all, it should be noted that, using the linearity property, the system defined in

(4.2) and (4.3) can be expressed as the sum of stochastic and deterministic subsystems. If

the deterministic subsystem is considered as a nominal trajectory, the stochastic part

represents the propagation of errors defined around the nominal trajectory which is

generated by the input $\hat{u} = M^{\#} y_k$ (for (4.2)) or $\hat{u} = M^* y_k$ (for (4.3)).

To prove the equivalence of the Kalman filter results for the systems defined in (4.2) and

(4.3), it will be shown that the optimal Kalman filter form of (4.3) has exactly the same

system model defined in (4.2).

The system noise "$B_k w_k - N_k M_k^* v_k$" and the observation noise "$T_k v_k$" of (4.3) are

correlated with each other. Therefore, as described in [Kailath et al., 2000 – Chapter 9.5],

the optimal Kalman filter for (4.3) must use the following model:

$$x_{k+1} = A_k x_k + N_k M_k^* \left(y_k - C_k x_k\right) - N_k \left(S_k \bar{R}_k \left(T_k y_k - T_k C_k x_k\right) + \tilde{v}_k\right) + B_k w_k \qquad (4.4a)$$

$$T_k y_k = T_k C_k x_k + T_k v_k \qquad (4.4b)$$

where,

$$\bar{R}_k = \left(T_k R_k T_k^T\right)^{-1} \tag{4.4c}$$

$$S_k = E\left\{\left(M_k^* v_k\right)\left(T_k v_k\right)^T\right\} = M_k^* R_k T_k^T \tag{4.4d}$$

$$E\left\{\tilde{v}_k \tilde{v}_k^T\right\} = M_k^* R_k M_k^{*T} - S_k \bar{R}_k S_k^T \tag{4.4e}$$

(4.4a) can be re-arranged as follows:

$$x_{k+1} = A_k x_k + N_k \left(\left(M_k^* - S_k \bar{R}_k T_k\right)\left(y_k - C_k x_k\right)\right) - N_k \tilde{v}_k + B_k w_k \tag{4.5}$$

Furthermore, using (2.51), it can be shown that:

$$\begin{aligned}
\left(M_k^* - S_k \bar{R}_k T_k\right) &= M_k^* - M_k^* R_k T_k^T \left(T_k R_k T_k^T\right)^{-1} T_k \\
&= \left(M_k^T R_k^{-1} M_k\right)^{-1} M_k^T R_k^{-1} \triangleq M^\#
\end{aligned} \tag{4.6}$$

Also,

$$\begin{aligned}
E\left\{\left(B_k w_k - N_k \tilde{v}_k\right)\left(B_k w_k - N_k \tilde{v}_k\right)^T\right\} &= Q_k + N_k \left(\left(M_k^* - M_k^* R_k T_k \left(T_k R_k T_k^T\right)^{-1} T_k\right) R_k M_k^*\right) N_k^T \\
&= Q_k + N_k \left(M_k^\# R_k M_k^{*T}\right) N_k^T \\
&= Q_k + N_k \left(M_k^T R_k^{-1} M_k\right)^{-1} N_k^T \\
&= E\left\{\left(B_k w_k - N_k M_k^\# v_k\right)\left(B_k w_k - N_k M_k^\# v_k\right)^T\right\}
\end{aligned} \tag{4.7}$$

Replacing (4.7) and (4.6) into (4.5) the following system model is obtained:

$$x_{k+1} = A_k x_k + N_k \left(M_k^\#\left(y_k - C_k x_k\right)\right) + B_k w_k - N_k M_k^\# v_k \tag{4.8}$$

(4.8) is exactly the same as (4.3a). Therefore, the optimal estimation solutions of (4.4) and (4.3) are algebraically equivalent as claimed above.

This result can be extended to the multi-INS implementations as follows:

Let $^A M_k^* \ldots {}^L M_k^*$ be L different matrices such that

$$^{A}M_{k}^{*}M_{k} = \ldots = {}^{L}M_{k}^{*}M_{k} = \mathrm{I} \tag{4.9}$$

Then, given an SRIMU with a configuration matrix M, it is possible to implement L different SINS all of which are run by independent sets of sensors. Hence (using the terminology defined in Chapter 3), the combined system model for the entire multi-INS system can be written as follows:

$$
\begin{aligned}
^{A}x_{k+1}^{\mathrm{nav}} &= A_{k}^{\mathrm{nav}}\,^{A}x_{k}^{\mathrm{nav}} + N_{k}\,^{A}M_{k}^{*}\left(y_{k} - C_{k}^{\mathrm{imu}}x_{k}^{\mathrm{imu}} - v_{k}^{\mathrm{imu}}\right) + w_{k}^{\mathrm{nav}} \\
&\vdots \\
^{L}x_{k+1}^{\mathrm{nav}} &= A_{k}^{\mathrm{nav}}\,^{L}x_{k}^{\mathrm{nav}} + N_{k}\,^{L}M_{k}^{*}\left(y_{k} - C_{k}^{\mathrm{imu}}x_{k}^{\mathrm{imu}} - v_{k}^{\mathrm{imu}}\right) + w_{k}^{\mathrm{nav}} \\
x_{k+1}^{\mathrm{imu}} &= A_{k}^{\mathrm{imu}}x_{k}^{\mathrm{imu}} + w_{k}^{\mathrm{imu}}
\end{aligned}
\tag{4.9a}
$$

$$T_{k}y_{k}^{\mathrm{imu}} = T_{k}C_{k}^{\mathrm{imu}}x_{k}^{\mathrm{imu}} + T_{k}v_{k}^{\mathrm{imu}} \tag{4.9b}$$

where, rows of T_{k} are the basis of the left null space of M_{k}, $\left\{{}^{i}x_{k}^{\mathrm{nav}}\right\}_{i=A}^{L}$ represents the navigation states for each SINS implementation and ${}^{A}x_{0}^{\mathrm{nav}} = \ldots = {}^{L}x_{0}^{\mathrm{nav}}$.

In (4.9) the system noise for each navigation model ($w_{k}^{\mathrm{nav}} - N_{k}\,^{i}M_{k}^{*}v_{k}^{\mathrm{imu}}$) and observation noise ($T_{k}v_{k}^{\mathrm{imu}}$) are correlated. Therefore, these cross-correlations must be removed for the Kalman filter. When such a removal operation is performed as shown in (4.4), the overall system model has exactly the same x_{k}^{nav} model for each SINS implementation. In this case, the overall system model can be represented as:

$$
\begin{aligned}
^{A}x_{k+1}^{\mathrm{nav}} &= \ldots = {}^{L}x_{k+1}^{\mathrm{nav}} = x_{k+1}^{\mathrm{nav}} = A_{k}^{\mathrm{nav}}x_{k}^{\mathrm{nav}} + N_{k}M_{k}^{\#}\left(y_{k} - C_{k}x_{k}^{\mathrm{imu}} - v_{k}^{\mathrm{imu}}\right) + w_{k}^{\mathrm{nav}} \\
x_{k+1}^{\mathrm{imu}} &= A_{k}^{\mathrm{imu}}x_{k}^{\mathrm{imu}} + w_{k}^{\mathrm{imu}}
\end{aligned}
\tag{4.10a}
$$

$$T_{k}y_{k}^{\mathrm{imu}} = T_{k}C_{k}^{\mathrm{imu}}x_{k}^{\mathrm{imu}} + T_{k}v_{k}^{\mathrm{imu}} \tag{4.10b}$$

This shows that multi-INS type implementations are nothing but just the repetitions of the same navigation states for each implementation in the overall state vector.

The key conclusions of this section can be summarized as follows:

i. The selection of nominal trajectory has theoretically no effect on the Kalman filter solution as long as the observations are optimally processed.

ii. If the nominal trajectory is generated by inputs other than $\hat{u}_k = M_k^{\#} y_k^{\text{imu}}$, then in the Kalman filter for the optimal solution, the cross-correlations between the system and observation noises must be corrected. Once this correction is done, the system model becomes exactly equivalent to the system model which is obtained with the nominal trajectory generated by $\hat{u}_k = M_k^{\#} y_k^{\text{imu}}$.

4.3 Optimal solution based on the equivalency of navigation states for multi-INS implementations

In the previous section, all the observations obtained from the redundancy of the sensors are represented using $T_k y_k^{\text{imu}}$ as described in Chapter 2. However, in the related literature (e.g. [Colomina et al., 2004], [Bancroft 2009]), the equivalence of the navigation states of different strapdown implementations are used as the only form of the redundancy observations in the multi-INS configurations instead of the $T_k y_k^{\text{imu}}$.

In this section, the relation between these equivalency based observations and the sensor based observations ($T_k y_k^{\text{imu}}$) are explained. Also, the conditions for which the navigation state equivalence type observations lead to optimal solution are derived.

The observation model for the multi strapdown implementations (whose system model is defined in (4.9a)) can be represented as follows:

$$y_k^{eq} = 0 = {}^A x_k^{nav} - {}^B x_k^{nav}$$
$$= {}^B x_k^{nav} - {}^C x_k^{nav}$$
$$\vdots$$
$$= {}^{L-1} x_k^{nav} - {}^L x_k^{nav}$$

(4.11)

At k=0, the states are all equivalent by definition. Therefore, y_0^{eq} has no effect.

At k=1:

$${}^A x_1^{nav} - {}^B x_1^{nav} = A_0^{nav} \left({}^A x_0^{nav} - {}^B x_0^{nav} \right) + N_0 \left({}^A M_0^* - {}^B M_0^* \right) \left(y_0^{imu} - C_0^{imu} x_0^{imu} - v_0^{imu} \right) + \left(w_0^{nav} - w_0^{nav} \right)$$
$$= N_0 \left({}^A M_0^* - {}^B M_0^* \right) \left(y_0^{imu} - C_0^{imu} x_0^{imu} - v_0^{imu} \right)$$

(4.12)

For the navigation applications N_k is a full column rank matrix. Therefore (4.11) can be

rewritten as:

$${}^A x_1^{nav} - {}^B x_1^{nav} = \left({}^A M_0^* - {}^B M_0^* \right) \left(y_0^{imu} - C_0^{imu} x_0^{imu} - v_0^{imu} \right) = 0$$
$$\vdots$$
$${}^{L-1} x_1^{nav} - {}^L x_1^{nav} = \left({}^{L-1} M_0^* - {}^L M_0^* \right) \left(y_0^{imu} - C_0^{imu} x_0^{imu} - v_0^{imu} \right) = 0$$

(4.13)

Let D_0 be as:

$$D_0 = \begin{bmatrix} {}^A M_0^* - {}^B M_0^* \\ \vdots \\ {}^{L-1} M_0^* - {}^L M_0^* \end{bmatrix}$$

(4.14)

Then (4.13) can be rewritten as:

$$D_0 y_0^{imu} = D_0 C_0^{imu} x_0^{imu} + D_0 v_0^{imu}$$

The same line of derivation can be used to verify that the reverse is also true (i.e.

$D_0 y_0^{imu} = D_0 C_0^{imu} x_0^{imu} + D_0 v_0^{imu} \Rightarrow y_1^{eq} = 0$). Furthermore, these derivations also hold for

any "k". Therefore:

$$y_{k+1}^{eq} = 0 \Leftrightarrow D_k y_k^{\text{imu}} = D_k C_k^{\text{imu}} x_k^{\text{imu}} + D_k v_k^{\text{imu}} \quad , \forall k \tag{4.15}$$

From (4.15) it can be seen that navigation state equivalency constraint at time "k" is equivalent to some form of sensor redundancy observations at "k-1".

In the previous section it was shown that the Kalman filter with the sensor redundancy observations in the form of $T_k y_k^{\text{imu}}$ is the optimal solution for the SRIMU systems.

Therefore, it is concluded that the Kalman filter for the system (4.9a) and observation in (4.11) is optimal if and only if $D_k \equiv T_k$ for $\forall k$. It should be noted that this equivalence is defined as the equivalency of range spaces of the corresponding matrices rather than an algebraic equivalence.

The consequences of this result are hard to see in this general matrix form. Therefore, in the next section these consequences are clarified using a fictitious navigation system example.

4.3.1 Simulated data results for multi-system implementations

4.3.1.1 Case I: Different Inertial Sensor Characteristics

In this section, several results for a (fictitious) multi-sensor based navigation system are presented and compared. The overall model for this (fictitious) system is as follows:

$$x_{k+1}^{\text{nav}} = \underbrace{\begin{bmatrix} 1 & 0 \\ 0 & 1 \end{bmatrix}}_{A^{\text{nav}}} x_k^{\text{nav}} + \underbrace{\begin{bmatrix} 1 & 0 \\ 0 & 1 \end{bmatrix}}_{N} u_k \tag{4.16a}$$

$$x_{k+1}^{\text{imu}} = A^{\text{imu}} x_k^{\text{imu}} + w_k$$

$$y_k^{\text{imu}} = \begin{bmatrix} {}^A y_k^{\text{imu}} \\ {}^B y_k^{\text{imu}} \end{bmatrix} = \underbrace{\begin{bmatrix} {}^A M \\ {}^B M \end{bmatrix}}_{M} u_k + x_k^{\text{imu}} + \underbrace{\begin{bmatrix} {}^A v_k^{\text{imu}} \\ {}^B v_k^{\text{imu}} \end{bmatrix}}_{v_k^{\text{imu}}} \tag{4.16b}$$

These equations represent the body velocity of a non-rotating system on a planar surface. u_k denotes the velocity increments (integral of body acceleration in a defined discretization period) (a_x, a_y) on each axis which are measured by 5 different accelerometer placed on the x-y plane as shown in Figure 4.1. The model parameters for the sensor error (x_k^{imu}) and navigation states (x_k^{nav}) are as follows:

$$A^{imu} = 0.99998 I_{5\times5} \tag{4.17a}$$

$$Q = E\left\{w_k w_k^T\right\} = \mathrm{diag}\left(\underbrace{2.495^{-9}}_{\chi}, 10\chi, 100\chi, 0.1\chi, 0.01\chi\right) \tag{4.17b}$$

$$R = E\left\{v_k^{imu} v_k^{imu^T}\right\} = \mathrm{diag}\left(\overbrace{\underbrace{4^{-6}}_{\chi}, 0.1\chi, 0.01\chi}^{{}^A R}, \overbrace{10\chi, 100\chi}^{{}^B R}\right) \tag{4.17c}$$

$$E\left\{x_0^{imu} x_0^{imu^T}\right\} = \mathrm{diag}\left(\underbrace{6.25^{-7}}_{\chi}, 0.1\chi, 0.01\chi, 10\chi, 100\chi\right) \tag{4.17d}$$

$$E\left\{x_0^{nav} x_0^{nav^T}\right\} = 1^{-4} I_{2\times2} \tag{4.17e}$$

In the above set of definitions all the values are selected in a way that all sensors have complimentary characteristics. As described in Chapter 3, the effectiveness of the redundancy measurements can be observed much easily under such complimentary configurations.
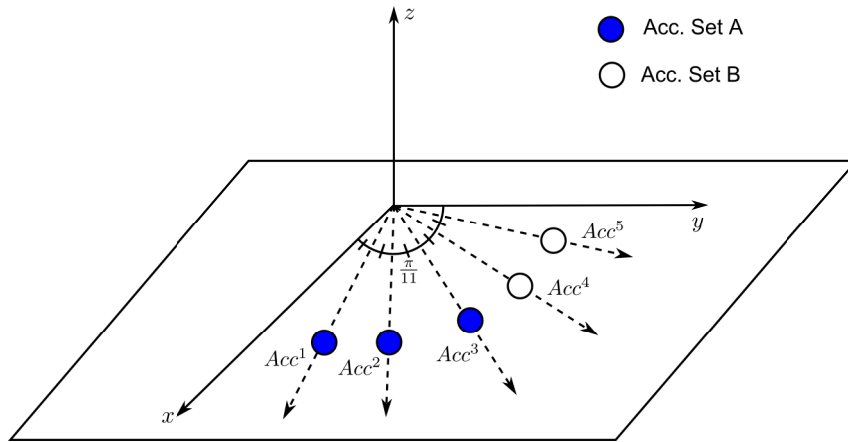
Figure 4-1 : Sensor configuration for the fictitious 2Dof navigation system

In this example, the 5 accelerometers are divided into 2 sub-sets to define 2 separate INS implementations for multi-INS based solutions. The first 3 accelerometers ($Acc^{1,2,3}$) in Figure 4.1 are referred to as Set-A, whereas the rest ($Acc^{4,5}$) are Set-B.

The configuration matrices for these sets of sensors are as follows:

$$
^{A}M = \begin{bmatrix} \cos(\pi/11) & \sin(\pi/11) \\ \cos(2\pi/11) & \sin(2\pi/11) \\ \cos(3\pi/11) & \sin(3\pi/11) \end{bmatrix} \tag{4.18a}
$$

$$
^{B}M = \begin{bmatrix} \cos(4\pi/11) & \sin(4\pi/11) \\ \cos(5\pi/11) & \sin(5\pi/11) \end{bmatrix} \tag{4.18b}
$$

$$
M = \begin{bmatrix} ^{A}M \\ ^{B}M \end{bmatrix} \tag{4.18c}
$$

For this system, 5 different solution methods were implemented both to compute the navigation solution and to estimate the individual sensor errors. These methods are summarized below.

Solution I: Optimal solution based on single INS implementation.

This is the direct application of Section 2.3.2. The system model for the Kalman filter is as follows:

$$\begin{bmatrix} x_{k+1}^{nav} \\ x_{k+1}^{imu} \end{bmatrix} = \begin{bmatrix} A^{nav} & -M^{\#} \\ 0 & A^{imu} \end{bmatrix} \begin{bmatrix} x_k^{nav} \\ x_k^{imu} \end{bmatrix} + \begin{bmatrix} -M^{\#} v_k^{imu} \\ w_k \end{bmatrix} + \begin{bmatrix} M^{\#} y_k^{imu} \\ 0 \end{bmatrix} \tag{4.19a}$$

$$Ty_k^{imu} = Tx_k^{imu} + Tv_k^{imu} \tag{4.19b}$$

where,

$$M^{\#} = \left(M^T R^{-1} M\right)^{-1} M^T R^{-1} \tag{4.19c}$$

$$T = LNull(M) \tag{4.19d}$$

In (4.19d) *LNull* represents the basis set of the left null space of its argument (i.e. $TM = 0$).

Solution II: Multi-INS solution with state equivalency constraints.

In this solution two separate navigation systems were implemented. The first used only the accelerometers in set A, whereas the second system used the set B. The state equivalency constraints for these 2 systems were used as the only form of redundancy observations. The overall system and observation model for this configuration is as follows:

$$\begin{bmatrix} {}^A x_{k+1}^{nav} \\ {}^B x_{k+1}^{nav} \\ x_{k+1}^{imu} \end{bmatrix} = \begin{bmatrix} A^{nav} & 0 & \begin{bmatrix} -{}^A M^* & 0 \end{bmatrix} \\ 0 & A^{nav} & \begin{bmatrix} 0 & -{}^B M^* \end{bmatrix} \\ 0 & 0 & A^{imu} \end{bmatrix} \begin{bmatrix} {}^A x_k^{nav} \\ {}^B x_k^{nav} \\ x_k^{imu} \end{bmatrix} + \begin{bmatrix} -{}^A M^{*\,A} v_k^{imu} \\ -{}^B M^{*\,B} v_k^{imu} \\ w_k \end{bmatrix} + \begin{bmatrix} {}^A M^{*\,A} y_k^{imu} \\ {}^B M^{*\,B} y_k^{imu} \\ 0 \end{bmatrix} \tag{4.20a}$$

$$y_k^{eq} = 0 = {}^A x_k^{nav} - {}^B x_k^{nav} \tag{4.20b}$$

where

$$^{A}M^{*} = \left({}^{A}M^{T}\,{}^{A}R^{-1}\,{}^{A}M \right)^{-1}\,{}^{A}M^{T}\,{}^{A}R^{-1} \tag{4.20c}$$

$$^{B}M^{*} = \left({}^{B}M^{T}\,{}^{B}R^{-1}\,{}^{B}M \right)^{-1}\,{}^{B}M^{T}\,{}^{B}R^{-1} \tag{4.20d}$$

Solution III: Multi-INS solution with both state equivalency constraints and sensor redundancy observations.

This solution is similar to Solution II. However, in this case, together with the equivalency constraints, the redundancy observation for set A was also processed as measurements in the Kalman filter. The observation model for this solution is as follows:

$$\begin{bmatrix} y_k^{eq} = 0 \\ {}^{A}T\,{}^{A}y_k^{imu} \end{bmatrix} = \begin{bmatrix} I & -I & 0 \\ 0 & 0 & {}^{A}T \end{bmatrix} \begin{bmatrix} {}^{A}x_k^{nav} \\ {}^{B}x_k^{nav} \\ x^{imu} \end{bmatrix} + \begin{bmatrix} 0 \\ {}^{A}T v_k^{imu} \end{bmatrix} \tag{4.21}$$

where

$$^{A}T = \begin{bmatrix} LNull\left({}^{A}M \right) & 0_{1\times 2} \end{bmatrix} \tag{4.22}$$

As can be seen from (4.22), the redundancy observation for set A is defined as the basis for the left null space of (4.20c) (The dimension of the null space is 1 as there are only 3 accelerometers in set A).

Solution IV: Single-INS implementation with redundancy observations derived from the equivalency constraints.

For this solution only one INS was implemented which was run with $\hat{u}_k = M^{\#} y_k^{imu}$. Only the sensor redundancy observations which were equivalent to the navigation state constraints were processed by the Kalman filter. Thus, the observation model is as follows:

$$D_k = \left[\left({}^A M^* \right) \left(- {}^B M^* \right) \right] \tag{4.23a}$$

$$D_k y_k^{\text{imu}} = D_k x_k^{\text{imu}} + D_k v_k^{\text{imu}} \tag{4.23b}$$

The system model is as defined in (4.19a). It should be noted that as $D_k M = 0$, the

observation and system noises are also independent for this configurations.

Solution V: Alternative implementations for optimal solutions

a. Kalman filter for correlated system and observation noises

For this case (which consisted of 2 distinct INS implementation), (4.20a) was used as the

system model and (4.19d) was used as the observation model. The Kalman filter

described in [Kailath et al., 2000 – Chapter 9.5] was directly implemented for these

models.

b. Redundancy observations derived from equivalency constraints.

This configuration was similar to Solution IV. However, in this case the following

complete observation model was used:

$$\begin{bmatrix} D_k \\ {}^A T \end{bmatrix} y_k^{\text{imu}} = \begin{bmatrix} D_k \\ {}^A T \end{bmatrix} x_k^{\text{imu}} + \begin{bmatrix} D_k \\ {}^A T \end{bmatrix} v_k^{\text{imu}} \tag{4.24}$$

Where D_k and ${}^A T$ is as defined in (4.23b) and (4.22).

As described in the previous section, these 2 solutions are in fact theoretically equivalent

to Solution I. However, they were included in the simulations to see whether the

numerical aspects have any noticeable effect on the solution.

In Figure 4.2, Acc^2 error estimation result for Solution I, II, V(a) and V(b) are presented.

As seen from this figure Solution II is not equivalent to the optimal solutions (Solutions I,

Va, Vb). The reason for this is that the equivalency constraint does not consider the extra

observation arising from the redundancy in Set A. These equivalency constraints are conceptually equivalent to the observation in (4.23a), whereas the optimal solution uses (4.24).
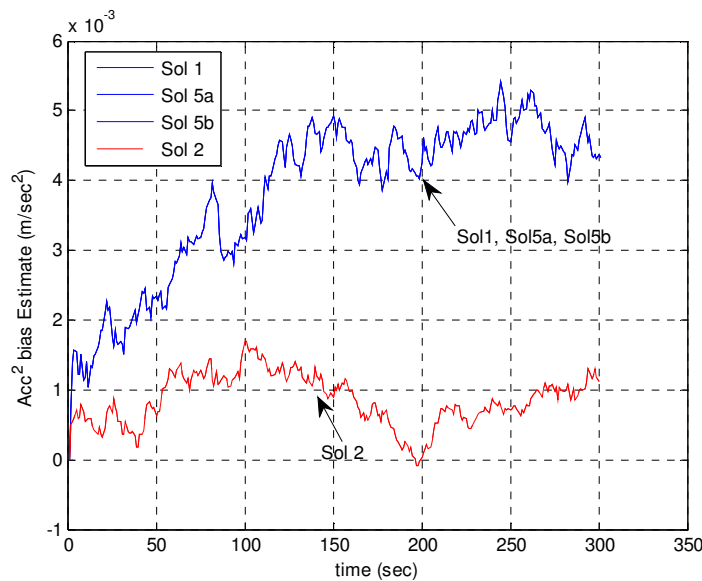
Figure 4-2 : Comparison of Acc^2 bias estimates for Solution I, II, V(a) and V(b).

Figure 4.3 represents the comparison of Acc^3 bias estimates for Solution I and III. As seen from this figure, when the missing sensor redundancy observation ($^A Ty_k^{imu}$) is augmented to the equivalency constraints based observation, the Kalman filter output for the multi-INS implementation becomes almost identical to the optimal results of Solution I. On the other hand, the small difference between the 2 curves verifies that they are not theoretically identical. Equation (4.15) explains the reason for this mismatch of the two results. As can be seen from (4.15), the equivalency constraint applied at time "k" is equivalent to the redundancy observation at time "k-1". Therefore equivalency constraint based observation is only equivalent to delayed state redundancy observations.
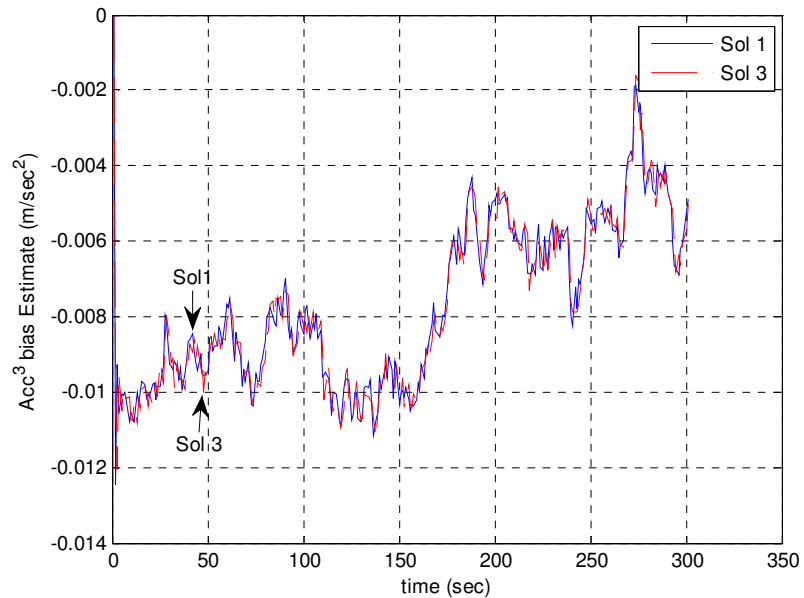
Figure 4-3 : Comparison of Acc^3 bias estimates for Solution I and III.

For navigation application point of view such a slight difference is not significant for any practical purposes. Furthermore, it should be noted that under some conditions, it is also possible to define exact equivalence between the predicted and filtered solution of these configurations. As an example, in Figure 4.4, the filtered Acc^4 bias estimates of Solution I and II and predicted bias estimate of Solution IV is presented. As seen from this figure, the filtered result of Solution II and predicted (only 1 sample delay) result of Solution IV is exactly identical.
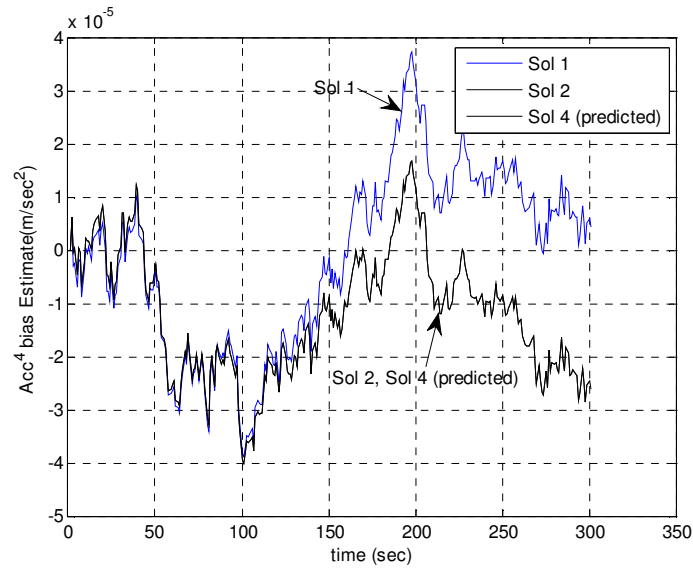
Figure 4-4 : Comparison of Acc^4 bias estimates for filtered results of Solution I, II and predicted result of Solution IV.

4.3.1.2 Case II: Identical Inertial Sensor Characteristics

In this section, the simulations were performed using the same system and sensor

configuration as defined in (4.16) and Figure 4.1. However, in contrast to previous

section, all sensors were assumed to be identical with the stochastic error model

parameters equivalent to parameters of Acc^1 (χ in (4.17)).

For this configuration, 3 types of solution method were implemented:

Solution I and II:

These configurations were exactly the same as the type of implementation presented in

Solution I and II of the previous section.

Solution IV:

In this solution no filtering was used at all. The two navigation solutions were computed using set A and B accelerometers as follows:

$$
{}^{A}\hat{x}_{k+1}^{\text{nav}} = A_k^{\text{nav}} \, {}^{A}\hat{x}_k^{\text{nav}} + N \, {}^{A}M^* \begin{bmatrix} Acc^1 \\ Acc^2 \\ Acc^3 \end{bmatrix}
\tag{4.25a}
$$

$$
{}^{B}\hat{x}_{k+1}^{\text{nav}} = A_k^{\text{nav}} \, {}^{B}\hat{x}_k^{\text{nav}} + N \, {}^{B}M^* \begin{bmatrix} Acc^4 \\ Acc^5 \end{bmatrix}
\tag{4.25b}
$$

where ${}^{A}M^*$ and ${}^{B}M^*$ is as defined in (4.20c-d).

Once these two separate navigation solutions were computed, the combined navigation solution was computed as the weighted average of these 2 solutions based on a MVU (minimum variance unbiased estimator) problem formulation as follows:

Let, the real navigation solution (x_k^{nav}) and the outputs of the 2 implemented INS has the following relation:

$$
\begin{bmatrix} {}^{A}\hat{x}_k^{\text{nav}} \\ {}^{B}\hat{x}_k^{\text{nav}} \end{bmatrix} = \begin{bmatrix} I \\ I \end{bmatrix} x_k^{\text{nav}} + \eta_k
\tag{4.26}
$$

Where x_k^{nav} is the combined output to be estimated for which ${}^{A}\hat{x}_k^{\text{nav}}$ and ${}^{B}\hat{x}_k^{\text{nav}}$ (the outputs of individual implementations) are considered as the 2 separate observations. η_k represents the fictitious observation noise whose covariance (Π_k) is equal to the error covariance of the navigation states for each INS. These error covariances were computed as in the Kalman filter (without any update cycle) with the system model defined in (4.20). Thus, the combined navigation solution is computed as follows:

$$
\hat{x}_k^{\text{nav}} = \left(\begin{bmatrix} I & I \end{bmatrix} \Pi_k^{-1} \begin{bmatrix} I \\ I \end{bmatrix} \right) \begin{bmatrix} I & I \end{bmatrix} \Pi_k^{-1} \begin{bmatrix} {}^{A}\hat{x}_k^{\text{nav}} \\ {}^{B}\hat{x}_k^{\text{nav}} \end{bmatrix}
\tag{4.27}
$$

In Figure 4.5, the comparison of the navigation solutions are presented for all 3 implementations defined above (Solution I, II and VI). As seen from this figure all 3 implementations have exactly identical navigation (velocity) solution.
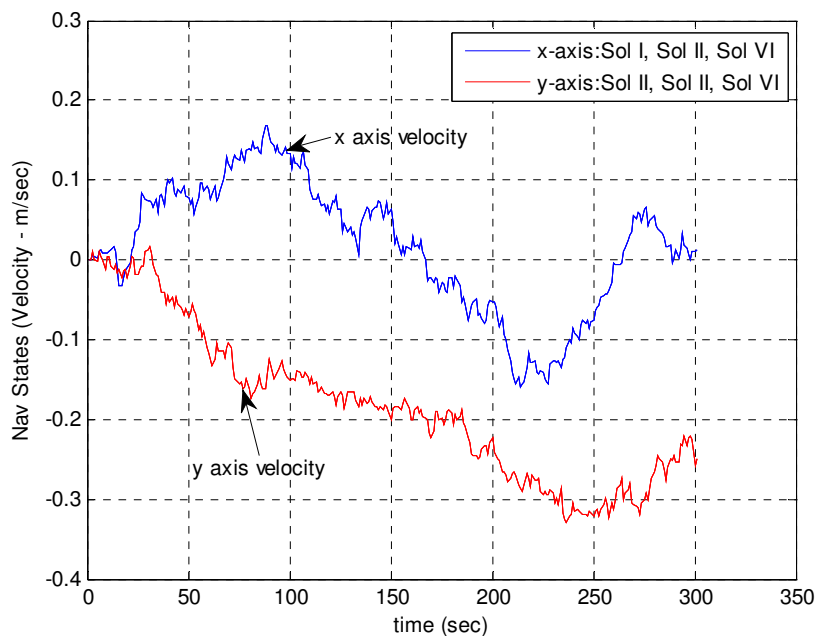
Figure 4-5 : Comparison of velocities for the solutions I, II and VI. The blue curve is the x-axis velocity computed by all 3 solutions and red curve is the y-axis velocity.

The reason for the theoretical equivalence of these solutions can be explained as follows: In Section 4.2, it is shown that the equivalency constraints are identical to some form of the redundancy observations. In Section 2.4.3 and 3.4.3, it was shown that when identical sensors are used in an SRIMU, the redundancy observations have no effect on the navigation solution for single-INS implementations. In Section 4.2, it was also showed that as long as the equivalent form of observations are used in the Kalman filter, the single and multi INS implementations are algebraically equivalent. Therefore, when

identical sensors are used, equivalency constraints can be completely ignored in multi-INS implementations. However, in this case, the knowledge of equivalence (Equation (4.11)) must be used to form the optimal average of individual implementations which leads to the MVU formulation defined in (4.26).

On the other hand, it should be noted that the equivalence of solutions VI and I-II are only limited to the navigation states. As shown in Section 3.5.1, even when all the sensors are identical, redundancy observation can still be used to perform sensor calibration. However, these sensor errors that are estimated do not have any effect on the navigation state error propagation unless the sensor configuration matrix changes.

4.4 Processing of the External PVA measurements in multi-INS implementations

All the discussion presented so far in this chapter has focused on the redundancy observations. However, in integrated navigation applications the system stability is dependent on external observations. Even with the SRIMU systems, it is not possible (at least with the currently available inertial sensor accuracies) to remove such dependence in most of applications.

For single-INS based SRIMU implementations the processing of external PVA measurements are exactly the same as the single IMU systems. As a matter of fact this is one of the reasons why single-INS implementations have more value for practical applications: this kind of implementation does not require significant modification in the existing integrated navigation software developed only for a single IMU.

On the other hand, as will be shown in the next section, single-INS based implementations have their own drawbacks (especially when there are significant

unknown bore-sight problems) and hence sometimes multi-INS implementations may become more favourable. For such implementations, the processing of external PVA observations in Kalman filter is not as trivial as the case for single-INS case.

In this section several methods for modeling external PVA observations in the multi-INS configurations are presented. Although all the presented methods are theoretically equivalent, they have different advantages and disadvantages from the implementation point of view. In this section, different methods are mainly compared in terms of ease of implementation. The robustness of these methods to the unknown bore-sight effects are discussed in the next section.

In order to simplify the notation in the following discussions only the direct PVA type observations are considered. Furthermore, it is assumed that the external observations are synchronized with the internal discretization time of INS implementations.

If it is assumed that a multi-INS configuration consists of L strapdown implementation each of which is run by an independent set of sensors located at the same point (but with arbitrary orientations), the main form of the observation model (including both the external observations and equivalency constraints) for such a configuration can be represented as follows:

$$
\left[\begin{array}{c} \overbrace{\begin{bmatrix} y_k^{\mathrm{nav}} \\ \vdots \\ y_k^{\mathrm{nav}} \end{bmatrix}}^{y_k^{\mathrm{nav}}} \\ \underbrace{\begin{bmatrix} {}^{1}y_k^{eq} = 0 \\ \vdots \\ {}^{L-1}y_k^{eq} = 0 \end{bmatrix}}_{y_k^{eq}} \end{array} \right] = \left[\begin{array}{c} \overbrace{\begin{bmatrix} H_k & & 0 \\ & \ddots & \\ 0 & & H_k \end{bmatrix}}^{H_k^{\mathrm{nav}}} \\ \begin{bmatrix} [\mathrm{I} \quad -\mathrm{I}] & & 0 \\ & \ddots & \\ 0 & & [\mathrm{I} \quad -\mathrm{I}] \end{bmatrix} \end{array} \right] \underbrace{\begin{bmatrix} {}^{A}x_k^{\mathrm{nav}} \\ \vdots \\ {}^{L}x_k^{\mathrm{nav}} \end{bmatrix}}_{x_k^{\mathrm{nav}}} + \underbrace{\left[\begin{array}{c} \begin{bmatrix} v_k^{\mathrm{nav}} \\ \vdots \\ v_k^{\mathrm{nav}} \end{bmatrix} \\ \begin{bmatrix} 0 \\ \vdots \\ 0 \end{bmatrix} \end{array} \right]}_{v_k} \qquad (4.28)
$$

where, $y_k^{nav} = H_k^{nav} x_k^{nav} + \begin{bmatrix} I & \cdots & I \end{bmatrix}^T v_k^{nav}$ represents the external PVA observations and

$\left\{ {}^i y_k^{eq} \right\}_{i=1}^{L-1} = 0$ are the state equivalency observations arising from the redundancy of the

sensors. It must be noted that v_k^{nav} for each sub-system in (4.28) represents the same

identical noise. In other words:

$$E\left\{ v_k v_k^T \right\} = \begin{bmatrix} ones(L)*R = \begin{bmatrix} R & R & \cdots \\ R & R & \vdots \\ \vdots & \cdots & \ddots \end{bmatrix} & 0 \\ & 0 & 0 \end{bmatrix} \qquad (4.29a)$$

where $R = E\left\{ v_k^{nav} v_k^{nav^T} \right\}$.

Therefore, some of the observations in (4.28) are in fact just the linear combination of the

others and hence do not carry any additional information at all. Furthermore, this form of

the observation model is the most problematic model in terms of the numerical

considerations. As $E\left\{ v_k v_k^T \right\}$ is not invertible, the inverse of the innovation process's

correlation is mainly determined by the correlation of the navigation states. However,

because of the equality constraints, the navigation state correlation also has a very low

condition number. Thus, in most cases, direct application of this observation model leads

to divergent Kalman filter results due to the almost rank deficient innovation correlation.

Therefore, equivalent observation models should be used for multi-INS implementations.

These equivalent models are obtained by removing some of the linear combination of

states from (4.28) which does not carry additional information. Although there are many

such ways of obtaining equivalent measurement models, in this study only the following

4 models are considered.

Model I: Measurement model based on a single sub-system.

$$
\begin{bmatrix} y_k^{\text{nav}} \\ {}^1y_k^{eq}=0 \\ \vdots \\ {}^{L-1}y_k^{eq}=0 \end{bmatrix} = \begin{bmatrix} H_k & 0 & \cdots & & 0 \\ I & -I & 0 & \cdots & 0 \\ & & \vdots & & \\ 0 & \cdots & 0 & I & -I \end{bmatrix} \begin{bmatrix} {}^A x_k^{\text{nav}} \\ \vdots \\ {}^L x_k^{\text{nav}} \end{bmatrix} + \begin{bmatrix} v_k^{\text{nav}} \\ 0 \\ \vdots \\ 0 \end{bmatrix}
\tag{4.30}
$$

Model II: Measurement model based on a combination of observations.

Let $^AG \ldots {}^LG$ be L invertible matrices such that $^AG + {}^BG + \ldots + {}^LG = I$. Then:

$$
\begin{bmatrix} y_k^{\text{nav}} \\ {}^1y_k^{eq}=0 \\ \vdots \\ {}^{L-1}y_k^{eq}=0 \end{bmatrix} = \begin{bmatrix} {}^AGH_k & {}^BGH_k & \cdots & & {}^LGH_k \\ I & -I & 0 & \cdots & 0 \\ & & \vdots & & \\ 0 & & \cdots & 0 & I & -I \end{bmatrix} \begin{bmatrix} {}^A x_k^{\text{nav}} \\ \vdots \\ {}^L x_k^{\text{nav}} \end{bmatrix} + \begin{bmatrix} v_k^{\text{nav}} \\ 0 \\ \vdots \\ 0 \end{bmatrix}
\tag{4.31}
$$

Model III: Measurement model based on a combination of states.

Let $^AJ \ldots {}^LJ$ be L invertible matrices such that $^AJ + {}^BJ + \ldots + {}^LJ = I$. Then:

$$
\begin{bmatrix} y_k^{\text{nav}} \\ {}^1y_k^{eq}=0 \\ \vdots \\ {}^{L-1}y_k^{eq}=0 \end{bmatrix} = \begin{bmatrix} H_k{}^AJ & H_k{}^BJ & \cdots & & H_k{}^LJ \\ I & -I & 0 & \cdots & 0 \\ & & \vdots & & \\ 0 & & \cdots & 0 & I & -I \end{bmatrix} \begin{bmatrix} {}^A x_k^{\text{nav}} \\ \vdots \\ {}^L x_k^{\text{nav}} \end{bmatrix} + \begin{bmatrix} v_k^{\text{nav}} \\ 0 \\ \vdots \\ 0 \end{bmatrix}
\tag{4.32}
$$

Model IV: Measurement model based on all sub-systems.

$$
\begin{bmatrix} y_k^{\text{nav}} \\ \vdots \\ y_k^{\text{nav}} \end{bmatrix} = \begin{bmatrix} H_k & & 0 \\ & \ddots & \\ 0 & & H_k \end{bmatrix} \begin{bmatrix} {}^A x_k^{\text{nav}} \\ \vdots \\ {}^L x_k^{\text{nav}} \end{bmatrix} + \begin{bmatrix} I \\ \vdots \\ I \end{bmatrix} v_k^{\text{nav}}
\tag{4.33}
$$

Below, it will be shown that these sets of observations are equivalent to (4.28). To show the equivalency it is sufficient to show that (4.30)-(4.33) can be generated from (4.28) using only linear transformations and vice versa. As the derivations of (4.30)-(4.33) from (4.28) is trivial, only the computation of (4.28) from (4.30)-(4.33) is provided below.

Model I:

According to (4.30) $^A x_k^{\text{nav}} = {}^B x_k^{\text{nav}} = \ldots = {}^L x_k^{\text{nav}}$. Therefore,

$y_k^{\text{nav}} = H_k {}^A x_k^{\text{nav}} + v_k^{\text{nav}} = H_k {}^B x_k^{\text{nav}} + v_k^{\text{nav}} \ldots$. This completes all the observations in (4.28).

Model II

It is sufficient to show that (4.31) is equivalent to (4.30). Using (4.31),

$$
\begin{aligned}
y_k^{\text{nav}} &= {}^A G H_k {}^A x_k^{\text{nav}} + \ldots + {}^L G H_k {}^L x_k^{\text{nav}} + v_k^{\text{nav}} \\
&= \left({}^A G + \ldots + {}^L G \right) H_k {}^A x_k^{\text{nav}} + v_k^{\text{nav}} \qquad (4.34) \\
&= H_k {}^A x_k^{\text{nav}} + v_k^{\text{nav}}
\end{aligned}
$$

Model III:

Similar to the previous case, using (4.32) it can be shown that:

$$
\begin{aligned}
y_k^{\text{nav}} &= H_k {}^A J {}^A x_k^{\text{nav}} + \ldots + H_k {}^L J {}^L x_k^{\text{nav}} + v_k^{\text{nav}} \\
&= H_k \left({}^A J + \ldots + {}^L J \right) {}^A x_k^{\text{nav}} + v_k^{\text{nav}} \qquad (4.35) \\
&= H_k {}^A x_k^{\text{nav}} + v_k^{\text{nav}}
\end{aligned}
$$

Model IV:

$$
y_k^{\text{nav}} = H_k {}^A x_k^{\text{nav}} + v_k^{\text{nav}} = H_k {}^B x_k^{\text{nav}} + v_k^{\text{nav}} \Rightarrow 0 = H_k \left({}^A x_k^{\text{nav}} - {}^B x_k^{\text{nav}} \right) \qquad (4.36)
$$

In almost all practical cases, H_k is not a full rank matrix. Therefore, in general (4.36) is

not equivalent to (4.28). However, in practice, even if H_k is rank deficient, the results of

this form of observations are close to the main form defined in (4.28). Therefore, for

practical applications this form can also be used as an alternative to (4.28). On the other

hand, as this model is not theoretically equivalent to other models, in this thesis it is not

used as a part of the comparisons.

In Model II and III, some kinds of weighting matrices are used to generate observations. A natural choice for these matrices is the MVU estimation coefficients of the corresponding states. As described in the previous section, at any time instant "k", the navigation states of each INS implementation can be considered as an observation for the kinematic states of the real system. The errors on these observations can be assumed to have zero mean and have a variance equal to the Kalman Filter covariance estimate. Hence this MVU problem can be formulated as:

$$\begin{bmatrix} {}^A\hat{x}_k^{\text{nav}} \\ \vdots \\ {}^L\hat{x}_k^{\text{nav}} \end{bmatrix} = \underbrace{\begin{bmatrix} \mathbf{I} \\ \vdots \\ \mathbf{I} \end{bmatrix}}_{U} x_k^{\text{nav}} + \eta_k \tag{4.37}$$

where $E\left\{\eta_k \eta_k^T\right\} = \Pi_k$ is the covariance of the Kalman filter (which is not a block diagonal matrix), ${}^A\hat{x}_k^{\text{nav}} \ldots {}^L\hat{x}_k^{\text{nav}}$ is the navigation result outputs of each INS and x_k^{nav} is the real kinematic state (PVA) of the system which has to be estimated from the observations $\begin{bmatrix} {}^A\hat{x}_k^{\text{nav}} & \ldots & {}^L\hat{x}_k^{\text{nav}} \end{bmatrix}$.

The MVU solution of x_k^{nav} in (4.37) can be computed as follows:

$$\begin{aligned} \hat{x}_k^{\text{nav}} &= \underbrace{\left(U^T \Pi_k^{-1} U\right)^{-1} U^T \Pi_k^{-1}}_{J} \begin{bmatrix} {}^A\hat{x}_k^{\text{nav}} \\ \vdots \\ {}^L\hat{x}_k^{\text{nav}} \end{bmatrix} \\ &= {}^A J \, {}^A\hat{x}_k^{\text{nav}} + \ldots + {}^L J \, {}^L\hat{x}_k^{\text{nav}} \end{aligned} \tag{4.38}$$

As (4.38) is an unbiased estimator, ${}^A J + \ldots + {}^L J = \mathbf{I}$. Therefore, these matrices can be used as the weighting coefficients in Model III.

Similar to the case presented above, G matrices for Model II can computed using the

MVU estimation formulation for $H_k x_k^{\text{nav}}$ as follows:

$$\begin{bmatrix} H_k{}^A \hat{x}_k^{\text{nav}} \\ \vdots \\ H_k{}^L \hat{x}_k^{\text{nav}} \end{bmatrix} = \underbrace{\begin{bmatrix} \mathrm{I} \\ \vdots \\ \mathrm{I} \end{bmatrix}}_{U} H x_k^{\text{nav}} + \eta_k \qquad (4.39)$$

where $E\left\{\eta_k \eta_k^T\right\} = H_k \Pi_k H_k^T$, $H x_k^{\text{nav}}$ is the combination of the states to be estimated and

$H_k{}^A \hat{x}_k^{\text{nav}} \ldots H_k{}^L \hat{x}_k^{\text{nav}}$ represents the observations provided by each INS. The MVU

estimate of $H_k x_k^{\text{nav}}$ can be computed as:

$$\widehat{H_k x_k^{\text{nav}}} = \underbrace{\left(U^T \left(H_k \Pi_k H_k^T\right)^{-1} U\right)^{-1} U^T \left(H_k \Pi_k H_k^T\right)^{-1}}_{G} \begin{bmatrix} H_k{}^A \hat{x}_k^{\text{nav}} \\ \vdots \\ H_k{}^L \hat{x}_k^{\text{nav}} \end{bmatrix} \qquad (4.40)$$

$$= {}^A G H {}^A \hat{x}_k^{\text{nav}} + \ldots + {}^L G H {}^L \hat{x}_k^{\text{nav}}$$

Again, as (4.40) is an unbiased estimator, ${}^A G + \ldots + {}^L G = \mathrm{I}$. Therefore these G matrices

can be used in the Model II.

It should be noted that as H_k is not an invertible matrix, $\widehat{H_k x_k^{\text{nav}}}$ of (4.40) is not

equivalent to $H_k \hat{x}_k^{\text{nav}}$ of (4.38).

In the above discussions, the MVU estimation formulations are described assuming linear

observation models. However, for the INS implementations, especially the attitude states

have a nonlinear relation. In Appendix B, the MVU estimation formulation for the INS

states are described. Although there is no difference for the Kalman filtering point of

view, the implementation of the above ideas for the navigation system must be performed

as described in Appendix B.

The ultimate aim in introducing different observation models is to derive a Kalman filter formulation whose final estimation performance least depends on the explicit state equivalency constraints $\left\{{}^{i}y_{k}^{eq}\right\}_{i=1}^{L-1} = 0$. This is because: i) as $R = 0$ for these observations, the equivalency constraints usually create numerical problems, ii) when there are unknown lever arm (and boresight) effects these constraints may degrade the overall system performance rather than supporting it.

In the next section, the effect of i) the selected observation model and ii) the Kalman filter update period for the equivalency constraints on the final navigation solution are further discussed based on simulated system examples.

4.5 Simulation Results For Multi-INS implementations

In this section, results of several multi-INS integration methods are presented for the 2D (3DoF) planar navigation system example introduced in Section 3.2. The multi sensor configuration for this system is presented in Figure 4.6. As seen from this figure, it is assumed that the SRIMU has 2 sets of IMUs each of which contains 2 accelerometers (on X-Y plane) and a gyroscope (on Z-axis). For the multi-INS implementation, Acc^1, Acc^2 and $Gyro^1$ is used to run INS A, whereas Acc^3, Acc^4 and $Gyro^2$ runs the INS B. The discrete time output model at 100hz for these sensors are as follows:

$$
y_k^{imu} = \begin{bmatrix} Acc^1 \\ Acc^2 \\ Acc^3 \\ Acc^4 \\ Gyro^1 \\ Gyro^2 \end{bmatrix} = \underbrace{\begin{bmatrix} 1 & 0 & 0 \\ 0 & 1 & 0 \\ 1 & 0 & 0 \\ 0 & 1 & 0 \\ 0 & 0 & 1 \\ 0 & 0 & 1 \end{bmatrix}}_{M} \begin{bmatrix} a_x \\ a_y \\ \omega_z \end{bmatrix}_k + x_k^{imu} + v_k^{imu} \tag{4.41a}
$$

$$x_{k+1}^{imu} = \mathrm{diag}\begin{pmatrix} 1 \\ 1 \\ 0.9999866 \\ 1 \\ 1 \\ 1 \end{pmatrix} x_k^{imu} + w_k \qquad (4.41b)$$

$$E\{w_k w_k^T\} = \mathrm{diag}\left(3.025^{-9}, 3.025^{-9}, 1.7^{-12}, 3.025^{-9}, 1^{-10}, 8.1^{-9}\right) \qquad (4.41c)$$

$$E\{v_k v_k^T\} = \mathrm{diag}\left(3^{-4}, 3^{-4}, 1^{-4}, 3^{-6}, 2.5^{-5}, 2.5^{-5}\right) \qquad (4.41d)$$

$$E\{x_0^{imu} x_0^{imu\,T}\} = \mathrm{diag}\left(1^{-4}, 1^{-4}, 2.5^{-7}, 1.0^{-4}, 6^{-8}, 6^{-9}\right) \qquad (4.41e)$$

As seen from the above error definitions, it was assumed Acc^1 and Acc^2 have identical characteristics which is worse than Acc^3 and Acc^4. The 3rd and 4th accelerometers have complementary characteristics in such a way that Acc^4 has better VRW characteristics but worse stability properties than Acc^3. Also, the initial stability covariance of Acc^3, Acc^4, $Gyro^1$ and $Gyro^2$ are selected to be substantially different from each other. For all simulations presented in the following section, the corresponding optimal solutions were computed using the optimal single-INS based SRIMU configuration described in Section 3.3. The reason for this is that the theoretically optimal multi-INS implementation (i.e. the Kalman filter processing the navigation states equivalency constraints at IMU-output frequency) is numerically very problematic. Especially, when the discretization of navigation state error propagation models is performed using 1st order Taylor series expansion, standard form of the Kalman filter cannot be used for the processing of equivalency constraints at this frequency. Therefore, instead of dealing

with such kind of numerical problems, the optimal solutions were computed using the optimal single-INS implementation.

The navigation and corresponding error propagation equations for this 2D (3DoF) navigation system are presented in Section 3.2. The trajectory that is used in the corresponding simulations is shown in Figure 4.7. As can be seen from this figure, the simulated system is allowed to accelerate/decelerate along only its x-axis.
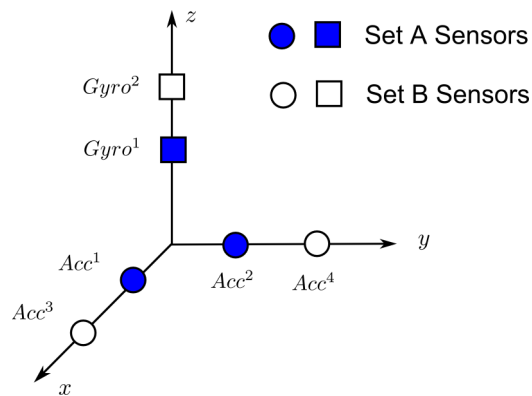
Figure 4-6 : Inertial Sensor configuration for the simulations.

In the first part of this section, using the simulated system i) the effect of Kalman filter update period for the equivalency constraints and ii) the selected external observation model type on the navigation performance are presented. In the second part (Section 4.5.2), the effect of unknown bore sight between the several sensor sets on the Kalman filter outputs are examined.
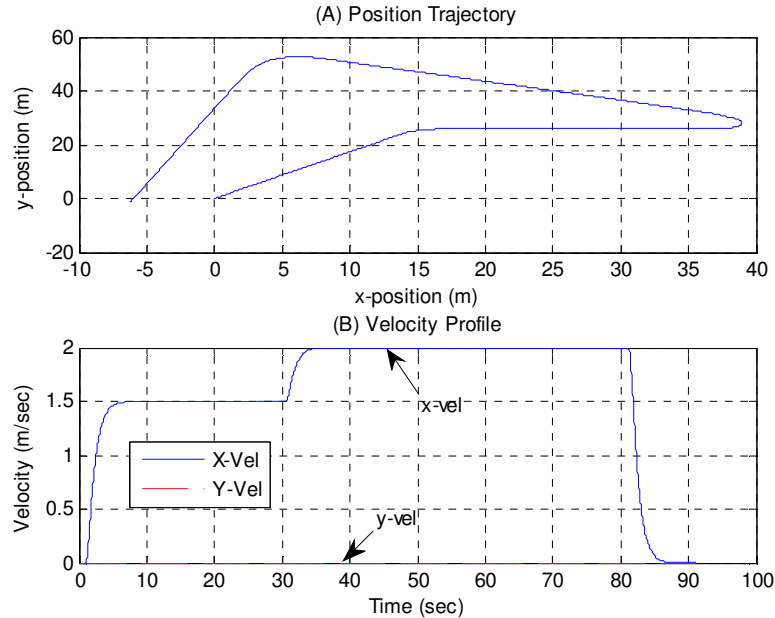
Figure 4-7 : Simulated trajectory. (A) is the simulated position and (B) is the

velocity defined in the body frame.

4.5.1 Effect of update period and observation models

In Figure 4.8, position results of several multi-INS configurations discussed in the

previous sections are presented. In the corresponding simulations no external navigation

aids were used. Hence, the Kalman filter in the optimal solution only processed the

redundancy observations.

The implemented configurations and the corresponding results that are compared in this

figure are as follows:

   i.   TT: True trajectory that is simulated by the trajectory generator.

   ii.   OP: Optimal result which was computed using the optimal single-INS

       implementation described in Section 3.3.

iii.   INS-A: Output of the (unaided) INS which was run using only the set A sensor

outputs.

iv.   INS-B: Output of the (unaided) INS which was run using only the set B sensor

outputs.

v.   A1: The average of INS-A and INS-B outputs. The computation of this average as

described in Appendix B. All navigation states were used in the MVU

formulation to compute the average.

vi.   A2: The sub-optimal average of INS-A and INS-B outputs. Only the position and

velocity states were used in the MVU formulation.

Figure 4-8 : Comparison of position (X-Y) results for several multi INS

configurations. Only in the optimal solution (OP) a Kalman filter is used.

From Figure 4.8, it can be seen that although no Kalman filter was used for multi-INS

solutions (other than the optimal solution which was obtained using a single-INS

implementation), AV2 turned out to be very close to the optimal solution (OP). This hints

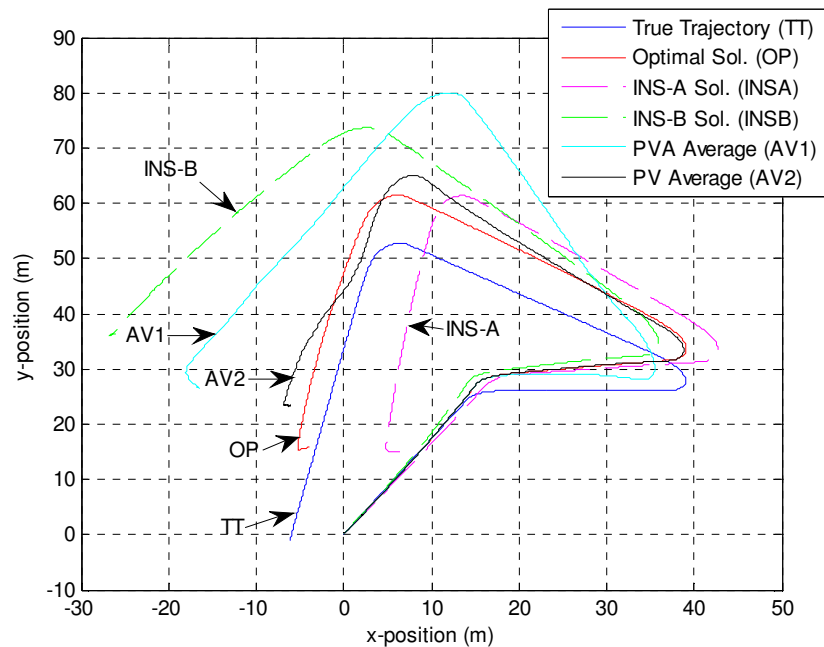the fact that, for multi-INS implementations, the apparent improvement is mostly

achieved by simple blending of the individual INS outputs rather than the error feedback

provided by the navigation states equivalency constraints.

On the other hand, as can be seen from Figure 4.8, only the initial part of the AV1 is

close to the optimal solution. Although, as described in Appendix B, AV1 corresponds to

the optimal blending of all navigation states, AV1 result deviated from the optimal (and

AV2) solution starting from approximately the 40th second of the simulation. The reason

for this deviation is the small angle assumption used in the MVU formulation of the

attitude states. As the attitude errors get bigger, this small angle assumption becomes

invalid and the linear estimation method described in Appendix B cannot be used. On the

other hand, as the attitude states were not included in the MVU formulation of the AV2,

the position result obtained with this method turned out to be more stable than AV1.

It should be noted that the same linearization problem also exists for the Type III

observation model (Equation 4.32) described in the previous section. In this observation

model all navigation states need to be combined using the weighting matrices $\left\{ {}^{i}J \right\}_{i=A}^{L}$.

When the attitude errors start to violate the small angle assumption, this type of

combination is not valid and hence type III observation models cannot be used for large

attitude errors.

In Figure 4.9, the x-axis velocity estimation errors together with the associated standard

deviations for the same simulation (and configurations) are presented (the standard

deviation of the average was computed using (Appendix B – Equation B.8)). As seen

from this figure, although the individual INS outputs have different error characteristics,

the error on the average output (AV2) stays close to the error on the optimal solution

especially for the initial part of the simulation.
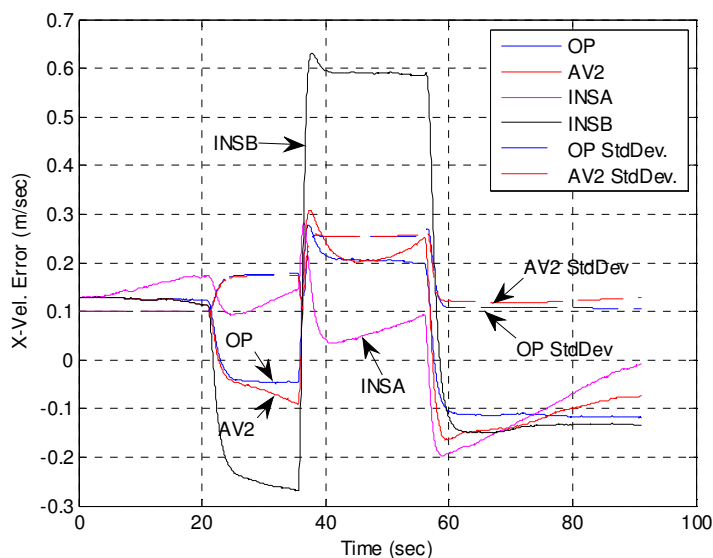
Figure 4-9 : Comparison of x-axis velocity results and the corresponding standard

deviations (1σ) for multi-INS implementations.

The above results suggest that as long as the best average of INS outputs are used as the

overall system output, the update frequency of the Kalman filter which processes the

navigation state equivalency constraints of a multi-INS implementation is not very

crucial (at least for the error models used in these simulations). To further verify this

point, comparison of position results for 5 multi-INS implementations each of which uses

a Kalman filter with a different update period is presented in Figure 4.10. In this figure,

each curve represents the combined output of individual INSs corrected by a Kalman

filter which processed navigation state equivalency constraints. However, for each

implementation a different update frequency was used for the Kalman filter. In KA1 it

was set to 12.5Hz. For KA2, KA3 and KA4 these update periods were 1, 10, and 20

seconds respectively. As can be seen from this figure, the position results are not affected

by the reduction of Kalman filter update period as much as 10 seconds.
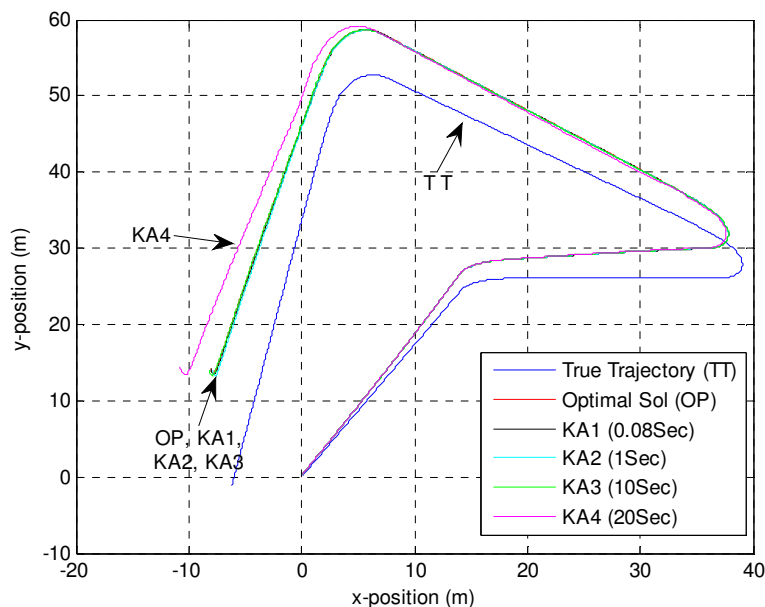
Figure 4-10 : Comparison of position results for Kalman filters with different

update frequencies. Because of the scale of the axis, OP, KA1, KA2 and KA3 curves

seem as a single curve. The combined outputs were computed as the optimal average

of position and velocity results of individual INSs.

In Figure 4.11, the set B\Y-axis accelerometer (Acc^4) bias estimation errors are

presented for the same 5 multi-INS implementations. As seen from this figure, as soon as

an equivalency constraint is processed by the Kalman filter, the bias errors can be reduced to the levels which can be obtained with the optimal configuration. Furthermore, again by noting the similarity between KA3 curve and the OP, KA1-2 curves, it can be concluded that for this configuration the reduction of Kalman filter update frequency up to 0.1Hz does not affect the sensor error estimation performance.
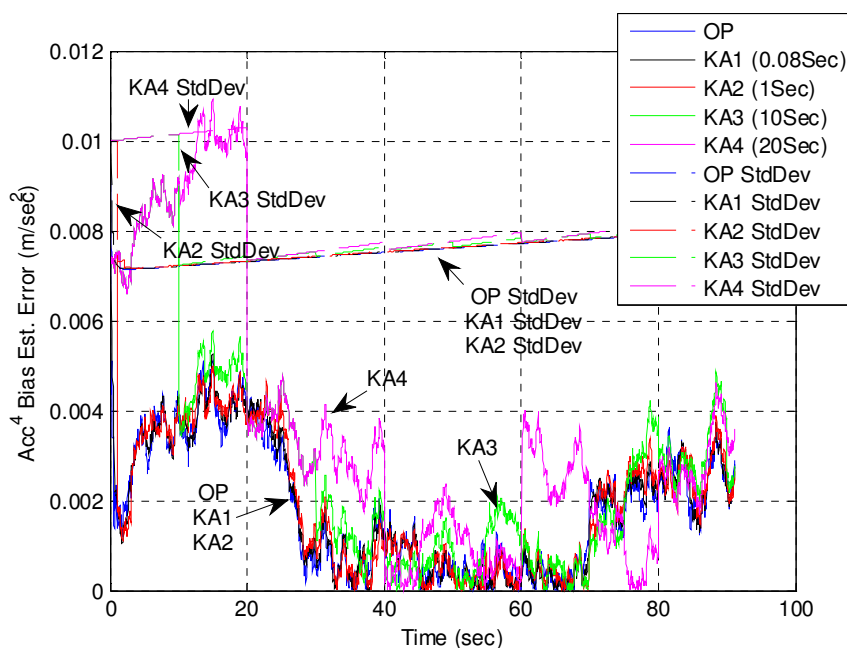
Figure 4-11 : Comparison of Acc^4 bias estimation errors. The dashed lines correspond to the standard deviation of the estimates whereas the solid lines represent the estimation errors.

In Section 4.3.2.1 it was shown that when all inertial sensors have identical stochastic error model parameters, the optimal solution can be obtained without implementing any Kalman filter for the equivalency constraints. The best weighted average of the individual INS outputs, becomes the optimal solution for these kind of multi-INS configurations. On

the other hand, as shown in Figure 4.8, when the magnitude of the attitude errors violate the small angle assumption (which is required to form the best averages) the averaging results tend to be incorrect. Therefore, in order to prevent the attitude errors of individual INS's to grow fast, it is advisable to use a Kalman filter with very low frequency (possibly in the order of 0.1Hz) to implement the equivalency constraints even for identical inertial sensor configurations.

In Section 4.4, it was shown that several observation models can be constructed for a given external PVA measurement in a multi-INS implementation. As all of these observation models are theoretically equivalent, selection of any of these models does not affect the system performance. On the other hand, if (for any reason) it is required to avoid implementing equivalency constraints, then the choice of observation model may change the individual strapdown results.

As an example, the comparison of position results of 3 different multi-INS implementations is presented in Figure 4.12 for the same simulation. However, in contrast to previous simulations, in this simulation it was assumed that an external position observation is available for the Kalman filter to process at 0.5Hz. Throughout the simulation, the navigation state equivalency constraints was processed by the Kalman filter for only 2 times at the 40th and 80th seconds.

In all 3 implementations presented in Figure 4.12, the external position observations were processed differently. In the first implementation (Figure 4.12.A), only INS B (the INS which was run by IMU set B in Figure 4.6), was directly aided by these position observations. Therefore, the measurement model for the external observations was as follows:

$$P_k^{Ext} = P_k^{INS-B} + v_k^{nav} \tag{4.42a}$$

In the second implementation (Figure 4.12b), the measurements were formed using the best average of individual INS outputs as explained in Section 4.4 (First row of (4.31)). Hence, the measurement model was in the following form:

$$P_k^{Ext} = \begin{bmatrix} {}^A G_k & {}^B G_k \end{bmatrix} \begin{bmatrix} P_k^{INS-A} \\ P_k^{INS-B} \end{bmatrix} + v_k^{nav} \tag{4.42b}$$

In the third implementation (Figure 4.12c), the position observations were used to aid both INS's (A & B) in an alternating fashion. At instant "k" only INS-A was aided whereas at "k+1" only INS-B was aided. The measurement model for this implementation can be represented as follows:

$$\begin{aligned} P_k^{Ext} &= P_k^{INS-A} + v_k^{nav} \\ P_{k+1}^{Ext} &= P_{k+1}^{INS-B} + v_{k+1}^{nav} \end{aligned} \tag{4.42c}$$

As mentioned above in all 3 implementations, the equivalency constraints were also processed by the Kalman filter only for 2 times during the entire simulation. The corresponding measurement models for these 2 equivalency constraint based observations can be represented as follows:

$$\begin{bmatrix} 0 \\ 0 \\ 0 \end{bmatrix} = \begin{bmatrix} {}^A P_k - {}^B P_k \\ {}^A V_k - {}^B V_k \\ S^{-1} \left({}^A C_b^n \, {}^B C_n^b \right) \end{bmatrix}_k \tag{4.43}$$

where P, V and C_b^n are the position velocity and attitude states of the individual INSs and "k" represents the index which corresponds to the only 40$^{\text{th}}$ and 80$^{\text{th}}$ seconds of the simulation. S^{-1} denotes an operator which converts a skew symmetric matrix into its vector form.
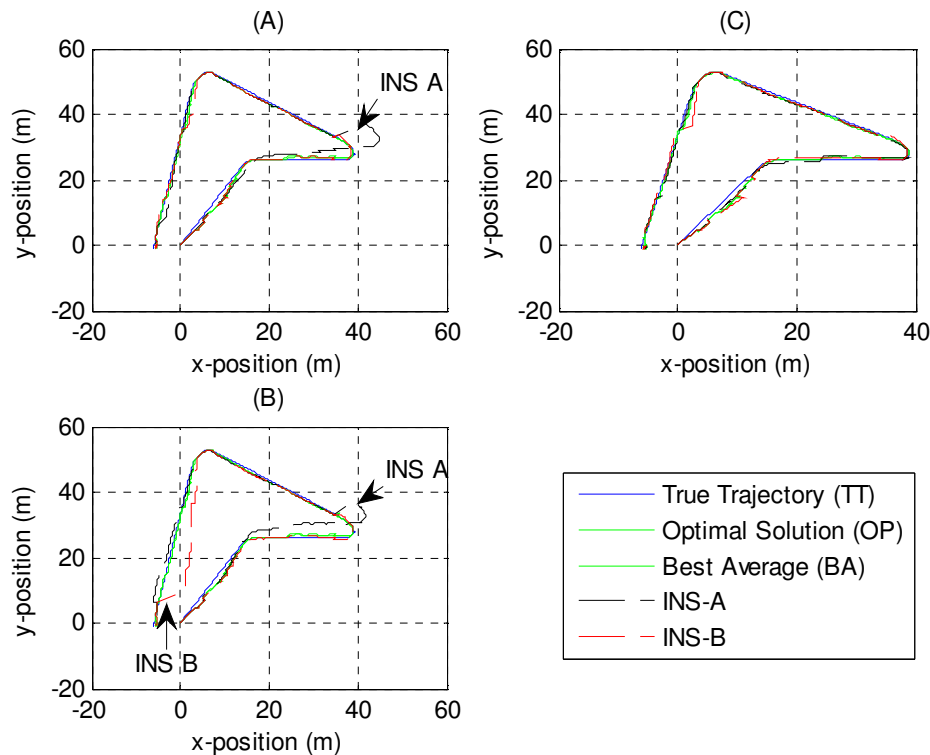
Figure 4-12 : Comparison of position outputs for 3 types of multi-INS implementation. In (A), measurement model (4.42a) was used. In (B) and (C), (4.42b) and (4.42c) were used respectively.

As seen from Figure 4.12, for all 3 configurations the combined results are almost identical to the optimal solution. However, for the first and second implementations (which uses observation models (4.42a) and (4.42b) respectively), the INS-A position errors tends to grow fast. This is natural for the first implementation because INS-A is not directly aided by the external position observations at all. However, although a combination of INS-A and INS-B states are used to form the measurements, the second implementation is not efficient to limit the error growth of the individual INSs either. As

can be seen in Figure 4.12B, the errors on both of the INS outputs in the second

implementation tend to grow faster than the other implementations.

For the third implementation, both INS's can be aided with the external observations

without using any equivalency constraints. In general, it has been observed in several

simulations that this kind of alternating aiding method provides the most feasible solution

for multi-INS configurations for which the frequency of equivalency updates for Kalman

filters are required to be reduced as much as possible.

4.5.2 Effect of Unknown Bore-Sight between multiple IMUs

In all discussions presented so far in this chapter, it was always assumed that the inertial

sensor configurations are known perfectly and remain rigid during the entire operation.

On the other hand, in practice there may be situations in which especially the relative

orientation of sensor sets with respect to each other cannot be fixed during the field

operation. As such relative motion between the sensors is completely ignored in the

SRIMU systems, the navigation results can be seriously damaged by these effects. In this

section, the effect of such changing (and unknown) bore-sight effects on the overall

navigation performance of a multi inertial sensor system will be presented based on

simulation results.

The same sensor configuration and simulation environment introduced in the beginning

of Section 4.5 was also used in the simulations of this section. However, in contrast to the

previous section, it was assumed that the sensor set B (in Figure 4.6) is not rigidly

connected along the z-axis and hence can undergo a free rotational motion about the z-

axis while preserving its position and internal orthogonality between the sensors. Under

this assumption, the simulated true heading angle profiles for the set A and B sensors are

presented in Figure 4.13. As seen from this figure, the heading angle of set B sensors

changes around the nominal heading angle of set A which is assumed to be perfectly

aligned with the system body frame.
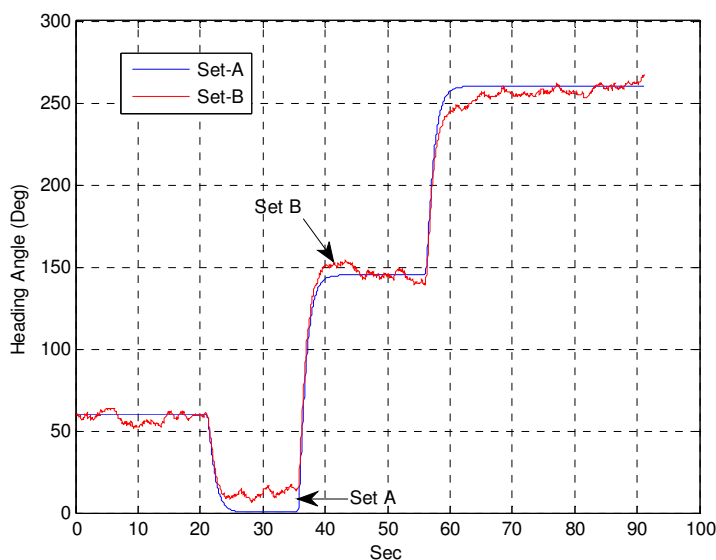
Figure 4-13 : Comparison of simulated heading angles of Set A and Set B sensors.

Set A sensors are assumed to be aligned with the system body frame. The standard

deviation of the difference between the heading angles is 6°.

For this simulated data set, 3 different multi-sensor navigation systems were

implemented. In all system designs, the relative motion between the two sets of sensors

was completely ignored. These systems can be summarized as follows:

System I: In this system, a single-INS configuration described in Section 3.3 (Figure 3.2)

was implemented without any modification. It was assumed that both sensor sets are

rigidly connected to the body frame of the system.

System II: In this system, two INSs were implemented. INS-A and INS-B processed the set A and set B sensors respectively. In a Kalman filter, the equivalency constraints for the entire navigation states (position, velocity and attitude) of these two INSs were processed at 1Hz. No modification was made in the design of the Kalman filter to consider the effect of relative motion between the sensors (i.e. no artificial measurement noise was injected for the equivalency constraints).

System III: This system is similar to system II. However in this case, only the equivalence of position states was used as the observation in the Kalman filter. As the separation between two sets of sensors did not change during the simulations, this configuration corresponds to some form of pseudo-optimal solution. It is not optimal because optimality requires the bore-sight effects to be modeled and augmented in the Kalman filter.

In Figure 4.14 and 4.15 the position and x-axis velocity results for all 3 systems are presented. As can be seen from these figures both the system I and II are significantly affected by the changing bore-sight between the sensor sets. Especially the velocity results are seriously degraded under these conditions. Every time the system undergoes a heading angle change, the x-axis velocity results for the system I and II converged to a wrong solution due to the unconsidered bore-sight effects.
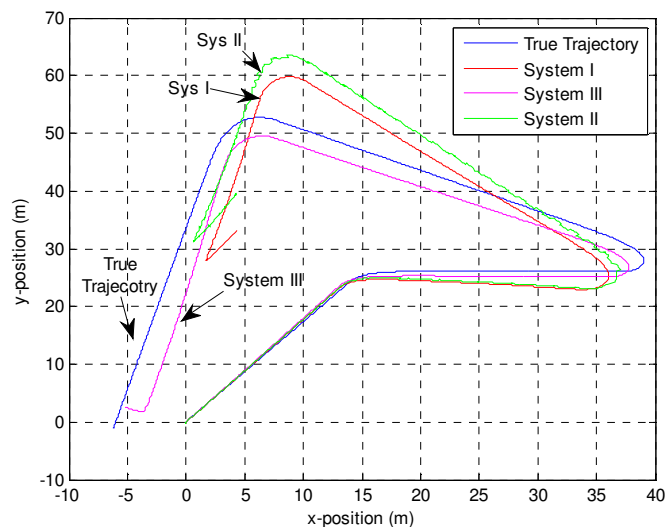
Figure 4-14 : Comparison of position results for the 3 systems
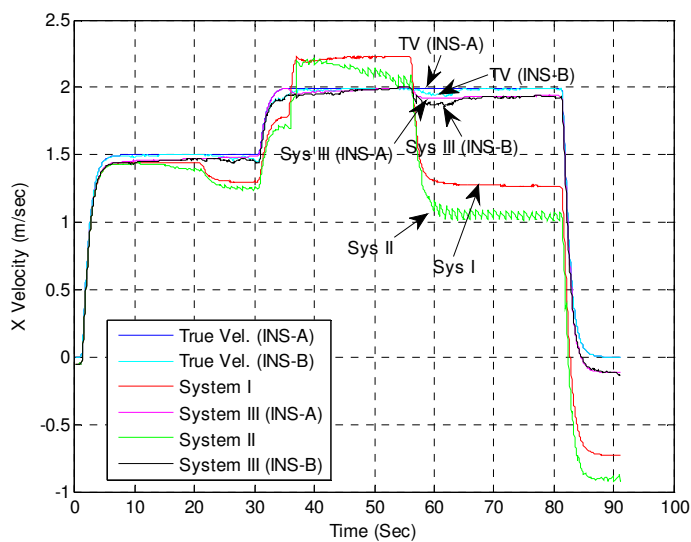
Figure 4-15 : Comparison of x-axis velocity results for the 3 systems. The INS-A and

INS-B results for the system III is shown separately
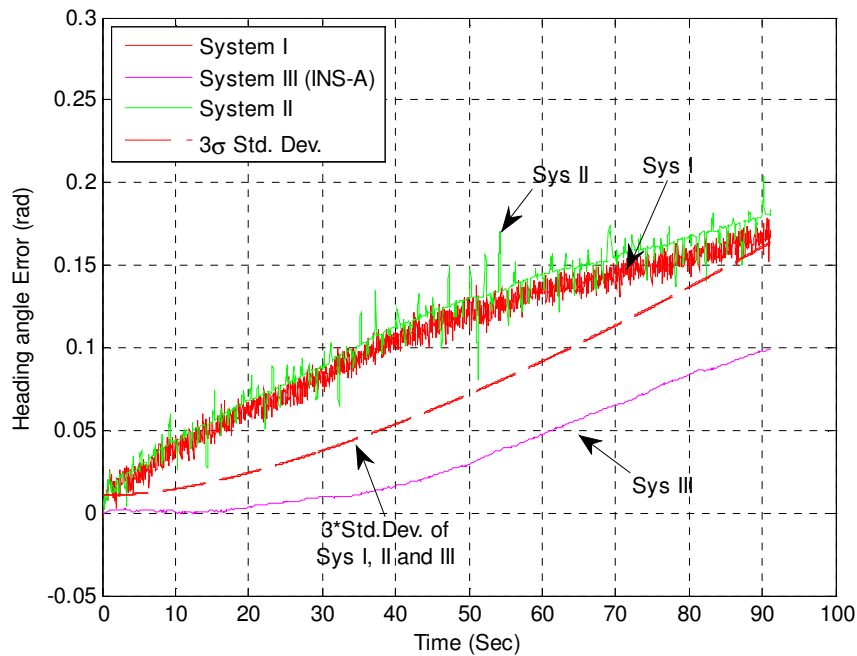
Figure 4-16 : Comparison of attitude estimation errors for the 3 systems. For System I and II the errors are defined as the difference between the combined output and the true INS-A attitude. Due to the scale of the figure, the 3σ std. dev. values for all systems seem like a single curve

The unknown bore-sight effects can also cause serious problems on the overall integrity of the Kalman filter for system I and II. In Figure 4.16 and 4.17, such problems are presented. In Figure 4.16 heading angle estimation error and the 3σ value of the corresponding Kalman filter standard deviation estimate are shown. As shown in this figure, the heading angle estimation error during the entire simulation exceeded the 3σ value which indicates that the Kalman filter covariance values cannot be relied on at all under these conditions. However, as system III does not contain any structural model mismatch, it does not suffer from such problems.

Similar situation can also be observed in Figure 4.17 where Acc^1 bias estimation error is presented together with the corresponding 3σ values. As seen from this figure, under changing bore-sight, the sensor error states estimates for system I and II may become completely unreliable whereas system III can continue to generate reliable results.
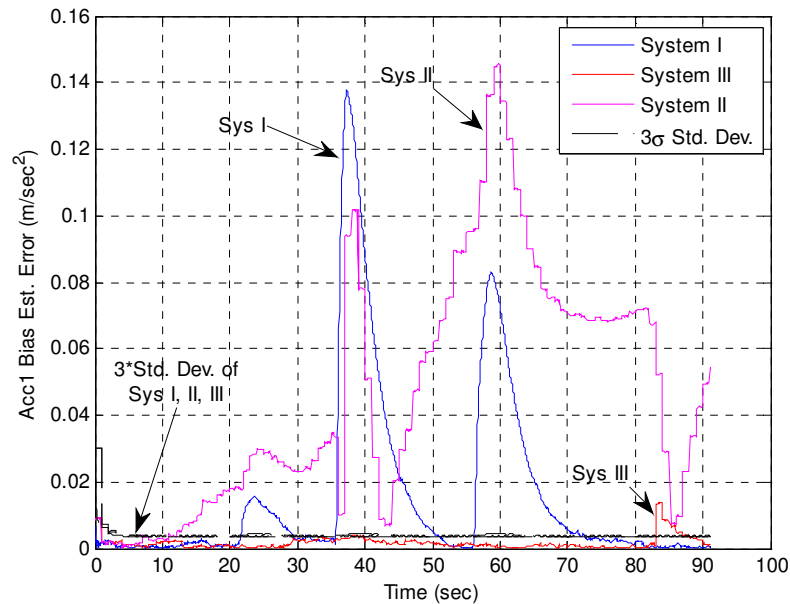
Figure 4-17 : Comparison of Acc^1 bias estimation errors and the Kalman filter standard deviation estimates for the 3 systems. Due to the scale of the figure, the 3σ (std. dev.) values for all systems seem like a single curve.

Another interesting observation that can be noticed from the Figures 4.14 to 4.16 is that the system I and II have comparable navigation error characteristics. Although these 2 systems have completely different internal structures, the effect of unknown bore-sight on the navigation solution turned out to be alike for these simulations. A similar effect can

also be seen in Figure 4.18 where the $Gyro^1$ bias drift estimation errors are shown. As

seen from this figure system I and II have very similar gyro drift estimation error.
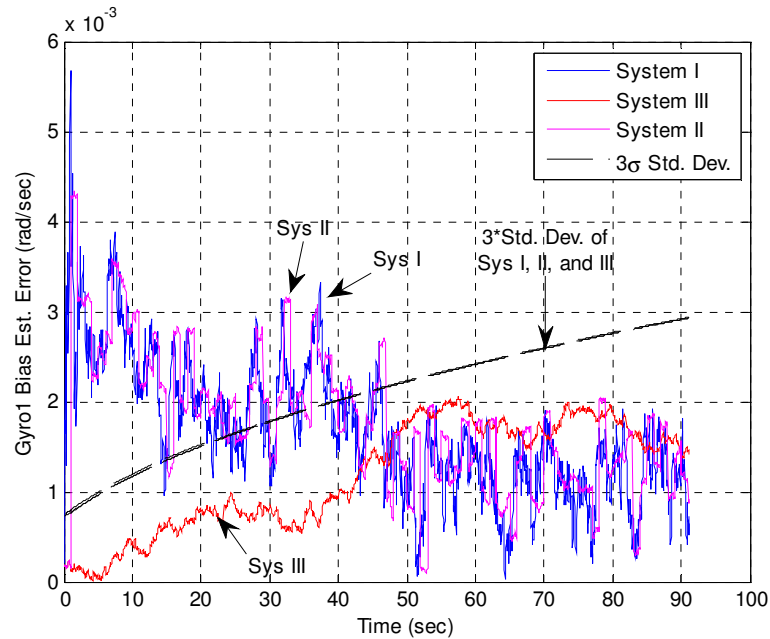
Figure 4-18 : Comparison of $Gyro^1$ bias estimation errors and the Kalman filter

standard deviation estimates for the 3 systems. Due to the scale of the figure, the 3σ

std. dev. values for all systems seem like a single curve.

When there are no bore-sight effects, single-INS implementation can always be used

instead of multi-INS implementations in order to obtain the optimal navigation solutions.

In general, single-INS implementations are easier to design and also they do not require

many modifications for the existing inertial navigation software. On the other hand, as

shown in the above simulations results, when there are significant bore-sight effects

between the inertial sensor sets, the multi-INS implementations can be better modified to

eliminate the effect of these unknown bore-sights which eventually leads to better

navigation solutions. However, it must be noted that in the above simulations an unrealistically exaggerated amount of bore-sight factor was simulated to present this point more clearly (the standard deviation of the bore-sight angle was 6° in the simulations). In the real applications, it is not required to deal with such big bore-sight problems. In general, it was observed in several other simulations that under realistic bore-sight conditions the single-INS implementations can generate as accurate results as any other (modified) multi-INS implementations. Therefore, in most practical applications the SRIMU based navigation system with a single-INS implementation is the most convenient choice to obtain the best navigation solutions.

Chapter Five: **Conclusions and Discussions**

In this thesis, a general framework for the design of inertial navigation systems using skew redundant inertial measurement units was presented. This general framework is capable of providing answers to most of the questions regarding the SRIMU configurations and the optimality of navigation results for such configurations.

5.1 Conclusions

Some of the key findings that have been addressed in this thesis are summarized below.

   i.   Redundancy Observations

In Chapter 2, it was proved that when there are redundant sensors, the projection of the sensor outputs to the left null space of the configuration matrix provides additional observations which can be used to self-calibrate the system.

   ii.   Effectiveness of Redundancy Observations

In Chapters 2 and 3, it was shown that the effectiveness of the redundancy observations is directly related with the error characteristics of the redundant sensors. If all sensors have identical error models, the redundancy observations do not provide any additional information about the kinematic variables which are used to drive the navigation algorithms.

   iii.   Optimal Navigation Solution

In addition to the optimal sensor fusion algorithm presented in Chapter 2, the optimal navigation solution for the SRIMU systems was derived in Chapter 3. Based on the simulations (Section 3.5), it has been shown that the pseudo-optimal solutions can be reliably used instead of the optimal solution without affecting the overall performance.

iv.   Multi-INS Implementations

It has been proved in Chapter 4 that multi-INS implementations are theoretically

equivalent to the single INS implementations. As multi-INS implementations are both

harder to implement and very problematic in terms of numerical considerations, single

INS implementations described in this thesis should be the preferred choice for the

SRIMU systems.

Although the presented framework is capable of providing valuable insights about the

SRIMU based navigation systems, it is not claimed that the application of this framework

will immediately lead to better INS designs with MEMS units. As mentioned above the

effectiveness of the SRIMU systems mainly depends on error characteristics of the

individual sensors. In practice, as most of the SRIMUs are formed using only identical

sensors, the corresponding redundancy does not provide any additional improvement

other than the simple averaging of the noise. However, as more specialized sensors for

specific applications are developed, it is believed that the use of sensors with

complementary characteristics in SRIMUs will become a standard procedure in the

future. For such SRIMU systems, the configurations presented in this study will

hopefully provide a reliable method for the computation of optimal navigation solution.

There are some other important aspects of the SRIMUs which are not discussed in this

thesis at all. One of the most important of such aspects is the determination of the sensor

orientations in the SRIMUs. As mentioned in Chapter 1, the former studies about the

sensor orientation problem is not sufficient to determine the optimal configuration for the

MEMS based SRIMUs. In this thesis, no assumptions are made about the sensor

orientations. The results presented in this thesis are valid regardless of any orientation.

However, some preliminary results suggest that sensor orientation can be extremely important especially for the robustness of the SRIMU based INSs. In a recent paper [Yuksel et al., 2010] such an example is provided. In that paper, it has been showed that when identical sensors are placed on the same axis with opposite directions the temperature induced errors can be automatically cancelled at the final kinematic variable estimates. Therefore, such a configuration becomes robust for unknown temperature effects. As that example suggests, further studies on the optimal orientation problem can provide very fruitful results for the effective SRIMU designs.

5.2 Contributions

1. This thesis presents a practical way of designing high accuracy inertial navigation systems using only low cost off-the-shelf inertial sensors. This is a major leap in the area of inertial navigation systems that has long been required. With the methods described in this thesis, any navigation system requirements can be fulfilled without limited by any physical (and commercial) constraints.

2. There have been some former efforts directed to achieve this goal with multiple-INS concepts. This thesis showed that such approaches are both impractical and suboptimal, and hence should be avoided.

5.3 Recommendation for Future Works

In the following sections, some further discussions and application areas for the framework described in this study are presented. These additional preliminary discussions summarized some important points where future studies on SRIMU based designs can be directed.

5.3.1 Application of Multi-Sensor approach to the Stationary INS updates

When an INS is stationary, the following observations can be used to aid (and self-calibrate) the system:

$$\vec{v}^b = 0$$
$$\dot{\vec{p}} = 0$$
$$\dot{C}_b^n = 0 \qquad\qquad\qquad\qquad\qquad (5.1)$$
$$C_b^n a^b = \bar{g}^n$$
$$\omega^b = C_e^b \bar{\omega}^e$$

where $\vec{v}^b, \vec{p}, C_b^n$ represents the velocity, position and attitude of the system respectively.

$\bar{g}^n$ is the local gravity vector and $\bar{\omega}^e$ is the earth rotation rate. a^b, ω^b denotes the acceleration and rotation rates sensed by the inertial sensors.

In order to avoid modeling any possible vibration effects during the stationary period, only the following subset can be used instead of (5.1):

$$\vec{v}^b = 0 \qquad\qquad\qquad\qquad\qquad (5.2a)$$

$$\omega^b = C_e^b \bar{\omega}^e \approx 0 \qquad\qquad\qquad\qquad\qquad (5.2b)$$

In (5.2b) it is assumed that the earth rotation rate is negligible with respect to gyroscope's intrinsic error sources which are almost always a valid assumption for the currently available MEMS sensors.

Although $\vec{v}^b = 0$ type observations (ZUPT – zero velocity update) can be easily processed with any straightforward Kalman filtering application, the implementation of $\omega^b = 0$ requires significant modification in the existing navigation models. The reason for such modifications can be seen from the associated observation model presented below:

$$y_k = \hat{\omega}_k^b = \delta\omega_k^b + v_k + v_k^{\text{vib}} \qquad\qquad\qquad\qquad\qquad (5.3)$$

where $\hat{\omega}_k^b$ is the gyroscope output, $\delta\omega_k^b$ is the sensor stability errors, v_k is the sensor additive white noise (ARW: angle random walk component) and v_k^{vib} is the observation noise due to the vibration (if there is any).

As can be seen from (5.3), the gyroscope ARW component, which is essentially the white disturbance noise for the INS attitude states, also appears as the measurement noise in this kind of formulation. Therefore, in order to process such an observation the form of the Kalman filter which considers the cross correlation between the measurement and system noises must be used (an example for such Kalman filters are described in [Kailath et al., 2000 –Chapter 9]). However, this form of the Kalman filter usually requires some changes in the existing navigation libraries.

Because of this difficulty, in most applications $\omega^b = 0$ type observations are simply ignored during stationary update periods. However, such an approach basically causes 2 problems:

i.   With only zero velocity updates azimuth errors cannot be stabilized. Therefore, during the stationary period the azimuth errors continue to grow unbounded.

ii.   Although the errors on the horizontal gyroscopes can be estimated by the feedback provided by the zero velocity updates, the vertical gyroscope errors (which mainly determine the azimuth error growth) cannot be calibrated at all.

Therefore, $\omega^b = 0$ type observations should be used as an integral part of ZUPT periods. This is especially important for MEMS units which require continuous calibration because of the unforeseeable effects of environmental factors on MEMS sensor outputs (this point will further be elaborated in Section 5.3).

Fortunately, the multi inertial sensor framework presented in this thesis provides a way to incorporate such sensor based observations in aided navigation applications with minimal change in the existing navigation libraries. In the multi-sensor approach to stationarity updates, $\omega^b = 0$ observations are processed as additional sensors in an SRIMU. Hence, with this approach, the navigation filter part of the INS can be used without any modification as presented below.

Using the same terminology introduced in Chapter 2, the inertial sensor outputs for any IMU can be represented as follows:

$$y_k = M \begin{bmatrix} a^b \\ \omega^b \end{bmatrix} + C_k x_k^{\text{imu}} + v_k^{\text{imu}} \tag{5.4}$$

where y_k is the inertial sensor outputs, M is the (SR)IMU configuration matrix. x_k^{imu} and v_k^{imu} represents the inertial sensor error states and additive white noises (A(V)RW) respectively.

When the system (and the IMU) becomes stationary, (5.4) can be augmented by the additional measurements arise from the stationarity. Therefore, in the stationary mode, the overall kinematic variable observation model can be described as follows:

$$\begin{bmatrix} y_k \\ \bar{\omega}^e \approx 0 \end{bmatrix} = \begin{bmatrix} M \\ 0 \quad I \end{bmatrix} \begin{bmatrix} a^b \\ \omega^b \end{bmatrix} + \begin{bmatrix} C_k \\ 0 \end{bmatrix} x_k^{\text{imu}} + \begin{bmatrix} v_k^{\text{imu}} \\ v_k^{\text{vib}} \end{bmatrix} \tag{5.5}$$

As seen from (5.5), the gyroscope stationarity observations do not cause any difference in the general form of kinematic variable observation model. During the normal mode of operation, the source of all kinematic variable observations is the inertial sensors, whereas when the system stays stationary, the knowledge of the stationarity also provides additional observations. As the general form of the kinematic variable observation model

is exactly the same as the form defined in Chapter 2, all the techniques described in this study can be immediately applied to this case without any modification.

As an example, let us assume an INS is constructed using the pseudo-optimal configuration described in Chapter 3. In this case when the system becomes stationary, the 1st stage IMU Kalman filter processes (5.5) to both estimate the best kinematic variables and self-calibrate the gyroscopes. During the stationary period the INS equations are executed using the optimal rotation rate estimates computed by this first stage. If there is no vibration (i.e. $v_k^{vib} = 0$) then the optimal rotation rate estimate becomes 0 and hence the azimuth error does not grow at all regardless of the stationary period duration.

In such a pseudo-optimal configuration, the zero velocity updates (i.e. $\bar{v}^b = 0$) is processed in the navigation filter (2nd stage filter) together with any other external navigation aid measurements. This navigation filter is an ordinary Kalman filter which is employed in any standard integrated navigation application.

As can be seen in this example, when an INS is designed using the framework described in this thesis, sensor and navigation domain observations can be completely separated from each other and processed in different Kalman filters. Due to this separation property, any kind of sensor measurement can be easily incorporated to the existing software without making any modification in the main navigation routines. Such an approach may provide INS designers an opportunity to develop more efficient (and robust) self-calibration and stationary alignment algorithms in the future.

5.3.2 Application of smoothers to multi inertial sensor systems

As can be seen in the previous section, the division of a single Kalman filter into 2 distinct stages provides great flexibility in the design of the navigation systems. With such a division, every observation related with the IMU can be processed in a separate structure and the remaining navigation operations can be implemented more easily. This is especially the case for the SRIMU systems. In these systems the sensor redundancy observations need to be processed much faster than any other navigation observations. Also, in contrast to the navigation observations, the sensor redundancy observations have usually simpler (more regular) forms. Therefore, whenever possible, it is highly desired to process the navigation and sensor redundancy observations separately. As presented in Chapter 3, the pseudo-optimal configuration provides a way for such a separation in the filtering applications. However, the question of whether or not such a separation is possible for the smoother applications has yet to be answered in this thesis.

Fortunately, as the smoother errors also have the Markovian property ([Kailath et al., 2000], [Verghese et al., 1979]), separation of IMU and navigation stages is possible for the smoother structures. Although, as in the case of filtering, the optimality is compromised in favor of ease of implementation, the separation can be performed in a way very similar to the pseudo-optimal configuration presented in Chapter 3. In the smoothing case, the 1st stage IMU and the 2nd stage navigation filters are replaced with any possible smoother forms. However, it must be noted that when a smoother is used in the 1st stage, the error model of the smoothed kinematic variables must be employed in the 2nd navigation stage.

Basically, any kind of smoother formula can be implemented in the navigation stage. In the existing literature, the "two-filters" ([Fraser et al., 1969]) and "RTS" ([Rauch et al., 1965]) formulas seem mostly to be the preferred choice of INS designers for navigation problems. However, we found that Bryson and Frazier formula as described in [Kailath et al., 2001] is marginally easier to implement than these formulations as it does not require any inversion of the covariance matrix.

For the IMU stage, again any one of these well-known smoother formulations can be used in theory. However, as mentioned above, the Markovion smoothing error models are also needed to be derived together with the smoother results for the navigation stage. In general, the derivation of these error model parameters is a very involved task. In [Bello et al., 1989] several formulations for the smoother error models are provided. Once a smoother structure is chosen for the IMU stage, any of the error model formulations defined in [Bello et al., 1989] can be implemented in the navigation stage.

On the other hand, we noticed that, although not widely used in the inertial navigation field, the smoother formulation of Weinart and Desai's complementary model approach ([Weinart 2001], [Desai et al., 1983]) is a much more suitable choice for the IMU stage than any of the smoother formulas mentioned above. The most important property of this formulation with respect to the other ones is that the smoother error models can be easily defined in this formulation as a simple by-product of smoothing computations.

In [Weinart 2001], a clear derivation of these types of smoothers and the associated error models are presented based on the complementary space approaches (the same formulation is also derived using innovation process approach in [Kailath et al., 1983]).

When the results of [Weinart 2001] are applied for the IMU states, the following forward

time Markovian error model is obtained for the smoothed estimates:

Let the system and observation model for the IMU is represented as follows:

$$
\begin{aligned}
x_{k+1} &= A_k x_k + B_k \omega_k \\
y_k^1 &= H_k x_k + v_k^1
\end{aligned}
\tag{5.6a}
$$

$$
E\left\{
\begin{vmatrix} x_0 \\ w_k \\ v_k^1 \end{vmatrix}
\begin{vmatrix} x_0 \\ w_k \\ v_k^1 \end{vmatrix}^T
\right\}
=
\begin{bmatrix}
\Pi_0 & 0 & 0 \\
0 & Q_k & 0 \\
0 & 0 & R_k
\end{bmatrix}
\tag{5.6b}
$$

Where x_k is the IMU stability errors and y_k^1 is the sensor redundancy observation which

is obtained as a result of multiplying all the sensor outputs with the left null space of

configuration matrix as descried in Chapter 2 (e.g. Chapter 2 - Equation 57).

Furthermore, let:

$$
\tilde{x}_k^s = x_k - \hat{x}_k^s
\tag{5.7}
$$

be the smother errors at time "k", where $\hat{x}_k^s$ denotes the fixed interval smoother results

for the system defined in (5.6) for the time interval $0 \le k \le n$.

In this case, as proved in [Weinart 2001], the forward time Markovian model for the $\tilde{x}_k^s$

can be represented as follows:

$$
\tilde{x}_{k+1}^s = \left(I + B_k Q_k B_k^T M_{k+1}\right)^{-1} A_k \tilde{x}_k^s + \overline{w}_k
\tag{5.8a}
$$

$$
M_k = H_k^T R_k^{-1} H_k - A_k^T \left(I + M_{k+1} B_k Q_k B_k^T\right)^{-1} M_{k+1} A_k
\tag{5.8b}
$$

$$
E\left\{\overline{w}_k \overline{w}_k^T\right\} = \left(I + B_k Q_k B_k^T M_{k+1}\right)^{-1} B_k Q_k B_k^T
\tag{5.8c}
$$

$$
E\left\{\tilde{x}_k^s \tilde{x}_k^{s^T}\right\} = \left(\Pi_0^{-1} + M_0^{-1}\right)^{-1}
\tag{5.8d}
$$

$$M_{n+1} = 0 \tag{5.8e}$$

This error model represents the time propagation of errors on the smoothed kinematic variable (acceleration/rotation rate) estimates. Therefore, when an INS is run by the smoothed kinematic variables, (5.8) must be used to represent the smoothed sensor errors in the 2nd navigation stage.

As can be seen from the above discussion, there is some flexibility in the application of smoothers for the multi-sensor case. Substantially different smoother formulations can be applied for each stage. In general, the improvement obtained by using a smoother instead of a filter in the first stage is quite marginal. In most cases, the 1st stage IMU filters converges to the steady state performances very quickly and this converged point is usually very close to the optimal smoother results. Therefore, for practical purposes, even if a smoother is employed in the navigation stage, a filter rather than a smoother can be preferred in the 1st stage without affecting the results too much.

Additional analysis and simulations are required to understand the cases for which IMU smoothers can be replaced with IMU filters for improved performance. Such further studies may also provide additional insights about whether or not some additional robustness properties can be gained with these smoother structures.

5.3.3 Application of Multi-Sensor approach to the traditional INS design process

As mentioned in the first chapter, the main motivation behind the use of the SRIMUs in INSs is to be able to satisfy the specified mission objectives by using only low cost MEMS inertial units. On the other hand, even if the mission objectives can be

theoretically satisfied without any redundant sensors, the developed framework can still be very useful for the standard single IMU based INS design process.

As described in [Maybeck 1982], the INS design process starts with the covariance analysis. Once the objectives are defined, a covariance analysis is performed to roughly determine the required IMU error specifications. However, covariance analysis method assumes that the inertial sensors under consideration have known error characteristics. Unfortunately, none of these error characteristics are defined in the specification sheets of the MEMS units. Currently, MEMS sensors' specification sheets contain only performance figures which are derived from the Allan variance tests. However, Allan variance characteristics of low cost MEMS units are usually among the least significant error components. In general, the errors induced the by external conditions (e.g. temperature, vibration etc) are more important than the short term stability properties characterized by the Allan variance results for the MEMS sensors.

An example of this situation is presented in figure 5.1 where the Allan standard deviations of 2 different gyroscopes are compared. The first gyroscope (G1) is a relatively expensive (and high accuracy) ADIS16120 unit ([ADIS16120]), whereas the second gyroscope (G2) is a very low cost L3G4200D unit which is currently used in the smartphones. According to the current market prices the G1 is approximately 200 times more expensive than the G2. However, Allan variance characteristics presented in Figure 5.1 shows that the short term error characteristics of the G1 are only 4 times better than the G2. Although the price and Allan variance comparison of these units seems quite inconsistent, a more detailed error analysis reveals the fact that G1 outperforms G2 in other more important aspects. As presented in [Yuksel et al., 2010], the G1 unit has a

very consistent temperature dependence which can easily be compensated with some

deterministic methods. Furthermore, with suitable compensation methods, the

repeatability errors of G1 can be almost completely removed. However, initial analysis of

G2 units showed that these units have significant temperature and repeatability errors

which cannot be compensated. Therefore, a covariance analysis for G2 units will lead to

completely wrong performance specification results if the analysis is performed based on

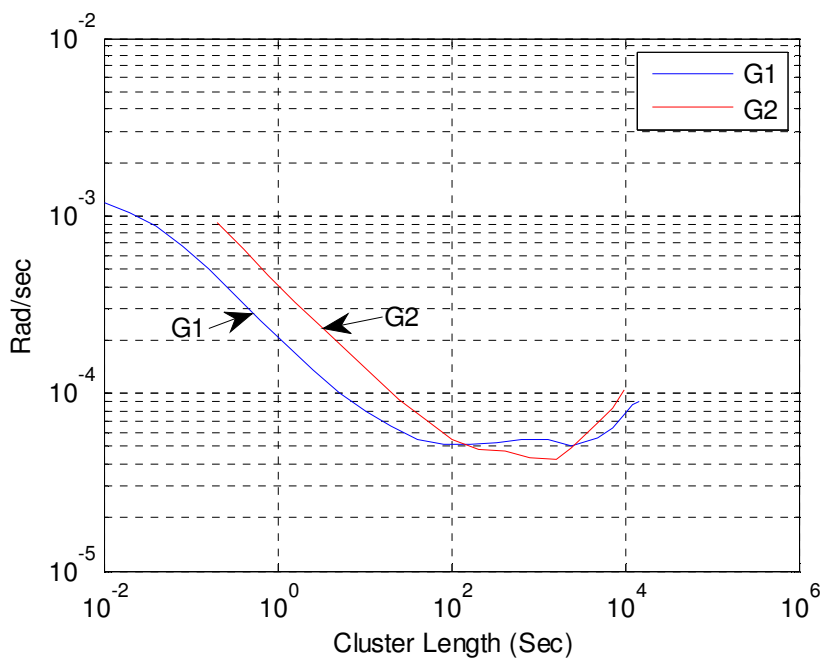only the Allan variance characteristics.

Figure 5-1 : Allan standard deviation comparison of 2 gyroscopes. G1: ADIS16120,

G2: L3G4200D.

In order to design a navigation system with units similar to G2, very extensive error

characterization tests such as the one described in [Yuksel et al., 2010] must be

performed prior to start of design process. However, this initial error characterization

phase are so time consuming and labor demanding that it is not possible to repeat it for a large variety of MEMS sensors just to find the most suitable sensor candidate for the INS design. Because of such difficulties, most INS design project fails even in the very initial phases.

On the other hand, the SRIMU based INS design methodology presented in this thesis can be used to avoid such difficulties in MEMS based INS designs. In this approach, only MEMS units which has completely known error characteristics (possibly due to the fact that it was used in a previous project) can be used in the covariance analysis to determine the approximate number of redundant sensors (of the specified kind) to achieve the mission objectives. Once such a sufficient SRIMU configuration is specified, the remaining INS design tasks can be started while a search for better (and newer) sensor can be simultaneously performed. As all the risks and expenses of the initial modeling phase are removed, the probability of successfully finishing an INS design project can be greatly increased in this approach.

APPENDIX A

The structure presented in Section 3.3 (Figure 3.3) corresponds to the case where the same observation is processed twice to form an optimal estimate of the overall state. In the first iteration, only the sensor error states are optimally estimated using the redundancy observations. This corresponds to the Schmidt-Kalman filter where the suboptimal gain is obtained by setting the rows of the optimal gain corresponding to the navigation states to zero. In the second iteration, the same observations are once more used to estimate only the navigation states.

In this appendix, the modified form of the Kalman filter recursions for which the same observation is applied twice is described.

Let $\hat{x}_k^-$ represent the best estimate of x_k computed using all the observations up to but not including y_k. Also, it is assumed that:

$$E\left\{ \underbrace{\left(x - \hat{x}_k^-\right)\left(x - \hat{x}_k^-\right)^T}_{\tilde{x}_k^-} \right\} = \Pi_k^- \tag{A.1a}$$

$$y_k = Hx_k + v_k \tag{A.1b}$$

$$E\left\{v_k v_k^T\right\} = R \tag{A.1c}$$

Let K_1 be any gain (not necessarily optimal in any sense). With this arbitrary gain, the new $\hat{x}_k^+$ estimate can be computed as follows:

$$\hat{x}_k^+ = \hat{x}_k^- + K_1\left(y_k - H\hat{x}_k^-\right) \tag{A.2}$$

Furthermore, the error is:

$$\tilde{x}_k^+ = x_k - \hat{x}_k^+ = \left(I - K_1 H\right)\tilde{x}_k^- - K_1 v_k \tag{A.3a}$$

$$E\left\{\tilde{x}_k^+ \tilde{x}_k^{+^T}\right\} = \Pi_k^+ = \left(I - K_1 H\right)\Pi_k^-\left(I - K_1 H\right)^T + K_1 R K_1^T \tag{A.3b}$$

It should be noted that $\hat{x}_k^+$ is not an optimal estimate. It is just an ordinary blending of $\hat{x}_k^-$

with y_k using (somehow) an arbitrary gain K_1. Therefore, $\tilde{x}_k^+$ is still correlated with y_k,

and hence, y_k can still be used to estimate $\tilde{x}_k^+$ as follows:

$$E\left\{\tilde{x}_k^+ \mid y_k\right\} = E\left\{\tilde{x}_k^+ \mid \underbrace{y_k - H\hat{x}_k^+}_{\tilde{y}_k^+}\right\} \tag{A.4}$$

Therefore (assuming Gaussian distributions), the best estimate of $\tilde{x}_k^+$ given y_k is:

$$\hat{\tilde{x}}_k^+ = R_{\tilde{x}_k^+ \tilde{y}_k^+} R_{\tilde{y}_k^+}^{-1} \tilde{y}_k^+ \tag{A.5a}$$

$$\begin{aligned}
R_{\tilde{x}_k^+ \tilde{y}_k^+} &= E\left\{\tilde{x}_k^+ \tilde{y}_k^+\right\} = E\left\{\tilde{x}_k^+ \left(H\tilde{x}_k^+ + v_k\right)\right\} \\
&= \Pi_k^+ H^T + E\left\{\tilde{x}_k^+ v_k^T\right\} \\
&= \Pi_k^+ H^T - K_1 R
\end{aligned} \tag{A.5b}$$

$$R_{\tilde{y}_k^+} = E\left\{\tilde{y}_k^+ \tilde{y}_k^{+^T}\right\} = H\Pi_k^+ H^T + R \tag{A.5c}$$

(It should be noted that when K_1 is the optimal gain, (A.5b) becomes algebraically 0.)

Thus, with the 2 successive updates from the same observation (the first being the

suboptimal, the second being the optimal), the modified form of the Kalman update

equations can be written as follows:

$$\hat{x}_k^+ = \hat{x}_k^- + K_1\left(y_k - H\hat{x}_k^-\right) \tag{A.6a}$$

$$\Pi_k^+ = \left(I - K_1 H\right)\Pi_k^-\left(I - K_1 H\right)^T + K_1 R K_1^T \tag{A.6b}$$

$$\hat{x}_k^{++} = \hat{x}_k^+ + \underbrace{\left(\Pi_k^+ H^T - K_1 R\right)\left(H\Pi_k^+ H^T + R\right)^{-1}}_{K_2}\left(y_k - H\hat{x}_k^+\right) \tag{A.6c}$$

$$\Pi_k^{++} = \left(I - K_2 H \right) \Pi_k^{+} \left(I - K_2 H \right)^T + K_2 R K_2^T + \left(I - K_2 H \right) R K_1^T K_2^T + K_2 K_1 R \left(I - K_2 H \right)^T \qquad \text{(A.6d)}$$

In the above equations $\hat{x}_k^{+}$ is the result of the first update, and $\hat{x}_k^{++}$ is the result of the

second. Therefore $\hat{x}_k^{++}$ corresponds to the optimal estimate of x_k given all observations

up to and including y_k.

In Figure 3.4, the 1$^{\text{st}}$ stage IMU Kalman filter realizes the first update. The equivalent

error models used in 2$^{\text{nd}}$ stage Kalman filter reflects the effect of this update in the

covariance calculation. Therefore, when the innovation process of the 1$^{\text{st}}$ stage filter

$\left(T_k y_k^{imu} - H_k^{rmimu} \hat{x}_{k|k} \right)$ is processed in the 2$^{\text{nd}}$ stage KF with the update equations shown in

(A.6c) and (A.6d), the overall structure becomes optimal.

APPENDIX B

In this appendix the solution of the following problem is presented:

Given the PVA (position, velocity and attitude in the form of direction cosine matrix) results ($^A\hat{x}\ldots\ ^L\hat{x}$) and associated covariance matrix "Π" of the zero mean (Gaussion) PVA errors of "L" INS implementation, compute the best minimum variance unbiased (MVU) PVA estimate of the system.

Before presenting the solution to the above problem, first it will be shown that the MVU estimates can be computed around a nominal value defined on one of the observations:

Let

$$\begin{bmatrix} ^A\hat{x} \\ \vdots \\ ^L\hat{x} \end{bmatrix} = \begin{bmatrix} I \\ \vdots \\ I \end{bmatrix} x + \eta \tag{B.1}$$

where $E\{\eta\} = 0$ and $E\{\eta\eta^T\} = \Pi$. Define $^i\delta x = x - {}^i\hat{x}$. Then

$$\begin{bmatrix} 0 \\ ^B\hat{x} - {}^A\hat{x} \\ \vdots \\ ^L\hat{x} - {}^A\hat{x} \end{bmatrix} = \underbrace{\begin{bmatrix} I \\ \vdots \\ I \end{bmatrix}}_{U} {}^A\delta x + \eta \tag{B.2}$$

Therefore,

$$^A\delta\hat{x} = \underbrace{\left(U^T\Pi^{-1}U \right) U^T\Pi^{-1}}_{J} \begin{bmatrix} 0 \\ ^B\hat{x} - {}^A\hat{x} \\ \vdots \\ ^L\hat{x} - {}^A\hat{x} \end{bmatrix} \tag{B.3}$$

where $^A\delta\hat{x}$ is the best MVU estimate of the errors on the $^A\hat{x}$ given all observations. As $x = {}^A\hat{x} + {}^A\delta x$, the best estimate of x ($\hat{x}$) is equal to $\hat{x} = {}^A\hat{x} + {}^A\delta\hat{x}$.

Furthermore, this idea can be generalized to any other observation. Hence:

$$\hat{x} = {}^{A}\hat{x} + J \begin{bmatrix} 0 \\ {}^{B}\hat{x} - {}^{A}\hat{x} \\ \vdots \\ {}^{L}\hat{x} - {}^{A}\hat{x} \end{bmatrix} = \ldots = {}^{L}\hat{x} + J \begin{bmatrix} {}^{A}\hat{x} - {}^{L}\hat{x} \\ {}^{B}\hat{x} - {}^{L}\hat{x} \\ \vdots \\ 0 \end{bmatrix} \tag{B.4}$$

The above way of computing the best estimates can be used for navigation states as follows:

Let $\left[{}^{A}P, {}^{A}V, {}^{A}C_{b}^{n} \right] \ldots \left[{}^{L}P, {}^{L}V, {}^{L}C_{b}^{n} \right]$ be the outputs (position, velocity attitude) of L navigation system. (it is assumed that there is no lever-arm/boresight effect between units.)

Using the ϕ-formulation, the attitude errors can be defined as follows:

$$\hat{C}_{b}^{n} = \left[I + S\left(\phi \right) \right] C_{b}^{n} \tag{B.5}$$

Therefore, using INS A as the nominal solution:

$$\begin{bmatrix} {}^{A}\delta\hat{P} \\ {}^{A}\delta\hat{V} \\ {}^{A}\phi \end{bmatrix} = J \begin{bmatrix} [0] \\ \begin{bmatrix} {}^{B}\hat{P} - {}^{A}\hat{P} \\ {}^{B}\hat{V} - {}^{A}\hat{V} \\ S^{-1}\left({}^{B}C_{b}^{n}{}^{A}C_{n}^{b} \right) \end{bmatrix} \\ \vdots \\ \begin{bmatrix} {}^{L}\hat{P} - {}^{A}\hat{P} \\ {}^{L}\hat{V} - {}^{A}\hat{V} \\ S^{-1}\left({}^{L}C_{b}^{n}{}^{A}C_{n}^{b} \right) \end{bmatrix} \end{bmatrix} \tag{B.6}$$

Where J is as defined in (A.3) and S^{-1} is the operator which converts skew-symmetric matrices into the corresponding vector form.

Using (B.6), the best PVA estimates can be computed as:

$$\hat{P} = {}^{A}\hat{P} + {}^{A}\delta\hat{P}$$
$$\hat{V} = {}^{A}\hat{V} + {}^{A}\delta\hat{V}$$
$$\hat{C}_b^n = \left[I - S\left({}^{A}\phi\right)\right] {}^{A}C_b^n$$

(B.7)

Furthermore, the covariance of this estimate is:

$$\Pi^{+} = \left(U^{T}\Pi^{-1}U\right)^{-1}$$

(B.8)

Errors on the estimated (combined) navigation states in terms of the errors on the

individual INSs can be represented as follows:

$$
\begin{bmatrix} \delta P \\ \delta V \\ \phi \end{bmatrix} = \begin{bmatrix} P - \hat{P} \\ V - \hat{V} \\ S^{-1}\left(\hat{C}_b^n C_n^b\right) \end{bmatrix} = \begin{bmatrix} {}^{A}\delta P \\ {}^{A}\delta V \\ {}^{A}\phi \end{bmatrix} + J \begin{bmatrix} [0] \\ \begin{bmatrix} {}^{B}\delta P \\ {}^{B}\delta V \\ {}^{B}\phi \end{bmatrix} - \begin{bmatrix} {}^{A}\delta P \\ {}^{A}\delta V \\ {}^{A}\phi \end{bmatrix} \\ \vdots \\ \begin{bmatrix} {}^{L}\delta P \\ {}^{L}\delta V \\ {}^{L}\phi \end{bmatrix} - \begin{bmatrix} {}^{A}\delta P \\ {}^{A}\delta V \\ {}^{A}\phi \end{bmatrix} \end{bmatrix}
$$

$$
= \begin{bmatrix} {}^{A}\delta P \\ {}^{A}\delta V \\ {}^{A}\phi \end{bmatrix} + {}^{B}J \begin{bmatrix} {}^{B}\delta P \\ {}^{B}\delta V \\ {}^{B}\phi \end{bmatrix} + \ldots + {}^{L}J \begin{bmatrix} {}^{L}\delta P \\ {}^{L}\delta V \\ {}^{L}\phi \end{bmatrix} - \underbrace{\left({}^{B}J + \ldots + {}^{L}J\right)}_{I - {}^{A}J} \begin{bmatrix} {}^{A}\delta P \\ {}^{A}\delta V \\ {}^{A}\phi \end{bmatrix}
$$

(B.9)

$$
= {}^{A}J \begin{bmatrix} {}^{A}\delta P \\ {}^{A}\delta V \\ {}^{A}\phi \end{bmatrix} + {}^{B}J \begin{bmatrix} {}^{B}\delta P \\ {}^{B}\delta V \\ {}^{B}\phi \end{bmatrix} + \ldots + {}^{L}J \begin{bmatrix} {}^{L}\delta P \\ {}^{L}\delta V \\ {}^{L}\phi \end{bmatrix}
$$

As can be seen from (B.9), the relation between the best navigation state estimate and

individual navigation systems outputs are equivalent to the relation between the error on

the best estimate ($\left[\delta P, \delta V, \phi\right]$) and the errors on individual systems ($\left[{}^{i}\delta P, {}^{i}\delta V, {}^{i}\phi\right]_{i=A}^{L}$).

Therefore, observation models presented in Section 4.4 (which are defined based on the

navigation states rather than the errors on the navigation states), is also valid for these error states.

As a final note, it should be noted that if only the combination of some of the navigation states are required (e.g. if only the best position estimate is required rather than the best PVA solution), then only the corresponding states can be used to form a solution (e.g. in (B.1) $x = P$). However, in this case the implicit information which is represented as the cross-correlation between the states are completely ignored (e.g. the cross correlation between P and V). On the other hand, as shown in Section 4.5, there are cases where such sub-optimality is generally preferred.

References

[ADIS16120]   ADIS16120 Low Noise Angular Rate Sensor Data Sheet Rev B, 2007, Analog Devices

[Arshal 1987]   Arshal G., "Error equations of inertial navigation", Journal of Guidance, Control, and Dynamics, 0731-5090 vol.10 no.4 (351-358), 1987

[Bar-Itzhack et al., 2002]   Bar-Itzhack, I.Y., and Harman, R. R., "In-Space Calibration of a Skewed Gyro Quadruplet," Journal of Guidance, Control, and Dynamics, Vol. 25, No. 5, 2002, pp. 852–859.

[Bancroft et al.,2008]   Bancroft J, G. Lachapelle, M. Cannon, and M. Petovello, "Twin IMU-HSGPS Integration for Pedestrian Navigation" , Proceedings of the ION GNSS, Savannah, GA, USA, 2008.

[Bancroft 2009]   Bancroft J., "Multiple IMU Integration for Vehicular Navigation", Proceedings of GNSS 2009, The Institute of Navigation, 2009.

[Bancroft 2010]   Bancroft J., "Multiple Inertial Measurement Unit Integration for Pedestrian Navigation", UCGE Report 20320, December 2010, University of Calgary, Calgary, Canada

[Bello et al., 1989]   Bello M. G., Willsky A. S., Levy B. C, Construction and application of discrete time smoothing error models, Journal of Int. Cont. 50, pp 203-233, 1989

[Carvalho et al.,   Carvalho, H.; Del Moral, P.; Monin, A.; Salut, G.; , "Optimal

1997]   nonlinear filtering in GPS/INS integration," Aerospace and

Electronic Systems, IEEE Transactions on , vol.33, no.3, pp.835-

850, July 1997

[Colomina et al.,   Colomina I., Gimenez M., Rosales J. J., Wis M., Gómez A., , "What

2003]   can skewed redundant IMU configurations contribute to

photogrammetry", Proocedings of ISPRS workshop, working group

1.5, Castelldefels, 2003.9.22-23, Castelldefel, ES

[Colomina et al.,   Colomina I., Gimenez M., Rosales J. J., Wis M., Gómez A.,

2004a]   Miguelsanz P., "Redundant IMUs for Precise Trajectory

Determination," in XXth ISPRS Congress Istanbul, 2004.

[Colomina et al.,   Colomina, I., Giménez, M., Rosales, J.J, "On the use of redundant

2004b]   inertial data for geodetic application", 17th ION GNSS International

Technical Meeting, Long Beach, USA, 2004

[Desai et al.,1983]   Desai U., Weinert H. Yusypchuk G., Discrete-Time

Complementary Models and Smoothing Algorithms: The

Correlated Noise Case, IEEE Trans. Automatic Control, Vol: 28 No:

4, 1983

[Fraser et al.,1969] Fraser D., Potter J. E., The optimum linear smoother as a

combination of two optimum linear filters, IEEE Trans. Automat.

Contr., AC-14, pp. 387-390, 1969

[Hall, 1982]   Hall, S. R., "Parity Vector Compensation For FDI," S.M. Thesis,

Dept. of Aeronautics and Astronautics, Massachusetts Inst. of
Technology, Cambridge, MA, Feb. 1982.

[Harrison et al.,1977]   Harrison, J.V., and Gai, E. G., "Evaluating Sensor Orientations forNavigation Performance and Failure Detection," IEEE Transactions on Aerospace and Electronic Systems, Vol. 13, No. 6, 1977, pp. 631–643.

[Ho, 1999]   Ho, J. H., "Sensor Redundancy Management/Fault Detection and Isolation of the Inertial Measurement Unit for a Land-Based Vehicle's Locating System," Ph.D. Dissertation, Dept. of Mechanical Engineering, Pennsylvania State Univ., University Park, PA, Oct. 1999.

[Kailath et al.,2000]   Kailath T., Sayed A. H., Hassibi B., "Linear Estimation", Prentice Hall, New Jersey USA, 2000.

[Kailath et al.,1984]   Kailath T., Wax M., A note on the complementary model of Weinert and Desai, IEEE Trans. Automatic Control, Vol 29 No:6, 1984

[Kaygisiz et al.,2003]   Kaygisiz, B.H.; Erkmen, A.M.; Erkmen, I.; , "GPS/INS enhancement using neural networks for autonomous ground vehicle applications," Intelligent Robots and Systems, 2003. (IROS 2003). Proceedings. 2003 IEEE/RSJ International Conference on

[Kleinert et al.,   Kleinert, M.; Schleith, S.; , "Inertial aided monocular SLAM for

2010]   GPS-denied navigation," Multisensor Fusion and Integration for

Intelligent Systems (MFI), 2010 IEEE Conference on , vol., no.,

pp.20-25, 5-7 Sept. 2010

[L3G4200D]   L3G4200D MEMS motion sensor: three-axis digital output

gyroscope, Doc ID 17116 Rev 2

[Maybeck 1982]   Maybeck S. P., Stochastic models, estimation and control Volume I,

Academic Press, USA, 1982

[Nordlund et   Nordlund, P.-J.; Gustafsson, F.; , "Sequential Monte Carlo filtering

al.,2001]   techniques applied to integrated navigation systems," American

Control Conference, 2001. Proceedings of the 2001 , vol.6, no.,

pp.4375-4380 vol.6, 2001

[Noureldin et   Noureldin, A.; El-Shafie, A.; El-Sheimy, N.; , "Adaptive neuro-

al.,2007]   fuzzy module for inertial navigation system/global positioning

system integration utilising position and velocity updates with real-

time cross-validation," Radar, Sonar & Navigation, IET , vol.1, no.5,

pp.388-396, October 2007

[Noureldin et al.,   Noureldin A., El-Shafie A., Bayoumi M.,. 2011. GPS/INS

2011]   integration utilizing dynamic neural networks for vehicular

navigation. Inf. Fusion 12, 1 (January 2011), 48-57

[Pittelkau 2005a]   Pittelkau M. E., "Calibration and Attitude Determination with

Redundant Inertial Measurement Units", AIAA Journal of

Guidance, Control, and Dynamics, Vol. 28, No. 4, July–August 2005, pp. 743–752

[Pittelkau 2005b]   Pittelkau, M. E., "Cascaded and Decoupled RIMU Calibration Filters", Paper No. AAS 05-466, Malcom D. Shuster Astronautics Symposium, Grand Island, NY, 12–15 June 2005. In Advances in the Astronautical Sciences, Vol. 122, Part I, 2006, pp. 273–288.

[Pittelkau 2005c]   Pittelkau, M. E., "Observability and Calibration of a Redundant Inertial Measurement Unit (RIMU)", AAS 05-105, AAS/AIAA Space Flight Mechanics Meeting, Copper Mountain, CO, 23–27 January 2005, in Advances in the Astronautical Sciences, 2005.

[Rauch et al.,1965]   Rauch H. E., Tung F., Striebel, Maximum likelihood estimates of linear dynamic systems, AIAA J., 3, pp. 1445-1450., 1965

[Sasiadek et al., 2000]   Sasiadek, J.Z.; Wang, Q.; Zeremba, M.B.; , "Fuzzy adaptive Kalman filtering for INS/GPS data fusion," Intelligent Control, 2000. Proceedings of the 2000 IEEE International Symposium on , vol., no., pp.181-186, 2000

[Savage 2000a]   Savage P. G., Strapdown Analytics, Strapdown. Associates Inc., Maple Plain, Minnesota, USA, 2000, vol. 1

[Savage 2000b]   Savage P. G., Strapdown Analytics, Strapdown. Associates Inc., Maple Plain, Minnesota, USA, 2000, vol. 2

[Skog et al., 2010]   Skog I., Nilsson J.O., Handel P., "Evaluation of zero-velocity detectors for foot-mounted inertial navigation systems," Indoor Positioning and Indoor Navigation (IPIN), 2010 International Conference on , vol., no., pp.1-6, 15-17 Sept. 2010

[Skoogh et al., 2006]   Skoogh, Daniel, Lennartsson, Anders, "A Method for Multiple Fault Detection and Isolation of Redundant Inertial Navigation Sensor Configurations," Proceedings of IEEE/ION PLANS 2006, San Diego, CA, April 2006, pp. 415-425.

[Sukkarieh et al., 2000]   Sukkarieh, S., Gibbens P., Brocholsky B., Willis K., Durrant-Whyte H. F., "A Low-Cost Redundant Inertial Measurement Unit for Unmanned Air Vehicles," The International Journal of Robotics Research, vol. 19, 2000

[Sturza 1988]   Sturza, M., "Skewed axis inertial sensor geometry for optimal performance". 8th AIAA/IEEE Digital Avionics Systems Conference, Oct. 1988, p. 128-135

[Tardif et al. 2010]   Tardif J.P., George M.; Laverne M., Kelly A., Stentz, A., "A new approach to vision-aided inertial navigation," Intelligent Robots and Systems (IROS), 2010 IEEE/RSJ International Conference on , vol., no., pp.4161-4168, 18-22 Oct. 2010

[Titterton et al. 2004]   Titterton, D. and Weston, J. "Strapdown Inertial Navigation Technology, 2nd Edition." Progress in Astro-

nautics and Aeronautics Series, Published by AIAA, 2004

[Verghese et al. 1979]   Verghese G., Kailath T., "A further note on backward Markovian Models", IEEE Trans. Inform. Theory, IT-25, pp:121-124, 1979

[Waegli et al. 2008]   Waegli A., Stephane G., Jan S., "Redundant MEMS-IMU integrated with GPS for Performance Assessment in Sports", Proceedings of IEEE/ION PLANS 2008, IEEE/ION PLANS 2008, Monterey, California, May 5-8, 2008

[Waegli 2009]   Adrian Weagli, "Trajectory determination and analysis in sports by satellite and inertial navigation", These EPFL, no 4288, Lausanne EPFL, Switzerland, 2009

[Weinart 2001]   Weinart H. L., Fixed Interval Smoothing for State Space Models, Kluwer Academic Publishers, USA, 2001

[Yuksel et al. 2010]   Yuksel Y.; El-Sheimy N., Aboelmagd N., "Error modeling and characterization of environmental effects for low cost inertial MEMS units," Position Location and Navigation Symposium (PLANS), 2010 IEEE/ION , vol., no., pp.598-612, 4-6 May 2010